SIGNAL DESIGN AND PROCESSING TECHNIQUES FOR WSR-88D AMBIGUITY RESOLUTION

PART - 4: Staggered PRT Technique

National Severe Storms Laboratory Report

prepared by: M. Sachidananda,
with contributions by: D.S. Zrnic and R.J. Doviak

October 2000

NOAA, National Severe Storms Laboratory
1313 Halley Circle, Norman, Oklahoma 73069

SIGNAL DESIGN AND PROCESSING TECHNIQUES FOR WSR-88D AMBIGUITY RESOLUTION
Part-4: staggered PRT

Contents

ooo000ooo

SIGNAL DESIGN AND PROCESSING TECHNIQUES FOR WSR-88D AMBIGUITY RESOLUTION

Part - 4: the staggered PRT technique

1. Introduction

The Operational Support Facility (OSF) of the National Weather Service (NWS) has funded the National Severe Storms Laboratory (NSSL) to address the mitigation of range and velocity ambiguities in the WSR-88D. This is the fourth report in the series that deals with velocity and range ambiguity resolution in the WSR-88D. The first two reports mainly dealt with uniform PRT transmission and phase coding techniques to resolve the range ambiguity. Although the phase coding techniques do not directly address the velocity ambiguity problem, their capability to separate overlaid echoes allows the use of shorter PRTs which, in turn, diminishes the occurrence of ambiguous velocities. In the third part, we considered the staggered PRT technique and its variants. The significant results in the Report 3 are a new staggered PRT sequence processing scheme in the spectral domain which significantly improves spectral moment estimates, and a clutter filtering method that recovers velocity information over the entire extended unambiguous velocity interval without any drop-out regions. The only assumption made in the algorithm is that there is no overlaid signal. This necessarily restricts the selection of the PRT T_1 to be sufficiently large for a given elevation so that the probability of overlay is small.

After the third report was submitted in July 1999, some more ideas were explored in an effort to further improve the staggered PRT scheme. Specifically, we tried to further improve the velocity estimate errors by optimizing the window weights. We also examined the possibility of increasing the unambiguous range to r_{a2}, by resolving the overlaid signal from corresponding to the shorter range r_{a1}. Exhaustive simulations were carried out to evaluate the performance of the staggered PRT decoding scheme and determine the limits of

spectral moment recovery within acceptable bonds under various conditions. This information is very useful in developing a data censoring strategy to discard or flag the bad data. The results from all these studies has been reported in this Part-4 of the report. In the light of these new results and an enhanced capability of the staggered PRT algorithm, we have revised the proposed WSR-88D scan strategy given in Table.5.3 of Report 3. The notations used in this report are the same as in Report 3. This study is essentially a continuation of the staggered PRT work. A brief introduction to the staggered PRT technique was given in Report 3, and a part of it is repeated here for the convenience of readers and to recall the symbols and notations used in the context of the staggered PRT processing.

2. The staggered PRT technique

Here, we describe the staggered PRT scheme briefly before we embark on a discussion of the new method of processing. In the staggered PRT technique (Zrnic and Mahapatra, 1985), two different pulse spacings, T_1 and T_2; ($T_2>T_1$), are used alternately (Report 3, Fig. 2.1a). Then, alternate pairs of return samples are used to compute autocorrelation estimates, R_1 at lag T_1 and R_2 at lag T_2. The velocity is estimated from the phase difference between the two using the formula,

$$\hat{v} = \lambda \, arg(R_1 R_2^*) \, / \, [4\pi(T_2-T_1)] \, . \qquad (2.1)$$

Thus, the difference in PRT, (T_2-T_1), determines the unambiguous velocity, v_a, for the staggered PRT technique and is given by

$$v_a = \pm \lambda \, / \, [4(T_2-T_1)] \; ; \;\; T_1 < T_2 \, . \qquad (2.2)$$

Zrnic and Mahapatra (1985) suggest a procedure to estimate mean velocity and signal power for echoes received within the time delay (T_1+T_2). In theory, this seems to be possible because the overlaid signals in any two consecutive samples are from two different

ranges and, therefore, are uncorrelated. Thus, the expected value of the overlaid signal contribution to the autocorrelation is zero, and the effective unambiguous range becomes

$$r_a = c(T_1+T_2)/2. \qquad (2.3)$$

Eq. 2.1 and 2.3 suggest that the staggered PRT is equivalent to a uniform PRT = (T_1+T_2) for the unambiguous range and a uniform PRT, $T_u = (T_2-T_1)$ for the unambiguous velocity, and each can be selected independently. However, the practical utility of this scheme is limited due to the quality of estimates. The overlaid signal increases the variance of the estimates because it acts as noise. Thus, the ratio of the overlaid signal powers is the equivalent signal-to-noise ratio (SNR), and for a reasonable accuracy of the estimates, the unwanted signal has to be at least 3 dB below the desired signal power.

Let $r_{a1} = cT_1/2$ and $r_{a2} = cT_2/2$ so that $r_a=r_{a1}+r_{a2}$, and $r_{a1} < r_{a2}$. If r_{a1} is chosen sufficiently large so that no echoes are received from ranges greater than r_{a1}, then the problem of overlaid echoes could be eliminated. If we choose PRTs such that we have no echoes from range greater than r_{a2} then for some of the range gates, the alternate samples have overlaid signal from another range gate separated by a delay time T_1, and the rest are free of overlaid signal. This situation, we call the "one-overlay" situation, is thought to be a good candidate for further extending the unambiguous range to r_{a2}, with some additional processing. This possibility has been explored in this report.

It is shown by Zrnic and Mahapatra (1985) that the standard error in the velocity estimate increases as the ratio $\kappa = T_1/T_2$ approaches unity, and a good choice is κ =2/3. Thus, the unambiguous range and unambiguous velocity are indirectly tied in practice via the estimate accuracy. However, compared to the uniform PRT, it is possible to achieve a much larger r_a and v_a because the limiting equation is $v_a\, r_{a2} = \{1/(1-\kappa)\}c\lambda/8$ for the staggered PRT scheme with one-overlay resolution. Report 3 indicates that κ =2/3 is optimum irrespective of the decoding algorithm, hence in this study we examine the κ =2/3 case only. Some discussion on other values of κ is available in Report 3.

3. Review of the staggered PRT sequence processing

The estimation of the spectral moments of the weather echo from the staggered PRT sequence is based on a few key ideas. The first idea is to view the non-uniform sample sequence as a product of a uniform sample sequence and a binary code sequence. Thus, the spectrum of the staggered PRT sequence can be viewed as a convolution in the spectral domain. Because of the singular nature of the convolution matrix, the de-convolution cannot be carried out. However, under certain conditions of narrow weather spectra, "magnitude de-convolution" can recover the spectral magnitudes, but not the complex coefficients (Sachidananda and Zrnic 2000). The phases are not required for estimating the spectral moments. Thus, the velocity estimation is identical to that of the pulse pair processing, except that the autocorrelation is not computed using the pairs of pulses but from the power spectrum. One of the major advantages of this procedure is that the standard errors in the velocity estimates are much lower than errors in estimates obtained by the conventional pulse pair processing. This comes about because, in the pulse pair processing of staggered PRT data (Zrnic and Mahapatra 1985), autocorrelations are computed at two different lags, T_1 and T_2, and the phase difference is used for computing the velocity, whereas in the new approach the autocorrelation for lag $(T_2 - T_1)$ is directly computed. Incidentally, this is a spin-off from the approach that we adopted to filter the clutter from the staggered PRT sequence. When the staggered PRT work was undertaken a method for clutter filtering was sought, because that was one of the major hurdles which prevented implementation of the staggered PRT technique in operational radars.

The second idea, central to the filtering of the clutter from the staggered PRT sequence, is a technique to recover the spectral coefficients of the weather signal in the region where the clutter and signal are overlapping in the spectral domain. Any conventional filtering technique cannot distinguish between the signal and the clutter power in a given spectral coefficient, and filtering one would automatically eliminate the other too. In this new procedure, the modulation properties of the code sequence, under the narrow spectra condition, are utilized to retain some fraction of the signal power while filtering the clutter power completely. An estimate of the complex clutter spectral coefficient is first obtained by

projecting the complex spectral code vector (appropriate column vector of the convolution matrix) onto a set of spectral coefficients where clutter is expected (5 coefficients for κ=2/3), and this estimated clutter vector is subtracted from the set of coefficients. Because of the linear independence between the different spectral code vectors, not all the weather signal power is filtered, except when the weather signal velocity also is close to zero (ground clutter is always around zero Doppler), and this residual signal power (and some additional information) is used to restore the signal to its original value. This is possible, because the residual power left in the spectral coefficient after the clutter is filtered is a known fraction of the original signal power. The correction factor can be easily computed provided the location of the original signal component can be determined. This is accomplished by obtaining an approximate velocity estimate with the partial signal power. The procedure fails only when the clutter filter is very wide and the approximate initial velocity estimate is not within $\pm v_d/5$ of the actual value. Without this last step, which is termed the "bias removal procedure", the velocity estimate is slightly biased because of the loss of signal power from the region of the spectrum from where the clutter is filtered. This bias becomes significant for larger clutter filter widths. The upper limit for the number of coefficients from which clutter can be filtered is a little more than half the number of the total spectral coefficients, and is generally sufficient to recover velocity in the presence of clutter as large as 50dB more than the signal power. If the clutter-to-signal ratio (CSR) is lower, a narrower clutter filter would be sufficient, and for sufficiently narrow clutter filter widths (e.g., n_c<7 for a number of T_u intervals N=160, and a number of staggered samples M=64), the bias correction may not even be necessary (for CSR less than about 15 dB). A very brief account of the spectrum reconstruction and the clutter filtering procedure is given below in the next two sub-sections to provide continuity for the reader.

3.1. Reconstruction of the signal spectrum

As indicated earlier in the introduction, unless indicated otherwise the stagger ratio, κ=2/3, is assumed in all our discussions and results in this report. If T_1 and T_2 are the PRTs, we select $T_1=2T_u$, and $T_2=3T_u$. Therefore, a uniform sample sequence can be

constructed for the sampling period T_u; then the corresponding code is 10100... etc., with ones representing the samples available, and the zeros, the missing samples. If the first sample is from the T_2 pulse transmission the code would be 10010... etc. If e_i is the uniform sample sequence and c_i is the code sequence, then the available stagger PRT sample sequence, v_i, can be written as

$$v_i = c_i\, e_i \;; \qquad i=1,2,3,\ldots N\,, \tag{3.1}$$

and in the transform domain this is a convolution represented by

$$\mathrm{DFT}(\, v_i\,) = \{\, \mathrm{DFT}(\, c_i\,) \star \mathrm{DFT}(\, e_i\,)\,\} \tag{3.2}$$

where the $\star$ represents circular convolution, and the DFT( ) represents the discrete Fourier transform of the sequence in brackets. N is the number of samples after inserting zeros for the missing samples. If M is the number of staggered PRT samples, then $N=5M/2$ for $\kappa=2/3$. We use capital letters to denote the spectral coefficients, and the corresponding time domain quantities are denoted by lowercase letters. The bold face letters denote matrices. Subscript index 'i' is used for the time domain quantities, and subscript index 'k' is used for the spectral coefficients. For example, $E_k = \mathrm{DFT}(e_i)$, are the spectral coefficients, and $\mathbf{E}$ is the column matrix of coefficients E_k. Eq. (3.2) can be written in matrix form as

$$\mathbf{V} = \mathbf{C}\,\mathbf{E}. \tag{3.3}$$

$\mathbf{V}$ and $\mathbf{E}$ are (Nx1) column matrices containing the spectral coefficients, V_k and E_k, of the corresponding time sequences, v_i and e_i, and $\mathbf{C}$ is the convolution matrix (size: NxN) whose column vectors are cyclically shifted versions of C_k. Because the convolution matrix is singular, we recover the magnitude spectrum using the magnitude deconvolution defined by

$$abs\{\mathbf{E}\} = [\; abs\{\mathbf{C}\}]^{-1}\; abs\{\mathbf{V}\}, \tag{3.4}$$

where $[\ abs\{\mathbf{C}\}]^{-1}$ is the magnitude deconvolution matrix. This reconstructs the exact magnitude spectrum only under the condition of "narrow" spectra; that is, the non-zero spectral coefficients of the signal e_i are spread at most $N/5$ coefficients, or the total spread is less than $2v_a/5$ for $\kappa=2/3$ (see Report 3 or Sachidananda and Zrnic 2000).

Once the magnitude spectrum is obtained, the spectral domain equivalent of the pulse pair algorithm can be used to estimate the mean power, p, mean velocity, v, and spectrum width, w. If the ground clutter is present, the echo time series is filtered using the procedure described briefly in the next sub-section, and then the magnitude deconvolution is applied.

3.2. Ground clutter filtering

The clutter filter capitalizes on the cyclic property of the convolution matrix and the assumption that the weather signal spectra are "narrow" (as defined earlier). The code spectrum has only 5 non-zero coefficients spaced 1/5th of the total (unambiguous velocity) span, hence, only 5 spectral coefficients will be involved at a time in the convolution process. Specifically, the power in each spectral coefficient is spread over these 5 coefficients, hence the problem of clutter filtering or the spectrum reconstruction can be split into $N/5$ equations with 5 variables each, in place of one equation with N variables. For example the equation

$$\mathbf{V}_r = \mathbf{C}_r\ \mathbf{E}_r, \qquad (3.5)$$

(see Report 3, Eq 3.7 for details) consisting of the rearranged matrices is a representation of $N/5$ equations together in matrix form. To understand the clutter filtering procedure it is sufficient to consider one such equation, say the k^{th} column of the matrices $\mathbf{E}_r$ and $\mathbf{V}_r$, and form a 5x5 matrix equation.

Consider an example with parameters $\kappa=2/3$, $M=64$ for which $N=160$, and let $k=1$. The corresponding equation is

$$\begin{bmatrix} V_1 \\ V_{33} \\ V_{65} \\ V_{97} \\ V_{129} \end{bmatrix} = \begin{bmatrix} C_1 & C_{129} & C_{97} & C_{65} & C_{33} \\ C_{33} & C_1 & C_{129} & C_{97} & C_{65} \\ C_{65} & C_{33} & C_1 & C_{129} & C_{97} \\ C_{97} & C_{65} & C_{33} & C_1 & C_{129} \\ C_{129} & C_{97} & C_{65} & C_{33} & C_1 \end{bmatrix} \begin{bmatrix} E_1 \\ E_{33} \\ E_{65} \\ E_{97} \\ E_{129} \end{bmatrix}. \quad (3.6)$$

The left hand side represents the convolved spectral coefficients (available from the measurement), and the coefficients E_k are for a uniform sequence of the signal plus the clutter. Under the condition of "narrow" weather spectra, only one of its five (E_1 or E_{33} or E_{65} or E_{97} or E_{129}) coefficients is non zero; the clutter can be present in the first coefficient (or in the last coefficient for a different k), because the clutter is at zero Doppler. The amplitude and the position of the signal coefficient that we are trying to recover is not known. Then it can be shown that the column vector, **V**, on the left is E_l times the first column vector of the convolution matrix, $\mathbf{C}_r$, plus the signal spectral coefficient (whichever is non zero) multiplied by the corresponding column vector of $\mathbf{C}_r$. Therefore, if we estimate the complex amplitude of the first column vector of $\mathbf{C}_r$ present in **V** and subtract it, all the clutter is removed. However, because of the non-orthogonality of the columns of $\mathbf{C}_r$, part of the signal power is also removed (signal is completely removed when it is also in the first coefficient, or at the zero Doppler). That is, the projection of the signal vector on to the clutter vector is also removed. The remaining part of the signal has certain relationship to the original signal and hence the original signal can be recovered using the bias removal procedure (see Report 3 for details).

3.3. Studies on the effect of windows

In most of the results presented in Report 3, the von Hann window was used. It is well known that the spectral moment estimates obtained by pulse pair processing have lower standard errors without the window (i.e., uniform weights) than with the window, because of the loss of power due to the window weights. The window becomes necessary to contain the clutter signal from spreading across the spectrum, and also for the spectrum width computation after magnitude deconvolution. This is a non-linear procedure, and it is difficult to compute the effect of window on the standard error in the width estimate theoretically. In the previous study, no effort was made to optimize the performance of the algorithm with respect to the window function. Here we examine this problem in more detail using simulation results to estimate standard errors and biases in the spectral moment estimates. First we evaluate the optimum window to be used when the clutter is absent, and later we examine the case with clutter. The optimum is different for these two cases.

3.3.1. Spectral moment estimation in the absence of ground clutter

The standard errors in the spectral moment estimates depend on several factors such as the wave length, PRTs, number of samples, spectrum width, etc. It is not easy to present all the data on the variation of the *sd(v)* with respect to all these parameters, nor is it necessary. Here, we consider the values relevant to the WSR-88D. In the vcp-11 (see Table.5.1a, Report 3), the complete volume scan takes about 5 minutes to cover the 14 elevations. For each radial, the dwell time is about 51 ms for lowest two elevations, and it is about 40 ms for higher elevations. With the sample overlap scheme (see Report 2, page-71), it is possible to reduce *sd(v)* by taking about 30 per cent overlapping samples. With rectangular window, this will result in an increased azimuthal smoothing of the velocity field (and other parameters), but with the von Han window the smoothing is marginal.

The pulse pair processing gives better estimates without the window (rectangular window is inherent), but, for width estimation, the window is required to avoid biased estimates. There are different estimators available for width estimation, but the one given by equation (6.27) of Doviak and Zrnic (1993) has the lowest standard error, and this estimator

produces a bias for low spectrum widths. This can be removed if window weighting is used. Of course, we have the option of using the window only for width estimation at the expense of more computation. The increase in the *sd(v)* appears to be related to the power loss due to the window. Hence, we examined different weighting functions, specifically the (von Hann)^p weights, and evaluated the performance of the algorithm. The exponents used are p=0, 0.25, 0.5, 1, and 2 (p=0 corresponds to no window or the rectangular window). A large number of simulations were carried out to obtain the standard error and the bias error in the mean power, the mean velocity and spectrum width estimates. These are in Figs. 3.1 to 3.3 for the three parameters; the mean of the simulation data is smoothed (curve fitted) for clarity. The simulation parameters are indicated in the figures. It can be seen that the spectrum width has a significant bias without the window (Fig. 3.1), but for all other windows, the bias is almost zero. We have examined exponents less than 0.25, but the bias could not be removed fully. The lowest exponent that works well is 0.25, which has a power loss factor of 1.93 dB. Power losses inherent to the von Hann window with the exponents, p = 0, 0.25, 0.5, 1, and 2, are 0, 1.93, 2.98, 4.23, and 5.6 dB, respectively. The *sd(v)* plot (Fig.3.2) indicates that the *sd(v)* for the first two cases is almost the same, and in fact, the second curve for exponent 0.25 is better in terms of the bias error for large spectrum widths. The mean power estimate (Fig.3.3) is best without the window (i.e., with rectangular window). Therefore, we conclude that the best method to adopt in the staggered PRT algorithm is, the mean power estimation using the time series samples directly, no window for the velocity estimation, and for width estimation (von Hann)$^{0.25}$ weighted time series. This, of course, increases the computation, because the FFT and magnitude deconvolution have to be carried out twice, with and without the window weights. But, because the degradation in the velocity estimate is marginal with (von Hann)$^{0.25}$ window, we can use it for both velocity and width estimation, thus, avoid one extra FFT and deconvolution operation.

The choice of PRTs determines the unambiguous range r_{al} as well as the number of samples available in a given dwell time. As mentioned earlier, the vcp-11 uses two dwell times, these are approximately 40 ms and 50 ms. Therefore, the performance of the

algorithm is evaluated for these two dwell times, and is presented in the form of contour plots in Figs. 3.4a and 3.5a. (The values are listed in tables 3.1 and 3.2.) The area left of the contour is the region of lower *sd(v)*, and for a given *sd(v)*, the contour can be approximated with a straight line. From these results an empirical relation can be derived which defines the region of velocity recovery within a specified standard error for any selection of PRTs. In fact, if we plot the *sd(v)* as a function of normalized width (normalized with respect to the unambiguous velocity), we find that the curves for different v_a are nearly the same for a given dwell time, as shown in Figs. 3.4b, and 3.5b, for the same set of data given in the contour plots. If we set an upper limit of 1 m s^{-1} for *sd(v)*, maximum normalized spectrum widths for velocity recovery are $w/2v_a$=0.045 and 0.05, for dwell times 40 ms and 50 ms, respectively (from Figs. 3.4b and 3.5b). These four figures provide an idea of the overall performance of the staggered PRT algorithm. It is seen that there is an upper limit for the spectrum width of the signal beyond which the velocity cannot be recovered with sufficient accuracy, and this upper limit is directly proportional to the unambiguous velocity. Hence, we cannot select low unambiguous velocities to increase the unambiguous range.

3.3.2. Ground clutter filtering and the window

The ground clutter is generally a concern at lower elevation scans. At elevations higher than about 5° the ground clutter is not a serious problem. The WSR-88D specifies 50 dB rejection for the ground clutter with a spectrum width of 0.28 m s^{-1} centered on zero Doppler. We use a Gaussian shaped spectrum with this width for the ground clutter in our simulation study, and specify clutter-to-signal ratio (CSR) as a parameter rather than the clutter rejection. We adopt this notation because our ultimate aim is to recover the spectral moments of the weather echo, and to achieve this, it is sufficient to filter enough clutter power to get a decent SNR (i.e., signal to residual clutter) so that the spectral moment estimates are accurate. The amount of filtering required depends on the CSR. Further, the clutter suppression ratio, α, defined as the ratio of the total clutter power to the residual clutter power after filtering, expressed in dB units, is a function of the filter width, hence,

any suppression can be obtained by suitably choosing the filter width. But this does not guarantee recovery of spectral moments of the weather signal, because there is an upper limit for the filter width beyond which the velocity cannot be recovered irrespective of the CSR. There is always an optimum clutter filter width for a given CSR and a clutter spectrum width. If the clutter filter width is allowed to be adjusted in the staggered PRT decoding algorithm based on an a-priori knowledge of the CSR, the performance of the algorithm can be optimized. It is obvious that the residual clutter power is spread throughout the spectrum, hence, can be treated as an effective noise. Thus, the effective SNR_e after filtering the ground clutter is equal to (α - CSR) dB (this assumes that other noise power is very small compared to the residual clutter power). The SNR_e has to be better than 10 dB to recover velocity of the weather echo with a good accuracy.

Other parameters that play important roles in the clutter filtering are the window function and the number of available staggered PRT samples, M, because, the suppression ratio is a strong function of these two parameters. This is illustrated in Figs. 3.6 to 3.8, where the clutter suppression ratio versus the normalized clutter filter width, $\zeta=w_f/w_c$, is shown for three different sample sequence lengths. The data is obtained from a large number of simulations, and their mean values are plotted. The filter widths used are discrete (indicated by the symbols: rectangle, triangle and circles) because the filter is implemented in the spectral domain where only discrete number of coefficients can be deleted (only odd numbers are used for n_c, the filter width in terms of the number of coefficients). With the inherent rectangular window, the clutter echo spreads much more across the extended spectrum, and α has an upper limit of 20 dB even with very large filter width. Therefore, it becomes necessary to apply some window to contain the spread of the clutter power. Instead of trying different window functions available, we chose to try the von Hann window weights raised to some power. As the exponent is increased the main lobe of the spectrum of the window function widens but the side lobe level decreases. Simulations with different exponents for the von Hann weights show that the best performance is for exponents near 1 and 2, hence α for only for these two exponents is plotted in Figs. 3.6 to 3.8. The curves for the ideal Gaussian spectrum and the rectangular window are also

presented for comparison. A common feature in all three figures is that, there is a cross over point between the two curves (von Hann and {von Hann}^{2}) for some filter width. For lower filter widths von Hann window gives better clutter suppression and for larger widths the {von Hann}^{2} window gives better α. Both these curves are very sensitive to the number of samples, M, as seen by comparing the three figures. By doubling M (compare M=32 and 64) α changes by about 10 dB for von Hann window (for large filter widths) and it is as much as 25 dB for the {von Hann}^{2} window. Thus, it can be concluded that for a large CSR (which requires large w_f/w_s), the{von Hann}^{2} window is better, and for a low CSR, (low filter widths) the von Hann window is preferable. The expected amount of clutter suppression in different situations can also be seen from these three figures and therefore the ability of the algorithm to recover the velocity can be inferred. There is an upper limit for the clutter filter width that can be used (for a given M); it is M/4 coefficients for large weather spectrum widths (more than about 4 m s^{-1}). The upper limit for the clutter filter width is less than M/4 coefficients for signals with narrow spectrum widths signals if the mean velocity is close to one of the values 0, $\pm 2v_a/5$, $\pm 4v_a/5$ (m s^{-1}) (for κ = 2/3) at which the clutter and signal spectra (convolved with the code spectrum) overlap. If the two spectra do not overlap, the upper limit for the clutter filter width can still be M/4 even for w < 4 m s^{-1}. Beyond this limit the bias removal part fails, because the error in the initial estimate of the velocity exceeds the maximum allowable ($v_a/5$ for κ=2/3).

For a typical WSR-88D dwell time of approximately 40 ms, the number of staggered PRT samples is about 32, if v_a is chosen to be $\pm$50 m s^{-1} (T_u = 0.5 ms). For this M it is best to use von Hann window up to ζ = 22, and achieve a clutter suppression of 40 dB, but the filter width is almost close to the maximum allowable for this ζ. However, if a 25 per cent larger number of samples can be utilized (M=40, using the sample overlap scheme, see Report 2, page 71) without slowing down the scan rate, we can achieve an additional 5 dB suppression with the von Hann window. For the lowest two elevations where the dwell time is about 51 ms, we get 51 samples per radial with 25 per cent sample overlap. It is also possible to use a larger overlap and {von Hann}^{2} window without much degradation in the estimates. The {von Hann}^{2} window has a much larger edge taper resulting in a lower

effective smearing (for the same overlap) of the estimates in azimuth (effective number of overlapped samples is much smaller because of the weights). For M=64 or more, a {von Hann}^{2} window is a better choice, as can be seen from Fig.3.8. It can also be observed from the figures that a larger number of samples allows a better suppression of the ground clutter for the same normalized clutter filter width.

Some sample velocity plots are shown in Figs.3.9 to 3.11. The estimated velocity is shown against the velocity input to the simulation program. 20 simulations are carried out at each of the velocities spanning the entire $\pm v_a$, at intervals of 1 m s^{-1}. The dots show the simulation points, and the continuous curve is the mean. The parameters used in the simulation are indicated in the figures. The first figure, Fig.3.9, is with M=32 and CSR=35 dB, which is almost the maximum limit for the recovery of the velocity. The clutter filtering algorithm starts failing first at the locations where the clutter and the signal overlap, i.e., at v_{in}=±20 and ±40 m s^{-1} as can be seen in Fig. 3.9. At these points the initial velocity estimate has an error greater than v_a/5, and hence the bias removal algorithm fails. The drop off at the extreme ends, ±50 m s^{-1}, is because of the aliasing. This kind of failure mode does not produce progressively increasing standard error. Thus we cannot put an upper limit to the standard error of the estimated velocity to define a cut off point. The standard error suddenly jumps because of the non-resolution of the ambiguity in the velocity estimate. Therefore, it is thought appropriate to exclude outliers in computing the standard error shown in the figure; a limit of velocity recovery is determined by putting a threshold of 10 per cent on the outliers. This is termed as *loss* expressed in percentage. In computing this *loss*, simulations are run with input velocities uniformly distributed over the entire unambiguous interval, $\pm v_a$, and the number of times the recovered velocity falls outside the interval $v_{in}\pm v_a/5$ is counted and expressed as a percentage of the total number of simulations. Generally these outliers fall predominantly in the spectrum overlap regions. (The outliers near the Nyquist velocity are not as detrimental because these can be corrected, nonetheless they are included in the *loss*.) In other regions the velocity is recoverable. The loss parameter is a function of the CSR, number of samples, clutter filter width etc. The CSR=35 dB in Fig. 3.9 is almost at the limit of velocity recovery with a *loss*=7.97% for the von

Hann window. An optimum clutter filter width of n_c=9 coefficients is used.

For the same set of simulation parameters, if {von Hann}^{2} window is used, we have a better velocity recovery performance (Fig. 3.10). The *loss* is reduced to 2.43%. The optimum clutter filter width is 7 coefficients for this window, which corresponds to $\zeta=w_f/w_c$=31.25. It is obvious from Fig. 3.6 that for this filter width {von Hann}^{2} window is better, and the results of simulation confirm this fact. Fig. 3.11 shows the effect of increasing the number of samples to 64. The velocity is recovered fully (*loss* is only 0.15%, mainly due to aliasing) even for a CSR=50 dB, with a much narrower filter width $\zeta=w_f/w_c$=24.6 (n_c=11 coefficients).

The performance of the clutter filtering algorithm is evaluated using a large number of simulations, and the results are tabulated in four tables, 3.3a to 3.3d, where optimum filter widths are used. The simulations are run with increasing clutter filter width, n_c, and the best is selected as the optimum value. For lower values of filter width, the estimated velocity gets biased towards the zero Doppler, as the clutter suppression is not enough to give a reasonable SNR_e after filtering. At larger than the optimum filter widths, the *loss* increases. The optimum is selected manually based on the results, and only these optimum results are shown in the tables. The last column is the *loss* parameter. If we use a limit of 10% for the *loss*, it is easy to determine the upper limit of CSR for a given spectrum width of the signal. Comparing the tables 3.3a and 3.3b for M=32 with von Hann and {von Hann}^{2} windows, respectively, it is clear that the second window performs better. For the CSR values used, the optimum filter widths are fairly wide. Only for n_c=5 or less, the first window is better, i.e., for low CSR values. For M=64 (tables 3.3c and 3.3d), similar conclusions can be drawn, except that the algorithm is able to recover velocities for much higher CSR.

The results in the four tables referred to above are presented in the graphical form to facilitate the selection of optimum filter width for a given situation. Figs. 3.12 to 3.15, show the optimum filter width as a function of CSR, with spectrum width as a parameter (i.e., plot of column 3 versus column 2 of the tables). The next four, Figs. 3.16 to 3.19, are plots of *loss* versus the CSR. The *loss* increases sharply with increasing CSR for the von Hann

window, but for the {von Hann}^{2} window, the increase is much slower. This behavior is seen for both values of M, 32 and 64.

The standard error in the velocity estimate (excluding the outliers) as a function of CSR is given in Figs. 3.20 to 3.23. In the case of the von Hann window, the *sd(v)* increases with increasing CSR because of inadequate filtering of the ground clutter. The side lobes of the ground clutter spectrum give rise to a poorer SNR after filtering. With the {von Hann}^{2} window, the side lobe power is reduced considerably, hence a better SNR is achieved after filtering, which is the reason for *sd(v)* remaining nearly constant with increasing CSR.

3.3.3. Conclusions

An exhaustive simulation of spectral parameter estimation, without and with different window functions, was carried out. In the absence of ground clutter some important observations are the following. The best mean power estimates are obtained with the staggered PRT samples directly. The mean power estimates obtained from the reconstructed spectrum (after the magnitude deconvolution procedure) have biases as well as a larger standard error. The larger is the power loss due to the window, the larger is the error. The velocity estimate is the best without the window, and the increase in the standard error with window depends on the loss of power associated with the window. Only for the spectrum width estimation the window produces improvements, especially in the bias error. The width estimator given by the equation (6.27) of Doviak and Zrnic (1993), which has the lowest standard error, along with the {von Hann}$^{1/4}$ window is the best combination. While the increase in the *sd(w)* is related to the loss of power due to the window, the bias error is a function of the spreading of the spectrum. The {von Hann}$^{1/4}$ window also keeps the degradation of the velocity estimate to a small value, thus, we can use the same window for both velocity and width estimation, which reduces the computation.

In the presence of the clutter, applying the window becomes necessary to contain the spreading of the clutter power, which prevents effective clutter filtering. There is an optimum clutter filter width for a given CSR and signal spectrum width. This optimum filter width is different for different window functions. For large CSR requiring wider clutter

filter, the {von Hann}^{2} window is found to perform better than the von Hann window. For normalized clutter filter widths of less than about 20, the von Hann window performs better.

4. Unambiguous range extension by overlaid signal separation

In the staggered PRT sampling "one-overlay" situation occurs if weather echoes extend to a maximum range, r_{a2}, corresponding to the delay time T_2. Fig. 4.1 shows a part of the PPI radar display for some typical parameters. For example, in the figure the first trip echo from a cell at 50 km and the second trip echo from a cell at 200 km, along a radial arrive at the same time at the radar. In general, the sample at delay time τ and $(T_1+ \tau)$ will overlap after T_2 pulse transmission. After the T_1 pulse transmission there is a clear range of r_{a1} without any overlay. We divide r_{a2} into three regions corresponding to the delay time $\tau \le T_u$, $T_u \le \tau \le 2T_u$, and $2T_u \le \tau \le 3T_u$. Signals from range gates corresponding to region-1 and region-3, require special processing whereas the ones coming from region-2 do not. There can also be ground clutter mainly in the region-1. The ground clutter region is usually insignificant for elevations higher than about 5°.

Note that echoes region-3 for T_1 pulse transmission overlap with echoes from the region-1 for the T_2 pulse transmission. Hence, only half the number of overlaid echo samples are available for these gates. However, if T_u is made an integer multiple of delay time $\delta\tau$, corresponding to the gate spacing (and also τ is made an integer multiple of $\delta\tau$) , for every gate at τ in the region-3 there would be a corresponding gate at $(\tau\text{-}2T_u)$ in the region-1. Therefore, we can get two samples for gates in the region-3 also, but one half of these samples contain overlaid echoes. The other half of the samples do not have overlay. For close-in ranges in the region-1 there can be ground clutter, which also will affect the overlaid signals from region-3.

The separation of these overlaid echoes and clutter filtering appeared to be tractable, and motivated us to examine this situation in more detail. In practice, several different combinations of the clutter, signal, and overlay can occur, and the computations have to be appropriately channeled in the staggered PRT algorithm. The algorithm for the no-overly situation with or without clutter has been treated earlier in section-3 (and in Report 3). In

this section, first we examine the one-overlay problem and develop a method for estimating the spectral moments of both the range gates involved. Later, we also address the situation where the ground clutter is present.

4.1. One-overlay resolution

Figure 4.2 shows the staggered PRT sampling scheme for one-overlay situation. As mentioned in section 4.0, the sample spacing, $\delta\tau$, (gate spacing) is chosen such that T_u, and τ are integral multiples of $\delta\tau$, so that there are $M/2$ common samples for region-1 and region-3. These common samples can contain overlaid echoes whereas the other half of the samples can not. T_u is the basic PRT from which T_1 and T_2 are derived; $T_1 = 2T_u$, $T_2 = 3T_u$, for the stagger ratio, $\kappa = 2/3$, which is used for all results in this section. The transmission sequence starts with T_2 pulse separation (i.e.,T_2 T_1 T_2 T_1 ...); the reason for this choice will be clear later when we discuss the processing algorithm. The sample sequence with a delay time τ (sampled by range gate (a)) is denoted by [v_1, v_2, v_3, v_4, ...etc.], and the samples at delay time ($T_1+\tau$, i.e., rage gate (b)) are represented by [v_1', v_3', v_5', v_7', ...etc.] Note that this set has only odd numbered samples available and these are within the T_2 pulse separation. The first sequence corresponds to the staggered PRT samples of range gate (a) and its odd numbered samples contain overlaid echo corresponding to range gate (b). Similarly, we can form the staggered PRT sequence for the range gate (b) by replacing the even numbered samples in the first set with the second set of samples, i.e., v_1, v_1', v_3, v_3', v_5, v_5', ...etc. The odd numbered and un-primed samples are the common samples and have contribution from ranges corresponding to both gates (a) and (b).

Now, to convert these non-uniform sequences into uniform sequences, we insert zeros in place of missing samples. The code sequence for the gate (a) sequence is [10010...] and for the gate(b) the sequence is [10100...], (Fig. 4.2b). Let us use the notation p_1, v_1, w_1, for the spectral moments signals sampled by gate (a) and p_2, v_2, and w_2, for the spectral moments of signals sampled by gate (b). To explain the one-overlay resolution algorithm, let us assume that p_2 is larger than p_1, and that we estimate the weaker signal velocity, v_1. If it can be recovered, then the stronger signal velocity can also be recovered, hence, we

concentrate on the weaker signal velocity. The same procedure applies with the sequences interchanged, if the gate (a) signal is stronger.

In order to understand the procedure, first let us examine the spectrum of the code sequences, [10000...], [00010...], which are the two components of the staggered PRT code [10010...], and the corresponding rearranged convolution matrices, $\mathbf{C}_{1r}$, $\mathbf{C}_{2r}$ such that $\mathbf{C}_{1r}+\mathbf{C}_{2r}= \mathbf{C}_{r}$. (see Report 3 for the definition and construction of the rearranged matrix). They are given by

$$abs\{\mathbf{C}_r\} = \begin{bmatrix} 1.0 & 0.309 & 0.809 & 0.809 & 0.309 \\ 0.309 & 1.0 & 0.309 & 0.809 & 0.809 \\ 0.809 & 0.309 & 1.0 & 0.309 & 0.809 \\ 0.809 & 0.809 & 0.309 & 1.0 & 0.309 \\ 0.309 & 0.809 & 0.809 & 0.309 & 1.0 \end{bmatrix} \tag{4.1}$$

$$phase\{\mathbf{C}_r\} = \begin{bmatrix} 0° & -72° & 36° & -36° & 72° \\ 72° & 0° & -72° & 36° & -36° \\ -36° & 72° & 0° & -72° & 36° \\ 36° & -36° & 72° & 0° & -72° \\ -72° & 36° & -36° & 72° & 0° \end{bmatrix} \tag{4.2}$$

$$abs\{\mathbf{C}_{1r}\} = abs\{\mathbf{C}_{2r}\} = \begin{bmatrix} 0.5 & 0.5 & 0.5 & 0.5 & 0.5 \\ 0.5 & 0.5 & 0.5 & 0.5 & 0.5 \\ 0.5 & 0.5 & 0.5 & 0.5 & 0.5 \\ 0.5 & 0.5 & 0.5 & 0.5 & 0.5 \\ 0.5 & 0.5 & 0.5 & 0.5 & 0.5 \end{bmatrix} \tag{4.3}$$

$$phase\{\mathbf{C}_{1r}\} = \begin{bmatrix} 0° & 0° & 0° & 0° & 0° \\ 0° & 0° & 0° & 0° & 0° \\ 0° & 0° & 0° & 0° & 0° \\ 0° & 0° & 0° & 0° & 0° \\ 0° & 0° & 0° & 0° & 0° \end{bmatrix} \tag{4.4}$$

$$phase\{\mathbf{C}_{2r}\} = \begin{bmatrix} 0° & -144° & 72° & -72° & 144° \\ 144° & 0° & -144° & 72° & -72° \\ -72° & 144° & 0° & -144° & 72° \\ 72° & -72° & 144° & 0° & -144° \\ -144° & 72° & -72° & 144° & 0° \end{bmatrix} \tag{4.5}$$

The coefficients of $\mathbf{C}_r$ are normalized so that the highest coefficient is unity. This is done to reveal the relative amplitudes of the coefficients. *In the actual algorithm, the normalization is with respect to the power* such that the sum of the magnitude square of each column elements (or row) equals one. It is particularly important to note that $\mathbf{C}_{1r}$ has all the elements same, and the elements of $\mathbf{C}_{2r}$ differ only in phase; all the magnitudes are same. Further, the mean value of each column of $\mathbf{C}_{2r}$ is identically zero, thus, the mean value of each column of $\mathbf{C}_r$ and $\mathbf{C}_{1r}$ is the same, equal to 0.5, or half the maximum coefficient. These observations are important for understanding the overlay resolution algorithm.

We start with the assumption that the signal spectrum is "narrow", i.e.,the spread of the non-zero spectral coefficients of the signal is limited to $2v_d/5$. Note that this assumption about the overlaid signal is not necessary for the overlay resolution algorithm to work. It is an assumption needed for the magnitude deconvolution procedure to reconstruct the spectrum. The gate (b) overlay signal is removed from gate (a) irrespective of its spectrum width, but the assumption is necessary because we need to recover the velocities corresponding to both gates, and the magnitude deconvolution is also applied to the gate (b)

signal (to recover its spectral moments). We will demonstrate later that the spectrum width of the overlay signal also plays an important role in the recovery of the velocity in the gate (a), because the decorrelation of the samples with time is a function of the spectrum width. Now, if we take the DFT of the full time series of the signal (samples at intervals T_u - no missing samples and no overlay) and rearrange the coefficients into a (5xM/2) size matrix, then each column will have only one non-zero coefficient. A convolution of this spectrum with any one of the code matrices ($\mathbf{C}_r$, $\mathbf{C}_{1r}$, or $\mathbf{C}_{2r}$) will spread the power only among the coefficients of the same column. Therefore, we can treat each column independently, and to understand the decoding scheme, it is sufficient to consider one such matrix equation, as we have done in the case of clutter filtering (see Eq. 3.6).

Let all the spectra be represented as a row-wise rearranged matrices of (5xM/2) size for our discussion; i.e., take the DFT of the time series sequence and rearrange the spectral coefficients row-wise to form the matrix of complex coefficients. The rearranged matrices are designated by the subscript 'r'. Denote the spectrum of non overlaid signal from gate(a) (samples at T_u interval) with $\mathbf{S}_{1r}$ and the corresponding spectrum of the overlaid signal from gate (b) with $\mathbf{S}_{2r}$. In terms of these two spectra, the staggered PRT signal from gate (a), with gate (b) overlay in one-half number of samples, can be represented as a sum of convolutions of these two spectra with the corresponding convolution matrices. The spectrum, $\mathbf{E}_{1r}$, of the time series, e_{s1} = [v_1, 0, 0, v_2, 0, ...] , which has gate(a) signal plus the gate(b) overlay in odd numbered samples is written as

$$\mathbf{E}_{1r} = \mathbf{C}_r \mathbf{S}_{1r} + \mathbf{C}_{1r} \mathbf{S}_{2r}. \qquad (4.6)$$

This is a set of M/2 equations, one for each column of the matrix, $\mathbf{E}_{1r}$. Let us examine one such equation. Let $\mathbf{e}_k$ = [E_1, E_2, E_3, E_4, E_5]^t be one such column (say k^{th} column) of $\mathbf{E}_{1r}$. And, let $\mathbf{a}_k$ = [0, 0, a_1, 0, 0]^t be k^{th} column of $\mathbf{S}_{1r}$, and $\mathbf{b}_k$ = [0, 0, 0, b_2, 0]^t be the k^{th} column of $\mathbf{S}_{2r}$, and in both, only one element is non-zero, by virtue of the "narrow" spectrum assumption. (The selection of a particular element as non-zero element is arbitrary in this example.) The matrix equation is

$$\begin{aligned} \mathbf{e}_k &= \mathbf{C}_r\, \mathbf{a}_k + \mathbf{C}_{1r}\, \mathbf{b}_k \\ &= [\mathbf{C}_{1r} + \mathbf{C}_{2r}]\, \mathbf{a}_k + \mathbf{C}_{1r}\, \mathbf{b}_k \\ &= \mathbf{C}_{1r}\, [\mathbf{a}_k + \mathbf{b}_k] + \mathbf{C}_{2r}\, \mathbf{a}_k \end{aligned} \qquad (4.7)$$

Now because, $\mathbf{C}_{1r}$ is a matrix with all elements same, the contribution of the overlay in all the elements of the column on the left hand side is a constant (complex), and also the contribution of the odd numbered samples of gate (a) signal is a constant. Therefore, if we subtract the mean value of the column from each element we effectively delete all the contribution of the gate (b). This is the reason for selecting the time series beginning with T_2 pulse. If not, the second convolution matrix (in the first row of equation 4.7) would be $\mathbf{C}_{2r}$ corresponding to the code [00100,...], which does not produce a constant contribution. This looks very simple, but the recovery of the signal mean velocity is not as simple, because, we need the ($\mathbf{C}_{1r}\mathbf{a}_k$) part (all elements of the column are the same) of the gate (a) signal.

Interestingly, from the properties of the convolution matrices involved, it can be inferred that the constant ($\mathbf{C}_{1r}\mathbf{a}_k$) is equal (in amplitude and phase) to one of the coefficients of the column ($\mathbf{C}_{2r}\mathbf{a}_k$), which is the original signal component (i.e., the 3rd element, a_1, in $a_k=[0,0,a_1,0,0]^t$, that we started with in the example). Therefore, the whole problem is reduced to determining which is the position of the original signal component in ($\mathbf{C}_{2r}\mathbf{a}_k$). Essentially, the problem is that we have one half of the samples with no overlay ($\mathbf{C}_{2r}\mathbf{a}_k$), and the spectrum of this set (with inserted zeros) consists of five replicas of the original spectrum with the relative phase shifts of the replicated spectra equal to the phase shifts of the code spectrum. By appropriate choice of sequence starting from T_2 pulse transmission, we make the contribution of the other half ($\mathbf{C}_{1r}\mathbf{a}_k$, which is overlaid) to be an identical spectrum (5 replicas) but with no relative phase shifts between the five components. Of the 5 replicas in the first set, only one has the same phase as the second set, and we need to identify it to resolve the ambiguity in the velocity.

To determine the position of the original signal component in the columns of ($\mathbf{C}_{2r}\mathbf{a}_k$),

we go through a series of steps. Each element of the column $\mathbf{C}_{1r}[\mathbf{a}_k + \mathbf{b}_k]$ has two parts, the gate(a) signal and the gate(b) overlay, and it is not possible to split it into two parts without additional information. This information is derived from the other set of $M/2$ samples, which contain only the overlaying signal. Take the set of samples, e_2 = [0, 0, v_1', 0, 0, 0, 0, v_3', 0, 0, ...etc.] and compute the DFT to get the rearranged matrix, $\mathbf{E}_{2r}$. The magnitude of the elements of the k^{th} column of this matrix (all magnitudes are the same) gives us an estimate of the magnitude of the overlay component in $\mathbf{C}_{1r}[\mathbf{a}_k + \mathbf{b}_k]$. If we compute $\{\mathbf{C}_{1r}[\mathbf{a}_k + \mathbf{b}_k] - \mathbf{C}_{2r}\mathbf{a}_k\}$, one of the elements of this column vector would have the same magnitude as the elements of the k^{th} column of $\mathbf{E}_{2r}$. Therefore, the column matrix, $\mathbf{g}$, given by the operation

$$\mathbf{g} = abs\ [\ |\ \mathbf{C}_{1r}[\mathbf{a}_k + \mathbf{b}_k] - \mathbf{C}_{2r}\mathbf{a}_k\ |\ -\ |\ \mathbf{E}_{2r}(k)\ |\ ] \qquad (4.8)$$

will have five values which are the differences between the five possible vectors and estimate of $\mathbf{E}_{2r}(k)$. The position of the element with the smallest magnitude is the most likely candidate for the correct position of the original signal component in $(\mathbf{C}_{2r}\mathbf{a}_k)$. This procedure is applied to all the columns to obtain an index array, $\mathbf{n}_k$, of $M/2$ elements (row matrix) containing the most likely row index of the original signal component in each column of $(\mathbf{C}_{2r}\mathbf{S}_{1r})$. Once the position of the element is known, we can reconstruct the gate(a) signal without the overlay by adding that component to the already available other half of the spectrum.

The magnitude deconvolution procedure to be performed after this step, to reconstruct the original magnitude spectrum, is explained briefly in section-3 (for more detailed explanation see Report 3, magnitude deconvolution). The above procedure essentially gives the most probable position of the correct element, but it can fail due to several reasons. The most important one is the correlation between the estimate of the overlaid signal component and the actual overlaid signal component. This correlation is a function of the spectrum width of the overlay signal; larger is the width, the lower is the correlation coefficient. The other parameter which limits the velocity recovery, is the overlay

power ratio, p_2/p_1. The criterion for success is that the uncertainty in the estimated magnitude of $\mathbf{C}_{1r}\mathbf{b}_k$ must be less than the magnitude of the spectral coefficients of $\mathbf{C}_{2r}\mathbf{a}_k$. This is roughly related to the overlay power ratio, but not necessarily for all the columns of the $\mathbf{E}_{1r}$. The p_2/p_1 ratio is the overall power ratio for the whole spectrum, but the overlay power ratio for each column can be completely different. The overlay power ratio for each column cannot be easily computed because we do not know the exact overlay power in each spectral coefficient.

Note that the spectral coefficients, $\mathbf{E}_{2r}$, are not obtained from the same set of samples as that present in the overlaid samples, but from a sample set which is delayed by T_1. The correlation between the overlaid samples and this set, is crucial for overlay resolution, i.e., the accuracy of our estimate of overlay component from the non-overlaid sample set for the same range gate, depends on the autocorrelation at lag T_1, and the spectrum width is a measure of the autocorrelation. Thus, if the overlaid signal has a narrow spectrum, the recovery is very good. This is an important point to note for the case of overlay resolution in the presence of the ground clutter. Further discussion of this topic is in Section 4.3.

Next we define a differential power ratio, R_p to indicate conditions for which velocity can be resolved, although we cannot quantify overlay resolution from R_p. By definition

$$R_p = 10\log\left(p_{tot}/\left|\sum_i |S_1(i)|-|S_2(i)|\right|^2\right),$$

where p_{tot} is the total power in the sequence $[v_1,0,v_2,0,0,v_3,0,v_4,0,0...]$, $S_1(i)$ is the complex spectrum coefficient of the sequence $[v_1,0,0,0,0,v_3,0,0,0,0,....]$, and $S_2(i)$ is the spectrum coefficient of the sequence $[0,0,v_2,0,0,0,0,v_4,..]$. In Fig. 4.3 is a plot of R_p as a function of spectrum width of overlay signal for different M and delay times T_1 and T_2, generated using simulated time series. We encounter both delays, T_1 and T_2, depending on whether the gate(b) signal is the overlay, or the gate(a) signal. It is seen that for larger number of samples, R_p is higher for narrow spectra, but for $w > 4$ m s^{-1} the difference is marginal.

Simulation study has shown that for $w < 3$ m s^{-1} the overlay resolution is very good, but beyond this width the failure rate becomes larger (quantitative results are given later in section 4.4). The proposed overlay resolution algorithm uses some of the known properties

of the spectrum to further improve the velocity recovery, without which it is difficult to recover velocity for overlay ratio more than about 5 to 10 dB.

For a typical Gaussian "narrow" spectrum we can determine the shape of the power spectrum in the $1/5^{th}$ spectrum interval, from one half of the samples without the overlay. From this shape we estimate the position of the minimum of the spectral power envelope function. Now, we know that the position of the spectrum is from one minimum to the next one, exactly $N/5$ (or $M/2$) coefficients, and there are five such segments in the entire spectrum. One of these segments is the correct signal. The DFT coefficients are cyclic, hence if the index exceeds N in the last segment it is to be joined with the beginning of the spectrum. Similarly, the rearranged matrix has five rows of $N/5$ coefficients, with row indices 1 to 5. Therefore, for any segment the row index can have at best two indices, and these two indices will be different by one. Further, the change over from one index to the next occurs at the minimum of the spectral power envelope function. Hence the correct index array, $\mathbf{n}_k$, can have only two segments, with index values differing by one in the descending order (cyclic over 5 to 1). With this known property, we can correct many of the missed indices in $\mathbf{n}_k$.

First, we determine the position of the minimum of the spectrum envelope. To do this, we smooth the envelope of the first $1/5^{th}$ of the spectrum ($M/2$ coefficients of $\mathbf{C}_{2r}\mathbf{S}_{1r}$, or the first row) into 6 to 8 segments and average the powers in these sets. Find the set that has lowest power, and position the minimum at the center of this segment. This, of course, is an approximate position, but is not critical because it is at the power minimum. Once the position of the minimum is obtained, we can cut index array, $\mathbf{n}_k$, into two pieces, and select the piece which has larger number of elements in it. Now, determine the index that has appeared maximum number of times in this segment of $\mathbf{n}_k$, and assign this index to all the elements of the segment as the most likely candidate. The index value for the other segment of $\mathbf{n}_k$ is determined as one less or one more, depending on whether it is on the right or on the left of the previous segment. The indices are in the descending order, and cyclic between 5 and 1. This modified index array, $\mathbf{n}_k$, when used in the reconstruction of the gate(a) signal spectrum, gives much better velocity recovery of the weaker signal velocity.

4.2. The one-overlay resolution algorithm

The steps involved in estimating the spectral moments from the staggered PRT time series with one-overlay, are listed below. In this algorithm, it is assumed that the gate(a) is in the region-1 and gate(b) is in the region-3. Explanations are given in curly brackets, {}. Lower case letters denote time domain quantities, and the upper case denotes spectral domain quantities. Bold fonts, both upper and lower case, are used for matrices in spectral domain.

1. Input the staggered PRT sample sequence, $[v_1, v_1', v_2, v_3, v_3', v_4, v_5, v_5',....]$.
{The sequence starts with T_2 pulse transmission; the number of transmitted pulses is M, and the total number of samples in the sequence is $3M/2$. Note that there are two samples (odd numbered samples) taken at delay times τ and $T_1+\tau$, after T_2 pulse transmission, and one sample (even numbered sample) after T_1 pulse transmission.}

2. Form four uniformly spaced sample sequences of length $N=5M/2$ by inserting zeros as follows:

$e_{s1} = [v_1, 0, 0, v_2, 0, v_3, 0, 0, v_4, ...]$; gate(a) signal + gate(b) signal overlay in v_1,v_3, etc.,

$e_{s2} = [v_1, 0, v_1', 0, 0, v_3, 0, v_3', 0, 0, ...]$; gate(b) signal + gate(a) signal overlay in v_1, v_3, etc.,

$e_1 = [0, 0, 0, v_2, 0, 0, 0, 0, v_4, 0, ...]$; gate(a) signal only,

$e_2 = [0, 0, v_1', 0, 0, 0, 0, v_3', 0, 0, ...]$; gate(b) signal only.

3. Compute the mean power estimates, p_1 , and p_2, from the sequences e_1 and e_2.

$$p_1 = \frac{4}{M}\sum_{i=2,4,...}^{M}|v_i|^2, \quad \text{and} \quad p_2 = \frac{4}{M}\sum_{i=1,3,5...}^{M}|v_i'|^2.$$

{Use the ratio, p_2/p_1, to decide the path of computation. If $|p_2/p_1|< 8$ dB, overlay separation procedure is applied in computing both gate(a) and gate(b) parameters. For $|p_2/p_1|> 8$ dB,

the overlay separation is applied only for recovering the weaker signal parameters, and the stronger signal parameters are estimated without removing the overlay. The steps below (#4 to # 15) are for recovering the weaker signal velocity.}

4. Compute the DFT of sequence e_{s1} and e_2, after multiplying by von Hann window weights, h_n.

$$E_1 = \mathrm{DFT}(e_{s1}\, h_n),$$

$$E_2 = \mathrm{DFT}(e_2\, h_n).$$

{The weaker signal velocity recovery is found to be the best with von Hann window.}

5. Rearrange the coefficients of E_1 and E_2 into 5xM/2 matrices.

$$E_1 \Rightarrow \mathbf{E_{1r}}, \text{ and } E_2 \Rightarrow \mathbf{E_{2r}}.$$

{Rearranged matrix is explained in Report 3, and κ=2/3 is assumed.}

6. Compute mean value of each column of $\mathbf{E_{1r}}$ and form a matrix $\mathbf{E_m}$ of the same size as $\mathbf{E_{1r}}$ with elements of each column as the mean value of that column.

$$\mathbf{E_m} = \begin{bmatrix} \overline{E_m(1)} & \overline{E_m(2)} & \cdots & \overline{E_m(\frac{M}{2})} \\ \overline{E_m(1)} & \overline{E_m(2)} & \cdots & \cdot \\ \overline{E_m(1)} & \overline{E_m(2)} & \cdots & \cdot \\ \overline{E_m(1)} & \overline{E_m(2)} & \cdots & \cdot \\ \overline{E_m(1)} & \overline{E_m(2)} & \cdots & \overline{E_m(\frac{M}{2})} \end{bmatrix}$$

where

$$\overline{E_m(k)} = \frac{1}{5}\sum_{i=1.}^{5} E_{1r}(i,k)\ ; \qquad k = 1,2,3,\ldots,\tfrac{M}{2}.$$

7. Compute the following matrices, **G** and **H**.

$$\mathbf{G} = abs\ [\ |\ 2\ \mathbf{E}_m - \mathbf{E}_{1r}\ |\ -\ |\ \mathbf{E}_{2r}\ |\ ],$$

and $$\mathbf{H} = [\mathbf{E}_{1r} - \mathbf{E}_m].$$

8. Find the row index of the smallest element in each column of **G**, to form an integer row vector $\mathbf{n}_k$, of $M/2$ elements. Note that $\mathbf{n}_k$ element values are any one of the row indices, 1 to 5.

9. Compute the row vector, $\mathbf{h}_1$, of the spectral power coefficients from the first row of $\mathbf{H} = [\mathbf{E}_{1r} - \mathbf{E}_m]$,

$$\mathbf{h}_1 = |\ 1^{st}\ \text{row of}\ [\mathbf{E}_{1r} - \mathbf{E}_m]\ |^2.$$

{All rows give the same result, because the coefficients have same magnitudes for all rows.}

10. Divide the row vector, $\mathbf{h}_1$, into 6 to 10 equal length segments depending on the number of elements ($M/2$ must be divisible by the number of segments to get equal length segments), and determine the segment which has the lowest power. Determine the index of the coefficient at the middle of this segment. Let k be this index. Note that $\mathbf{h}_1$ and $\mathbf{n}_k$ have the same length, $M/2$.

{The number of segments can be selected conveniently based on the number of samples. The indicated value, between 6 to 10, is not very critical. For M=64, 8 is found to be a good choice.}

11. Divide $\mathbf{n}_k$ into two segments, the first segment - elements 1 to k, and the second segment - elements k+1 to $M/2$. Two cases to be considered are $k > M/4$, and $k < M/4$.

If $k > M/4$, then, find the index, x, that appears maximum number of times in the first segment of $\mathbf{n}_k$, and replace all the elements of the first segment of $\mathbf{n}_k$ with x. The elements of the second segment of $\mathbf{n}_k$ is replaced by (x-1). If (x-1) is zero, the value is set to 5 (indices are cyclic, 1 to 5).

If $k < M/4$, then find the index, x, that appears maximum number of times in the second segment of $\mathbf{n}_k$, and replace all the elements of the second segment of $\mathbf{n}_k$ with x. The

elements of the first segment of $\mathbf{n}_k$ is replaced by (x+1). If (x+1) is 6, the value is set to 1.

12. Now, select the $\{\mathbf{n}_k(k)\}^{th}$ element of k^{th} column of **H**, k=1,2, ...M/2, to form a row vector of M/2 elements, and repeat these rows five times to form the complete 5xM/2 size correction matrix, $\mathbf{E}_{1c}$. The recovered spectrum of the weaker signal, $\mathbf{E}_t$, is obtained by adding the correction matrix to **H**.

$$\mathbf{E}_t = [\mathbf{H} + \mathbf{E}_{1c}] = [\mathbf{E}_{1r} - \mathbf{E}_m + \mathbf{E}_{1c}] \ .$$

{Note that the matrix **H** corresponds to the spectral components of sequence e_1, and $\mathbf{E}_{1c}$ is the recovered spectrum of the sequence [v_1, 0, 0, 0, 0, v_2, 0, 0, 0, 0, ..etc.] with the gate(b) overlay part removed from these samples. The spectrum **H** is computed the way it is indicated in step# 7, to reduce computation - one DFT operation less.}

13. Apply the magnitude deconvolution to the matrix, $\mathbf{E}_t$, to reconstruct the complete spectrum of the weaker signal, $\mathbf{S}_{1r}$, (see Report 3 for magnitude deconvolution.)

$$abs\{\mathbf{S}_{1r}\} = [abs\{\mathbf{C}_r\}]^{-1} \ abs\{\mathbf{E}_t\},$$

and rearrange $abs\{\mathbf{S}_{1r}\}$ into a column matrix $\mathbf{S}_1$.

14. Compute the autocorrelation $R(T_u)$, (Eq. 3.6 of Report 3) using the elements of $\mathbf{S}_1$ and the mean velocity from the phase of $R(T_u)$.

$$R(T_u) = \frac{1}{N}\sum_{k=0}^{N-1} |S_1(k)|^2 \, e^{j2\pi k/N},$$

$$v_1 = (v_a/\pi)\ arg\{R(T_u)\}; \qquad v_a = \lambda/(4T_u).$$

15. The spectrum width is computed using the equation (6.27) of Doviak and Zrnic, (1993).

$$w_1 = (\lambda / 2\pi T\sqrt{2})\,|\ln(p/|R(T_u)|)|^{1/2}\,\mathrm{sgn}(\ln(p/|R(T_u)|)).$$

{Here, the mean power, p, is computed from the reconstructed spectrum, it is not the estimate obtained earlier in step #3.}

16. For gate(b) mean velocity, v_2, and spectrum width, w_2, the following steps are used:

(i) If $|p_2/p_1| < 8$ dB, follow the procedure in steps #4 through #15, with gate(a) and gate(b) sequences interchanged (Interchange the indices 1 and 2).

(ii) If $|p_2/p_1| > 8$ dB, ignore the overlay signal and use steps #13 to #15, i.e., magnitude deconvolution to estimate the stronger signal parameters.

{Note that the code matrices are different for gate(a) and gate(b), however, the deconvolution matrix is the same for both.}

4.3. Overlay and the ground clutter

For ranges in the region-3, the first trip echo can have ground clutter overlaid on the signal. Because half the number of samples are common for gates in the region-1 and region-3, the ground clutter will be present in all the samples for gate(a), and in only half the number of samples for gate(b). The mean power estimate, p_1, (computed in step# 3 of the algorithm, section 4.2) will have ground clutter power added to the gate(a) signal power, whereas, p_2 will not be contaminated by the ground clutter power. As mentioned earlier in section 4.1, if the spectrum width of the overlay signal is narrow ($w<3$ m s^{-1}), it can be effectively removed and the weaker signal velocity can be estimated accurately. Because the ground clutter spectrum width is very narrow ($w_c<0.5$ m s^{-1}), the gate(b) parameters, v_2, and w_2, can be easily estimated using the overlay resolution algorithm (steps #4 through #15). For this very narrow ground clutter width, v_2 can be recovered for overlay power ratio (or the same as clutter-to-signal ratio, CSR, for gate(b) signal if gate(a) signal is absent) in excess of 50 dB. The ground clutter and the gate(a) signal are overlaid as far as the gate(b) is concerned. When the gate(a) signal is also present, and is stronger than the gate(b) signal, then its spectrum width, rather than the CSR will limit the v_2 recovery. Because of the presence of ground clutter, which needs to be filtered, the difficulty is faced only in estimating the gate(a) parameters.

There are situations that need to be considered depending on the relative powers of the gate(a), gate(b) and the ground clutter. First problem we face is in deciding the signal power in p_1. If an estimate of the clutter power is available from the clutter map, then we can subtract it to get p_1 of gate(a). Now, we compute p_2/p_1 and if it is less than -8dB, we ignore the gate(b) overlay. The time series for gate(a) is processed using the clutter filtering algorithm (see Report 3) to filter the clutter, and then estimate its parameters. If p_2/p_1 >-8dB, we need to filter the clutter first, and then apply the overlay resolution algorithm of section 4.2. How effective this combination of algorithms is in recovering v_1 has not been tested, mainly because it involves a lot of simulation runs, and this situation is likely to be encountered only in a small number of gates very close to the radar, in low elevation scans. Further, the staggered PRT is proposed for higher elevation scans because of other considerations, and at the higher elevation scans the ground clutter may not be as serious a problem as it is at the lowest elevations.

4.4. Simulation results and discussion

In order to evaluate the performance of the overlay resolution algorithm given in section 4.2, a large number of simulations were carried out with different input parameters. There are a number of variables to be considered such as, the overlay power ratio, p_2/p_1, spectral moments of the two signals involved, PRTs, SNR, number of samples, etc. We selected two sample sequence lengths, M=32 and 64, a large SNR (>30 dB) for both signals, a typical weather radar wavelength of 10 cm, and a basic PRT, T_u=0.5 ms with a stagger ratio κ=2/3 (which gives an unambiguous velocity, v_a=50 m s^{-1} and r_{a2}=225 km), for most of our simulation results presented in this section. The most critical and difficult parameter to estimate is the weaker signal velocity, and this parameter is used to determine performance of the algorithm. In general, if the weaker signal velocity can be recovered, all other parameters are also recoverable. First, we present some sample scatter plots of the estimated velocity, v_1, of the weaker signal versus the velocity input to the simulation program to illustrate the quality of estimates.

In Fig. 4.4 is a typical scatter plot with parameters almost at the limit of velocity

recovery. The parameters are as indicated in the figure. The parameter *"loss"* is the percentage of the number of times the velocity recovery failed (i.e., the number of outliers) in 2020 simulations, with input velocities uniformly distributed over $\pm v_a$. The standard error, *sd(v)*, is computed leaving out the missed velocity points, or the outliers. There are some outliers at the extreme edge of the velocity interval, $\pm v_a$, which are due to the aliasing and not due to the failure of the algorithm. The rest of the outliers (a region of velocity error, $|v_1 - v_{in}| > v_a/5$) appear in bands because of the mode of failure of the algorithm; it is not able to resolve the ambiguity. This is more apparent for narrow spectrum widths as shown in Fig. 4.5, for a different set of parameters. If the spectrum width of the overlay is narrow, but the signal spectrum width is broad, then the standard error in the velocity estimate increases, which is because of the width itself, but the velocity recovery is very good. Fig. 4.6 shows the effect of a larger signal spectrum width. Note that the 4.0 % loss indicated in Fig. 4.6 is mainly due to the aliasing, and, of course, a few outliers due to the large *sd(v)*. These three figures, 4.4 to 4.6, are generated using 32 staggered PRT samples. The effect of increasing the number of samples is shown in Fig. 4.7. With M=64 we are able to recover the velocity for a overlay ratio as high as 40 dB, with only 5.3% loss for spectrum widths 3 m s^{-1} for both w_1 and w_2.

Next six figures present the performance limits of the algorithm in terms of the maximum resolvable overlay ratio, the standard errors, and the loss parameter, for different spectrum widths. We approximately fix *loss*=10% as the limit of velocity recovery. From a large number of simulation results with varying parameters, only the ones at the limit of recovery are selected, and the following figures are generated. Figs. 4.8 and 4.9 show the maximum overlay ratio (with loss=10% criterion) for M=32 and 64, respectively. It is clear from these figures, that for narrow spectra, the performance is good, but for widths greater than 4 m s^{-1} the performance deteriorates rapidly. The next two figures, 4.10 and 4.11, are plots of the loss parameter at the $\{p_2/p_1\}_{\max}$, as obtained from simulations. Some of the values are lower than 10 % because of the discrete values of the parameters used in the simulation. We selected the value closest to 10% among the available set of results. It can also be noted that for large spectrum widths, some of the values are more than 10% (see

Fig. 4.10). The reason is that, for these parameters we did not get values less than that indicated, and we selected the lowest ones possible, although they are higher than 10%. Lastly, the *sd(v)* achieved at these limiting overlay ratios is shown in Figs. 4.12 and 4.13. It is to be noted that the *sd(v)* is computed from the estimates that are within the $|v_I - v_{in}| > v_a/5$ interval. The reason for adopting this approach is that the overall *sd(v)* (including all the outliers) is not a monotonic increasing function; it is discontinuous because of the nature of the failure mode of the algorithm.

4.5. Considerations for an overall staggered PRT algorithm

In this report as well as in Report 3, the staggered PRT algorithm has been discussed with the aim to solve several long standing problems such as, spectral moment estimation, ground clutter filtering, overlay resolution etc. In an operational environment, we encounter some of these situations individually or in combination. In an operational environment, the situation may vary from gate to gate, hence, in a practical algorithm it is necessary to have a decision mechanism to route the computation along an appropriate path. For example, the gates in the region-2 sample simple staggered PRT echoes without any overlay and the ground clutter contamination, thus, only the magnitude deconvolution procedure need to be applied (i.e., the clutter filtering and overlay resolution are not required). The region-1 and region-3 time series needs to be processed together. It is also most desirable to incorporate some type of data censoring into the algorithm so that bad data is identified.

Different situations that may be encountered in the operational environment are the following:

(a) Echo time series samples without any contamination, i.e., no ground clutter and no overly. The range gates in the region-2 fall in this category, provided the PRTs are selected appropriately for "one-overlay". The gates in other regions may also fall in this category.

(b) Echo time series with ground clutter contamination, but no overlay.

(c) Echo time series with overlay, but no ground clutter.

(d) Echo time series with both ground clutter and overlay present.

The last three situations are for ranges in regions-1 and 3. Further, the clutter is usually present only for ranges close to the radar. In each one of these situations, the routing of the computations again depends on the relative power levels of the signals (one or two) and the ground clutter involved. The computations can be divided into three basic modules; (i) clutter filtering, (ii) overlay resolution, and (iii) the magnitude deconvolution and the pulse pair processing (spectral domain equivalent). The time series needs to be weighted by an appropriate window function before the start of the processing; a {von Hann}$^{1/4}$ window when there is no overlay resolution or the ground clutter filtering, a {von Hann}^{2} window when clutter filtering is to be carried out, and a {von Hann} window when overlay resolution algorithm is applied. The clutter filtering including the magnitude domain deconvolution algorithm is given in Report 3, and the overlay resolution algorithm is in this report (see section 4.2). These two algorithms include the decision criteria used within the algorithms based on the relative power levels of the signals and the clutter involved. All these basic modules need to be integrated into a single program with appropriate decision logic to route the computations. It is also desirable to include the data censoring part, so that the erroneous estimates are identified before they are passed on to the users. The following is an overall decision tree for the staggered PRT scheme, from which the path of computation can be determined.

An overall schematic of the staggered PRT algorithm

Begin

1. Input: gate#, T_1, T_2, M, elevation, time series, etc.

2. **If** the gate# in region-2
   2.1. apply staggered PRT algorithm[(c)] to estimate p, v, w, ->output -> **end (1)**

3. **If** the gate# in region-1 and region-3 (input $3M/2$ samples for both gates).
   3.1. **If** ground clutter is present
      3.1.1. estimate p_1, p_2, from time series, and clutter power, p_c (from clutter map).
      3.1.2. subtract clutter power from p_1, $p_1=p_1-p_c$.
      3.1.3. estimate CSR_1, and $\{p_1/p_2\}$

3.1.4. **If** CSR_1>-10 dB, apply {von Hann}^{2} window and clutter filter[(a)] to gate(a) seq.

3.1.4.1. **If** $\{p_1/p_2\}$> 8dB, apply staggered PRT algorithm to gate(a) seq. and overlay resolution algorithm to gate(b).

3.1.4.2. **If** $\{p_1/p_2\}$< 8dB, apply overlay resolution algorithm[(b)] to gate(a) and gate(b) sequences (gate(b) needs overlay resolution because of clutter).

3.1.5. **If** CSR_1<-10dB, ignore clutter, and apply von Hann window

3.1.5.1. **If** $\{p_1/p_2\}$> 8dB, apply staggered PRT algorithm to gate(a) seq. and overlay resolution algorithm to gate(b).

3.1.5.2. **If** -8dB<$\{p_1/p_2\}$< 8dB, apply overlay resolution algorithm to gate(a) and gate(b) sequences.

3.1.5.3. **If** $\{p_1/p_2\}$< -8dB, apply staggered PRT algorithm to gate(b) and overlay resolution algorithm to gate(a).

3.1.6. output $p_1, v_1, w_1, p_2, v_2, w_2$. - > **end (2)**

3.2. **If** ground clutter is absent

3.2.1. estimate p_1, p_2, from time series, and the ratio, $\{p_1/p_2\}$.

3.2.2. **If** $\{p_1/p_2\}$> 8dB

3.2.2.1. apply staggered PRT algorithm to gate(a) seq.

3.2.2.2. apply overlay resolution algorithm to gate(b) seq.

3.2.2.3. output $p_1, v_1, w_1, p_2, v_2, w_2$. - > **end (3)**

3.2.3. **If** -8 < $\{p_1/p_2\}$< 8dB

3.2.3.1. apply overlay resolution algorithm to gate(a) seq. and gate(b) seq.

3.2.3.2. output $p_1, v_1, w_1, p_2, v_2, w_2$. - > **end (4)**

3.2.2. **If** $\{p_1/p_2\}$<- 8dB

3.2.2.1. apply staggered PRT algorithm to gate(b) seq.

3.2.2.2. apply overlay resolution algorithm to gate(a) seq.

3.2.2.3. output $p_1, v_1, w_1, p_2, v_2, w_2$. - > **end (5)**

end

Notes:

(a) For clutter filtering steps see Report 3.

(b) The overlay resolution algorithm (for weaker signal).

1. convert staggered sequence to uniform sequence (insert zeros).
2. apply {von Hann} window.
3. apply overlay resolution steps (see section 4.2).
4. apply magnitude deconvolution.
5. use pulse pair algorithm to compute p, v, w.

(c) The staggered PRT algorithm:

1. convert staggered sequence to uniform sequence (insert zeros).
2. apply {von Hann}$^{1/4}$ window.
3. apply magnitude deconvolution.
4. use pulse pair algorithm to compute p, v, w.

5. Revised scan strategy for the WSR-88D

The scan strategy proposed in Table 5.3, Report 3, was based on the data available at that point in time, on the SZ phase coding scheme, and the staggered PRT scheme. The staggered PRT algorithm assumed no overlaid echoes in the time series. To ensure this, T_1 must be large enough to give a clear range r_{a1} for any given elevation. Therefore, the maximum range requirement of WSR-88D is equated to r_{a1}, and the PRTs were determined accordingly. Since the algorithm is based on the "narrow" spectrum assumption, which requires that the unambiguous velocity be large enough to ensure that this criterion is satisfied, the scheme could be used only for higher elevation scans, where the range required is sufficiently small. We had planed to work on the resolution of the one-overlay echo but at that time we did not know if a solution existed. With the success of the one-overlay resolution algorithm developed in this report, it might be possible to use the staggered PRT at lower elevations than proposed in Report 3. Nonetheless, there remains substantial testing of the staggered PRT scheme before implementation on the network. We are very confident that the staggered PRT with clutter filtering capability and censoring of overlaid echo in the T_2 interval will significantly improve the WSR-88D data. Thus we recommend this simpler procedure be implemented first on the KOUN1. From the tests we would determine the overall quality of the scheme and the lowest elevation at which it can effectively be used. Thus, in the first implementation on the network, these and higher elevations could use the staggered PRT whereas at the lowest elevations the radar would transmit the phase coded signals. Meanwhile, extensive tests should be made to determine the overall effectiveness of the one-overlay resolution algorithm. If the one-overlay resolution algorithm passes the tests it could be used for the intermediate elevation angles on the WSR-88D. With these caveats it is deemed appropriate to revise the scan strategy proposed in Report 3.

Table 5.1 gives the set of parameters required for the staggered PRT scheme with

one-overlay resolution for each of the elevation scans of the vcp-11. The dwell times and the scan rates are the same as that of the vcp-11 of the WSR-88D. For the lowest two elevations, the dwell time is increased by combining the two scans (long and short PRT) into a single staggered PRT scan to get more samples (antenna azimuth rotation rate is decreased). But for other scans, the antenna rotation rate is kept the same. The PRTs are selected such that r_{a2} is equal to the maximum range required for each elevation to cover a height of 18 km. The addition of the overlay resolution part to the algorithm has made it possible to increase the unambiguous range by a factor 1.5, as compared to that without the overlay resolution. This allows us to select shorter PRTs, resulting in a larger unambiguous velocity. It can be observed from Table 5.1 that, even at 2.4° elevation, the spectrum width of the signal for which velocity can be recovered is about 4.24 m s^{-1}, and the standard error in the velocity estimate is not excessive. Hence, it might be possible to use the staggered PRT scheme for elevations 2.4° and higher. For elevations higher than 10° the range requirement is small, and the overlay resolution algorithm is not needed.

Table 5.2 gives the revised scan parameters for the proposed vcp-11. It is proposed to use staggered PRT down to 2.4° elevation, leaving only the first two scans as before. The lowest two scans retain the long PRT to get a clear reflectivity over 460 km, and SZ(8/64) phase coded short pulse scan, which gives an unambiguous range of 234 km. The SZ phase coding scheme can recover velocities if two echoes are overlaid. They can be from any two of the four possible trips in the 460 km range. But here it is assumed that the echoes are restricted to the first two trips, and the indicated range, 234 km, is for the first two trip overlay. The staggered PRT overlay resolution scheme is proposed for elevations 2.4° to 10°, and the staggered PRT scheme without the overlay resolution from 12° to 19.5°. The PRT is kept constant for elevation 7.5° and higher, because it achieves a sufficiently large v_a (83.33 m s^{-1}). (Further increase might exceed the transmitter Klystron duty cycle.) The lowest PRT used is 0.6 ms.

It may be noted that, for elevations 2.4° and 3.35°, the unambiguous range is reduced by approximately 25 km (303 and 247 km are reduced to 274 and 225 km, respectively) so that echoes with a larger spectrum width can be accommodated. Perhaps,

the performance of the SZ phase coding scheme and the staggered PRT scheme with overlay resolution are comparable for 2.4°. While the SZ phase coding scheme allows overlay resolution for $p_1/p_2 = 20$ dB over a range 234 km, the overlay ratio that can be resolved using the staggered PRT is only 5 dB, but over a 274 km range. The sd(v) is somewhat larger for the staggered PRT scheme as compared to the SZ phase coding scheme, but allows a larger v_a. (Compare the rows corresponding to 2.4° in Table 5.2 of this report and Table 5.3 of Report 3.) The staggered PRT scheme is also simpler in terms of the computation and the radar pulsing scheme. Therefore, the staggered PRT is selected for this elevation. For higher elevations, clearly the staggered PRT is superior. Although uniform PRT scheme is sufficient for elevations 7.5° and above, we have chosen to retain the staggered PRT for all the higher elevations; this is because it allows a much larger v_a which completely eliminates the velocity folding at the expense of some additional computation (these are already in place for the lower elevations).

The data in the last four columns of the Table 5.2 is generated using extensive simulations with the PRTs of each elevation individually. The $\{p_2/p_1\}_{\max}$ is obtained by increasing the overlay ratio in steps until the recovery of the weaker signal velocity failed in 10% of the simulations. The standard errors in the spectral moment estimates is calculated leaving out these outliers for which the velocity ambiguity is not resolved. The spectrum widths of the two signals involved are set to 4 m s^{-1}, which is approximately the median value for weather echoes. The PRTs are set to the values proposed for each elevation, and the number of samples, M, is calculated from the dwell time. The staggered PRT overlay resolution algorithm requires that M is divisible by 4, hence, the nearest multiple of 4 is selected for the simulation. These values are given in brackets in column 4 of the Table 5.2. The simulation results are listed in Tables 5.3a to 5.3c. The first 8 columns are the input parameters, and the rest are the standard errors in the three spectral moments of the two echoes involved and the *loss* parameter. The *loss* parameter is computed for both velocities, $loss_1$ for v_1 and $loss_2$ for v_2. The cutoff overlay ratio is fixed approximately at $loss_1$=10%.

Figures 5.1 to 5.3 show important results from these tables in graphical form. The three important parameters, $loss_1$ of the weaker signal velocity, and the *sd(v)* of the two

velocity estimates, are shown as a function of the overlay ratio, p_2/p_1, in figures 5.1, 5.2, and 5.3, respectively. These plots for $w_1=w_2=4$ m s^{-1} are representative of the performance of the algorithm. For narrower widths the overlay resolution performance is better, and for larger widths, it is poorer. The $loss_1$ parameter increases sharply beyond a certain overlay ratio (Fig.5.1). The standard error in the weaker signal velocity estimate is larger for the lower elevations, because the "narrow" spectrum criterion is satisfied to a lesser degree as we decrease the unambiguous velocity. The $sd(v_1)$ trace is stopped at the point where the loss reaches 10% (Fig. 5.2). The overlap in the staggered PRT spectrum affects the ambiguity resolution part of the overlay resolution algorithm, producing a larger standard error. The spectrum corresponding to the second half of the samples with overlay is not reconstructed accurately enough, if the "narrow" spectrum criteria is not satisfied. This effect can also be seen in the stronger signal velocity for low overlay ratios (Fig. 5.3).

6. Data censoring

The section-6 of Report 3, contains a fairly detail discussion on the data censoring for the staggered PRT as well as the SZ phase coding schemes. Two approaches considered were, (1) rejection criterion based on the combination of several parameters estimated for each range gate, and (2) the censoring criterion based on the spatial continuity/variance of the data field. The second approach is based on the high degree of spatial and temporal continuity of the weather data, and is best implemented off line, after the data is collected. Here we will concentrate on the first approach, which depends more on the scheme used for generating the data fields; specifically the staggered PRT and the SZ phase coding schemes.

In the first approach, the data censoring part consists of a set of pre-determined limits for some of the parameters, such as, the CSR, SNR, overlay ratio, spectrum width etc., and a series of comparisons to determine whether all these parameters are within the pre-set limits. This comparison can be made a part of the overall staggered PRT or the SZ algorithm, so that the bad data is censored. From the simulation study it is known that the limits on the parameters indicated above, depend on the scheme, the PRT, the spectrum widths, and many other parameters. The hard part is determining these limits, and it requires extensive

simulation. As an example, the overlay ratio, $\{p_2/p_1\}_{max}$=5dB, in Table 5.2, for elevation 2.4°, is determined from the simulation data tabulated in Table 5.3a. To generate the 21 rows of this table for 2.4°, takes about 30 minutes of computer time. This is for one set of widths, w_1=w_2=4 m s^{-1}. To study the dependence of the $\{p_2/p_1\}_{max}$ on the spectrum widths, we need to run simulations for many combinations of the widths covering at least up to 8 m s^{-1}. And this procedure has to be repeated for all the elevations, because each elevation has a different set of PRTs, number of samples, etc.

Further, the limits derived using simulation are applicable only to Gaussian spectra, an assumption inherent in the time series simulation. In practice, not all spectra fall in this category, hence, the shape of the spectrum also needs to be examined, in order to achieve a high rejection capability of bad data. This study can be carried out only with real weather data collected using the staggered PRT pulsing scheme.

In this report, a procedure for the data censoring is indicated. The actual values for the upper limits for the parameters to be supplied to the program are not available at this time. They need to be generated using simulations as indicated for both the SZ phase coding and the staggered PRT schemes. These values are specific to a given situation, such as, elevation, PRT, dwell time, number of samples, etc. Without repeating much of the discussion given in section-6 of Report 3, we proceed with the parameters and the decision logic required for the data censoring procedure.

There does not seem to be a need for evaluation of these suggested data censoring schemes, because they involve only comparisons with preset limits, and these limits can be derived using simulation. The evaluation of the data censoring algorithm is meaningful only on the actual radar data.

6.1. The data censoring for the SZ phase coding scheme

As per the proposed vcp-11 (Table 5.2), this is applicable for the lowest two elevation scans where SZ coding is proposed for the short PRT scan. The parameters that can be used for data censoring are signal-to-noise ratio (SNR), the clutter-to-signal ratio (CSR), the overlay power ratio, $\{p_1/p_2\}$, and the spectrum widths, w_1 and w_2. The information regarding

the clutter, i.e, the gate wise distribution of the clutter power, clutter spectrum width, w_c, (also the clutter filter width required, w_f), have to be stored in a clutter map for each elevation (0.5° and 1.45°). The $\{p_1/p_2\}$ ratio is computed from the long PRT data, and an estimate of the spectrum width of the two overlaid range gates, when not contaminated by the clutter, can also be obtained from the long PRT data. If there is clutter present in one of the range gates (the one closer to the radar), it is necessary to filter the clutter before power, and spectrum width are estimated. Note that the spectrum width estimated using the SZ phase coded short PRT time series is under estimated for very large widths because of the spectrum overlap, although the standard error can be much less than that using the long PRT.

The $\{p_1/p_2\}_{max}$ for which velocity recovery of the two overlaid signals is possible, is a function of the spectrum widths and the system phase error (phase error in the phase shifter and the transmit-receive RF path - see report-2). It is about 40 dB for 0.2° phase error for $w_1=w_2=4$ m s^{-1}, for one set of parameters used in the simulation (see Fig.4.3, report-2). At this limit, obviously, the estimated widths will have significant error. Therefore, although we can derive the dependence of $\{p_1/p_2\}_{max}$ on the input spectrum widths using simulation, we cannot base our data censoring on the estimated width. Here, we use the widths estimated from the long PRT data, which is not affected by the SZ decoding, although it has a larger variance due to the smaller number of samples. We use these widths to compute the limits on the $\{p_1/p_2\}$ ratio. The following scheme can be adopted for data censoring, and can be included in the overall SZ decoding algorithm. The actual limits on $\{p_1/p_2\}$, and the clutter map need to be generated for the specific PRT and other parameters used during each scan, and supplied to the algorithm.

The steps in the data censoring algorithm for the SZ phase coding scheme

1. From the long PRT estimate the following parameters: CSR, SNR_1, SNR_2, w_1, w_2, p_1, p_2. {The CSR is only for the range gates indicated in the clutter map.}

2. Set limits for data censoring: $\{CSR\}_{max}$, $\{SNR_1\}_{min}$, $\{SNR_2\}_{min}$, $\{p_1/p_2\}_{max}(w_1,w_2)$, $\{p_2/p_1\}_{max}(w_1,w_2)$.

{Note that $\{p_1/p_2\}_{max}$ is a strong function of w_1 and a weak function of w_2. This is the overlay

ratio for the 2nd trip signal, i.e., first trip is the overlay affecting the recovery of velocity, v_2 . The other is the overlay ratio for the 1st trip signal.}

3. Use **SZ-1** or **SZ-2** algorithm for estimating the spectral moments (see report-2).

4. Flag the velocity data: (a) if $SNR_1 < \{SNR_1\}_{min}$, flag v_1.

(b) if $SNR_2 < \{SNR_2\}_{min}$, flag v_2.

(c) if $CSR > \{CSR\}_{max}$, flag v_1 (only when clutter is present).

(d) if $\{p_1/p_2\} > \{p_1/p_2\}_{max}$, flag v_2.

(e) if $\{p_2/p_1\} > \{p_2/p_1\}_{max}$, flag v_1.

6.2. The data censoring for the staggered PRT scheme

The comments made at the beginning of the previous section are applicable here also. The data censoring decision is based on the same set of parameters as the SZ phase coding, i.e.,CSR, SNR_1, SNR_2, w_1, w_2, p_1, p_2, however, the limiting values for comparison depend on the path the algorithm takes in the overall staggered PRT decoding scheme. The path taken by the computation in the staggered PRT algorithm can be divided into four groups. (1) when there is no overlay and no clutter, (2) when there is clutter, but no overlay, (3) when there is overlay, but no clutter, and (4) when there is both clutter and overlay. These four groups have to be further divided based on the relative power levels of clutter and the two signals involved. These divisions will lead to nine different paths. There are essentially three major computational blocks, (a) clutter filtering, (b) overlay resolution, and (c) the magnitude deconvolution plus the pulse pair estimation of spectral moments. Each path will end with the block (c). Extensive simulation study is required to generate the cutoff limits on CSR, $\{p_2/p_1\}$, etc., and these are functions of the spectrum widths.

The spectrum widths of the signals can be estimated either from the staggered PRT time series directly (power is estimated directly), or from the reconstructed spectrum after the magnitude deconvolution. While the first estimate has inherently larger standard error, the second estimate is biased low for large widths because of the spectrum overlap. This happens for lower elevations where the unambiguous velocity, v_a, cannot be made sufficiently large. For elevations 4.5° and higher, neither the spectrum width estimate, nor the clutter are

problems. A check on the limiting overlay ratio alone is sufficient for data censoring. Thus, the data censoring requires more comparisons for the lower elevations (2.5° and 3.35°). The limiting ratios, i.e., CSR, SNR_1, SNR_2, $\{p_1/p_2\}_{max}$ (w_1,w_2), and $\{p_2/p_1\}_{max}$ (w_1,w_2), need to be obtained from simulations for each of the elevations separately, and a look-up table generated, as an input to the data censoring part of the algorithm.

The steps in the data censoring procedure for the staggered PRT scheme

1. Estimate the parameters, CSR_1 (where applicable), SNR_1, SNR_2, $\{p_1/p_2\}$, w_1, w_2.

2. Obtain the limiting values, $\{CSR_1\}_{max}$, $\{SNR_1\}_{min}$, $\{SNR_2\}_{min}$, and $\{p_1/p_2\}_{max}$, from the look-up table of limits.

3. Flag the velocity data: (a) if $SNR_1 < \{SNR_1\}_{min}$, flag v_1.

(b) if $SNR_2 < \{SNR_2\}_{min}$, flag v_2.

(c) if $CSR > \{CSR\}_{max}$, flag v_1 (only when clutter is present).

(d) if $\{p_1/p_2\} > \{p_1/p_2\}_{max}$, flag v_2.

(e) if $\{p_2/p_1\} > \{p_2/p_1\}_{max}$, flag v_1.

7. Conclusions

The Report 3 introduced an algorithm for the clutter filtering and spectral moment estimation from the staggered PRT sequence. In the current report further developments of the staggered PRT technique are presented. These include several improvements of the algorithm. Specifically, the effect of window is examined in detail, and it is determined that the optimum window functions for various processing modules are different. The {von Hann}^{2} window is found to perform best with the clutter filtering, and the von Hann window is the best when overlay resolution algorithm is applied. When neither of these two are used, i.e., no overlay and no clutter situation, the {von Hann}$^{1/4}$ performs the best.

Most important contribution of this report is a method to resolve "one-overlay" situation in the staggered PRT scheme. This results in an increased unambiguous range, from r_{a1} to r_{a2}. However, there are limits on the maximum overlay ratio which can be resolved. The method is fairly involved and therefore would require significant testing on the KOUN1

before a decision can be made whether to include it on the WSR-88D network.

We have also examined the possible parameters that can be used for censoring the bad data, and suggested a methodology for incorporating this part in the staggered PRT and the SZ phase coding algorithms.

Finally, the alternative vcp-11 scan strategy proposed in the Report 3 has been revised based on the latest findings on the performance of the staggered PRT algorithm. The staggered PRT scheme has been suggested for most elevations except for the lowest two, where the long PRT and the SZ phase coded transmissions in two successive scans are retained as proposed earlier. It is important to bear in mind that the proposed vcp-11 hinges on the successful tests of the one-overlay resolution algorithm that will involve considerable effort. Because of this uncertainty and time required for development, the simpler scheme or its variants, as described in Report 3, should first be implemented on the network.

----oooo0000oooo----

8. Figures and tables

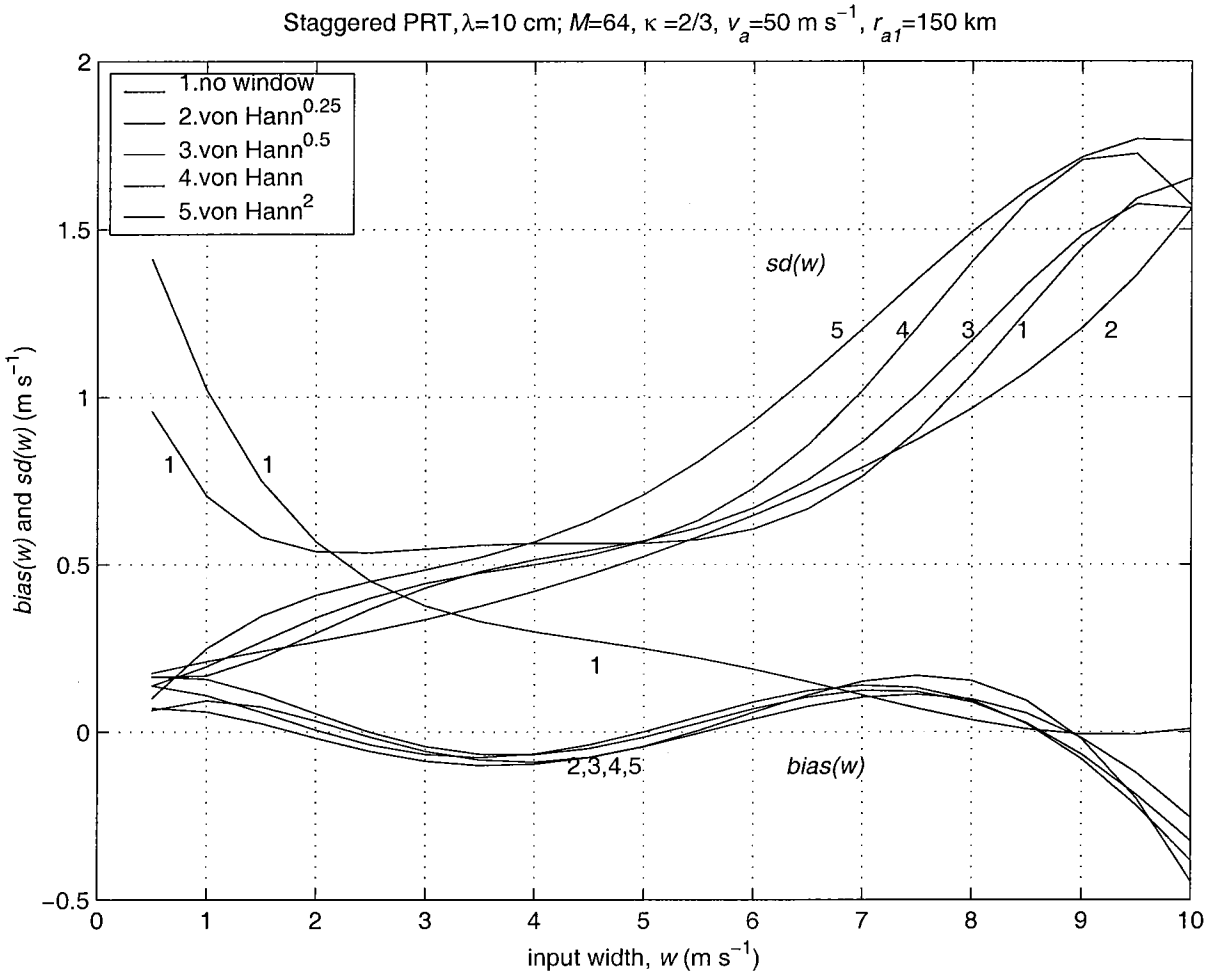

Fig. 3.1. The effect of window function on the bias and standard error in the spectrum width estimate. The *sd(w)* and *bias(w)* are shown as a function of input width for window functions, {von Hann}^{p}, with $p = 0$, 0.25, 0.5, 1, and 2. Simulated data is fitted to obtain smooth curves.

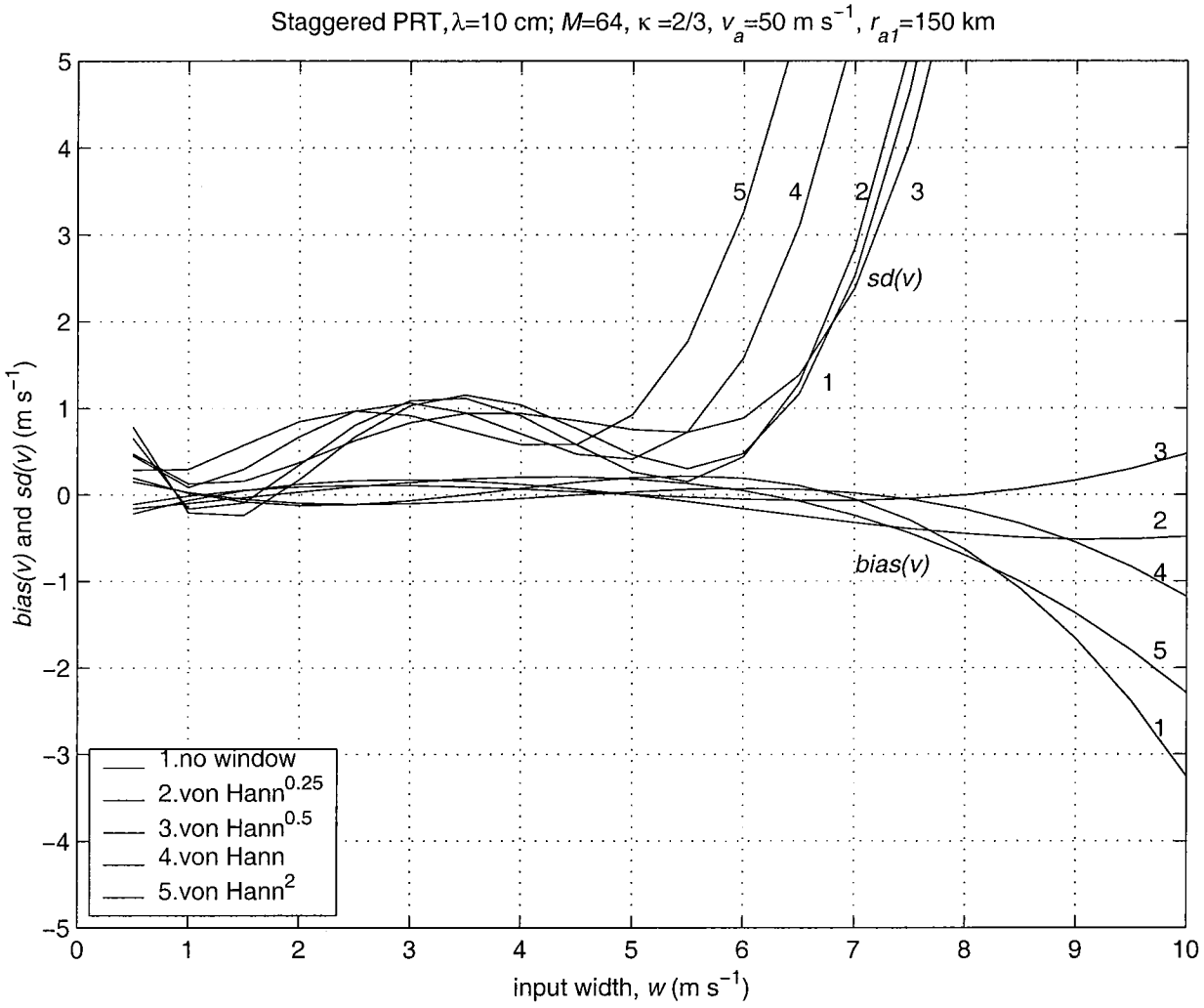

Fig. 3.2. The effect of window function on the bias and standard error in the mean velocity estimate. The *sd(v)* and *bias(v)* are shown as a function of input width for window functions, {von Hann}^{p}, with p = 0, 0.25, 0.5, 1, and 2. Simulated data is fitted to obtain smooth curves.

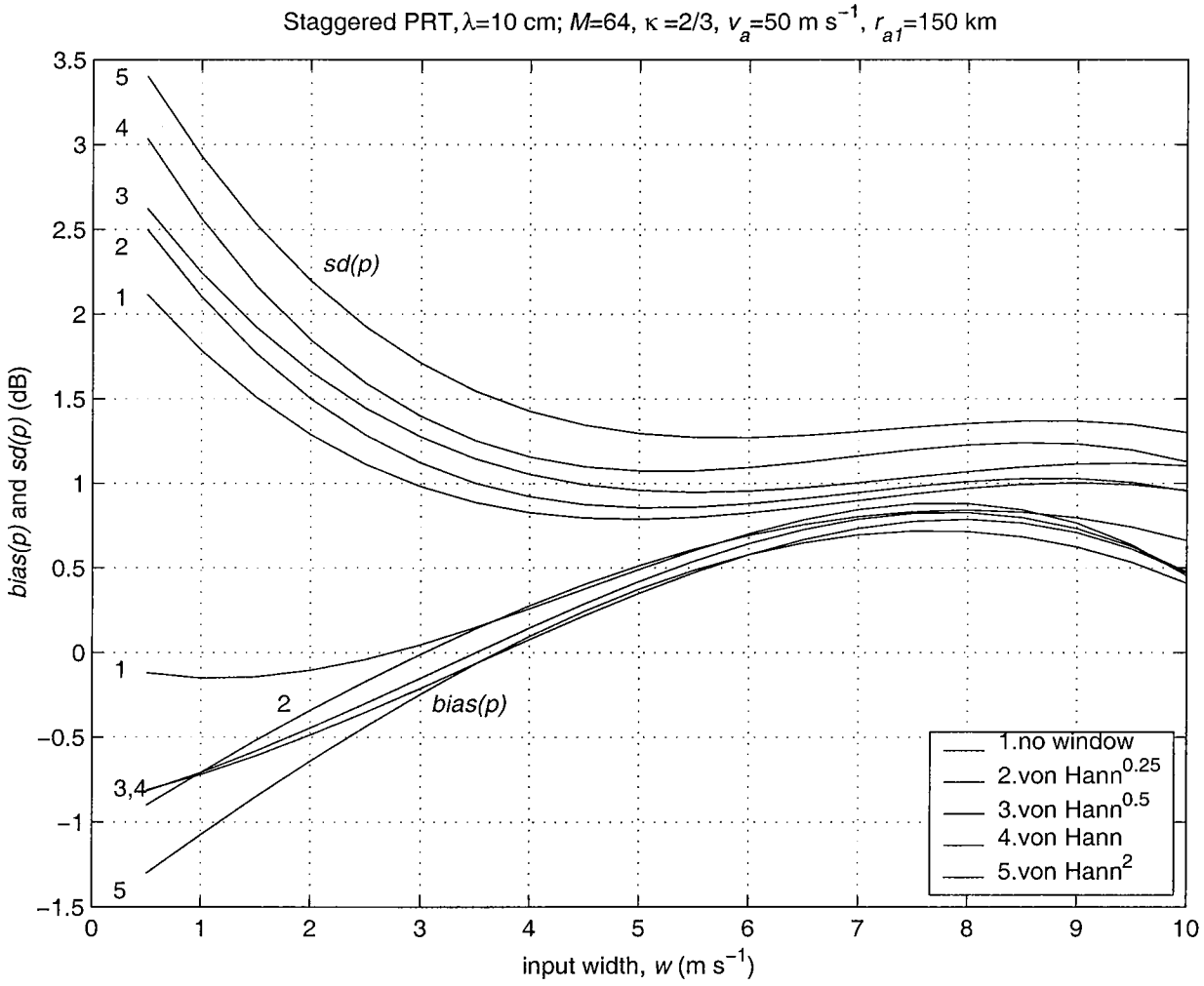

Fig. 3.3. The effect of window function on the bias and standard error in the mean power estimate. The *sd(p)* and *bias(p)* are shown as a function of input width for window functions, {von Hann}^{p}, with p = 0, 0.25, 0.5, 1, and 2. Simulated data is fitted to obtain smooth curves.

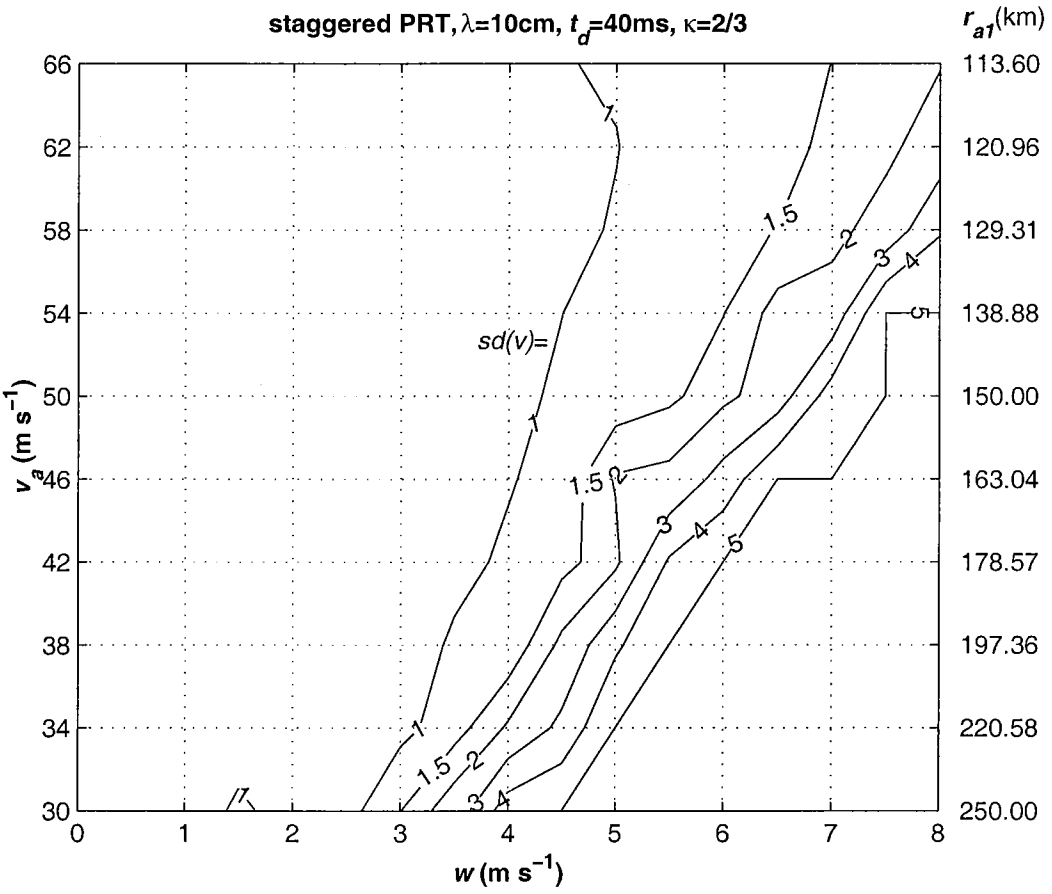

Fig. 3.4a. Contour plot of $sd(v)$ as a function of spectrum width of the signal, w, and the unambiguous velocity, v_a, for dwell time t_d=40ms and κ=2/3. Each value is obtained from 800 simulations (20 at each of the 40 velocity bins spread uniformly across $\pm 0.8 v_a$). The unambiguous range, r_{a1}, corresponding to the v_a is given on the right side vertical axis. No window is used.

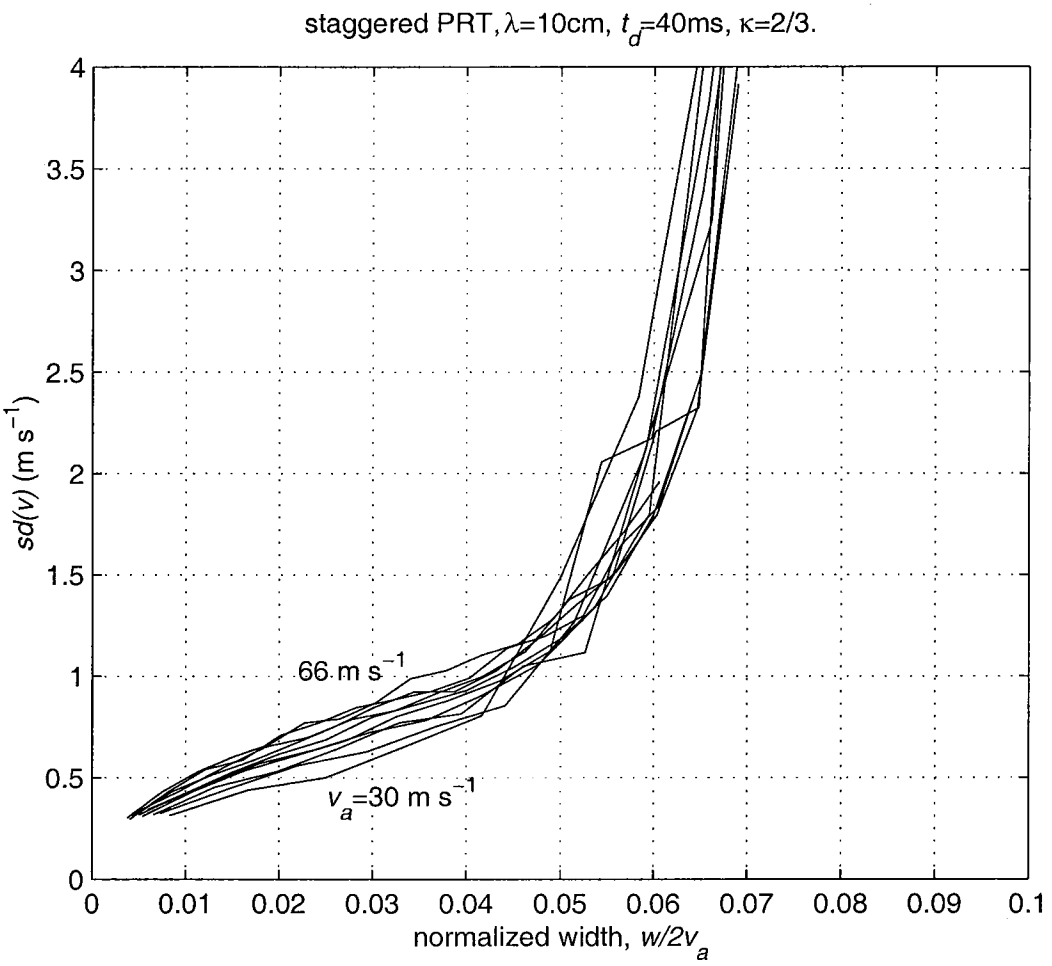

Fig.3.4b. Standard error, *sd(v)*, as a function of normalized width, $w/2v_a$, for different unambiguous velocities from 30 to 66 m s^{-1} (or different T_u). The data is same as in Fig.3.4a.

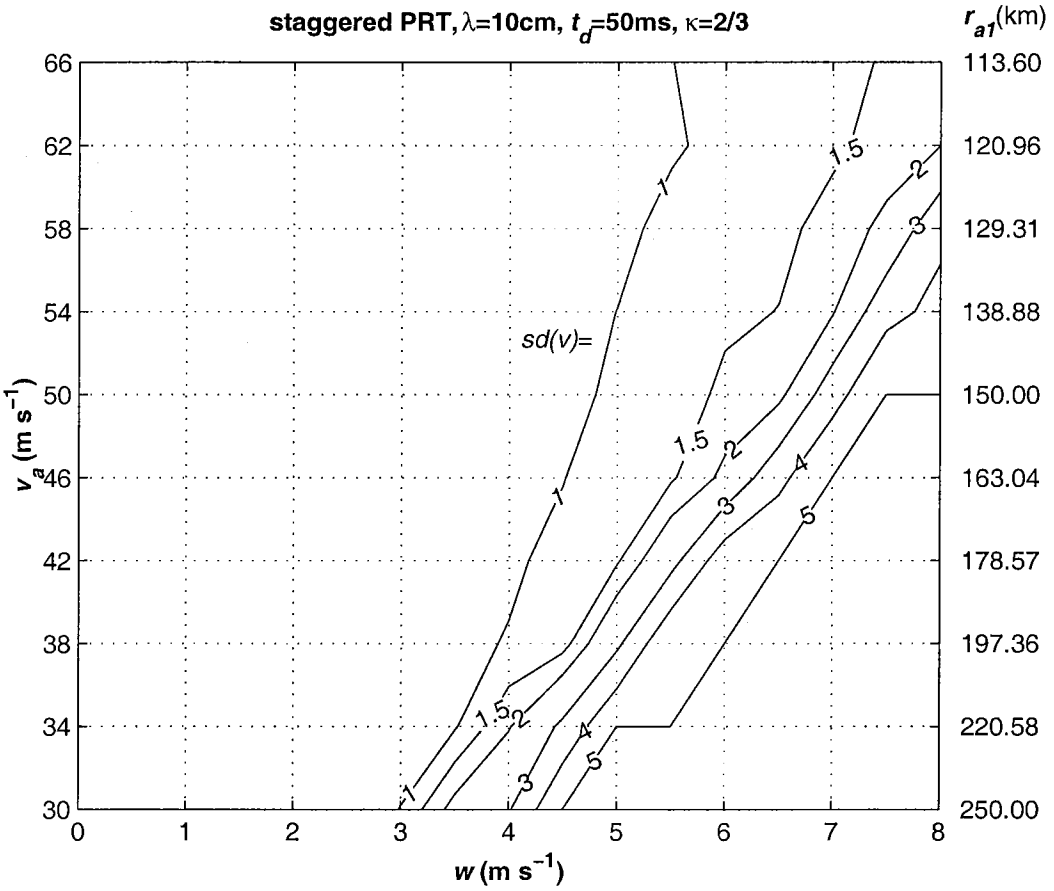

Fig. 3.5a. Contour plot of $sd(v)$ as a function of spectrum width of the signal, w, and the unambiguous velocity, v_a, for dwell time t_d=50ms and κ=2/3. Each value is obtained from 800 simulations (20 at each of the 40 velocity bins spread uniformly across $\pm 0.8 v_a$). (This figure is same as Fig.3.4a, but dwell time is 50 ms.)

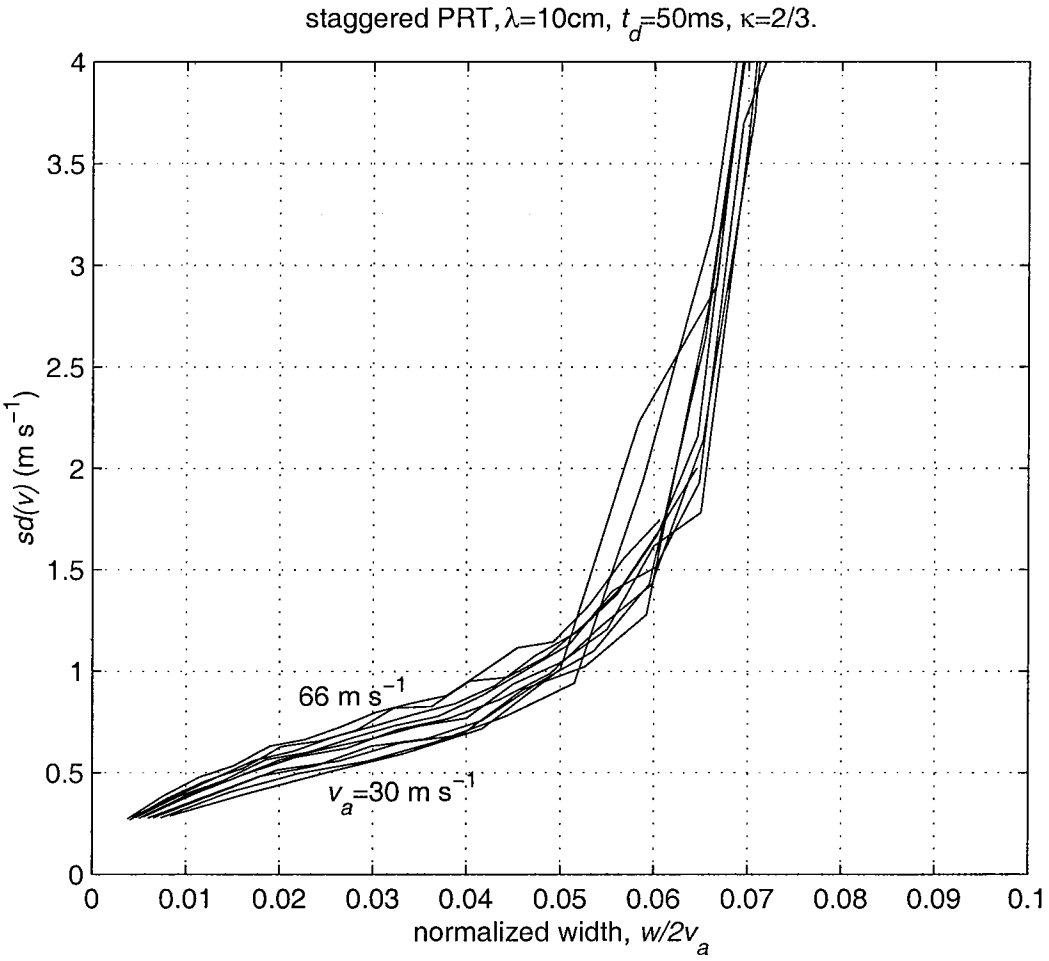

Fig.3.5b. Standard error, *sd(v)*, as a function of normalized width, $w/2v_a$, for different unambiguous velocities from 30 to 66 m s^{-1} (or different T_u). The data is same as in Fig.3.5a.

Table. 3.1. *sd(v)* as a function of w and v_a for λ=10 cm, t_d=40 ms, κ=2/3 staggered PRT transmission. Each values is obtained from 800 simulations (20 simulations at each of the 40 velocity bins spread uniformly over $\pm 0.8 v_a$.) Units are m s^{-1}.

$w \setminus v_a$	30	34	38	42	46	50	54	58	62	66
0.5	0.31	0.33	0.32	0.34	0.31	0.32	0.33	0.31	0.29	0.30
1.0	0.44	0.45	0.45	0.46	0.43	0.42	0.43	0.43	0.43	0.43
1.5	1.16	0.56	0.53	0.57	0.53	0.53	0.55	0.52	0.54	0.53
2.0	0.65	0.63	0.64	0.64	0.61	0.62	0.65	0.59	0.59	0.60
2.5	0.81	0.75	0.77	0.72	0.68	0.69	0.70	0.67	0.71	0.66
3.0	1.49	0.85	0.82	0.78	0.80	0.80	0.79	0.75	0.77	0.77
3.5	2.38	1.27	1.05	0.91	0.88	0.87	0.83	0.85	0.84	0.79
4.0	4.57	2.08	1.12	1.06	0.98	0.93	0.92	0.92	0.88	0.87
4.5	7.01	3.24	2.13	1.33	1.12	1.04	1.00	0.93	0.93	0.99
5.0	10.77	7.82	3.82	1.80	2.06	1.18	1.12	1.02	0.99	1.03
5.5	12.36	9.76	6.34	4.12	2.17	1.40	1.38	1.18	1.14	1.10
6.0	15.32	13.13	9.02	6.69	3.38	1.80	1.49	1.35	1.20	1.16
6.5	16.09	15.41	13.40	9.81	5.15	2.48	2.21	1.52	1.30	1.28
7.0	16.85	17.27	15.54	11.75	8.70	4.47	2.32	1.80	1.65	1.51
7.5	16.83	18.65	17.16	14.92	10.37	8.41	5.86	2.32	1.84	1.71
8.0	17.63	19.56	18.94	18.45	14.79	11.18	6.73	3.92	2.42	1.96

Table. 3.2. *sd(v)* as a function of w and v_a for λ=10 cm, t_d=50 ms, κ=2/3 staggered PRT transmission. Each values is obtained from 800 simulations (20 simulations at each of the 40 velocity bins spread uniformly over $\pm 0.8 v_a$.) Units are m s^{-1}.

$w \setminus v_a$	30	34	38	42	46	50	54	58	62	66
0.5	0.29	0.28	0.28	0.28	0.28	0.28	0.28	0.28	0.27	0.27
1.0	0.40	0.40	0.40	0.38	0.39	0.39	0.38	0.38	0.38	0.38
1.5	0.51	0.50	0.51	0.48	0.49	0.47	0.46	0.47	0.46	0.48
2.0	0.59	0.56	0.56	0.53	0.58	0.56	0.56	0.56	0.52	0.54
2.5	0.72	0.65	0.65	0.63	0.62	0.62	0.60	0.61	0.63	0.63
3.0	1.01	0.78	0.69	0.67	0.71	0.67	0.67	0.68	0.66	0.66
3.5	2.23	0.94	0.91	0.76	0.77	0.73	0.73	0.73	0.71	0.73
4.0	2.90	1.94	1.02	0.94	0.86	0.77	0.78	0.79	0.82	0.80
4.5	6.28	3.18	1.28	1.10	0.99	0.94	0.88	0.84	0.83	0.84
5.0	9.22	5.56	2.80	1.43	1.22	1.04	1.00	0.93	0.95	0.88
5.5	11.67	9.20	4.91	2.64	1.43	1.21	1.13	1.08	0.97	1.00
6.0	14.87	12.09	7.78	4.62	2.14	1.62	1.40	1.19	1.07	1.12
6.5	15.42	14.73	10.88	7.73	3.73	1.78	1.51	1.38	1.23	1.14
7.0	16.61	16.02	13.97	10.37	6.43	3.60	1.93	1.67	1.41	1.32
7.5	16.98	17.39	16.78	13.11	11.24	5.84	3.70	2.16	1.69	1.56
8.0	17.37	18.79	18.67	16.94	13.21	9.88	4.27	3.79	2.00	1.75

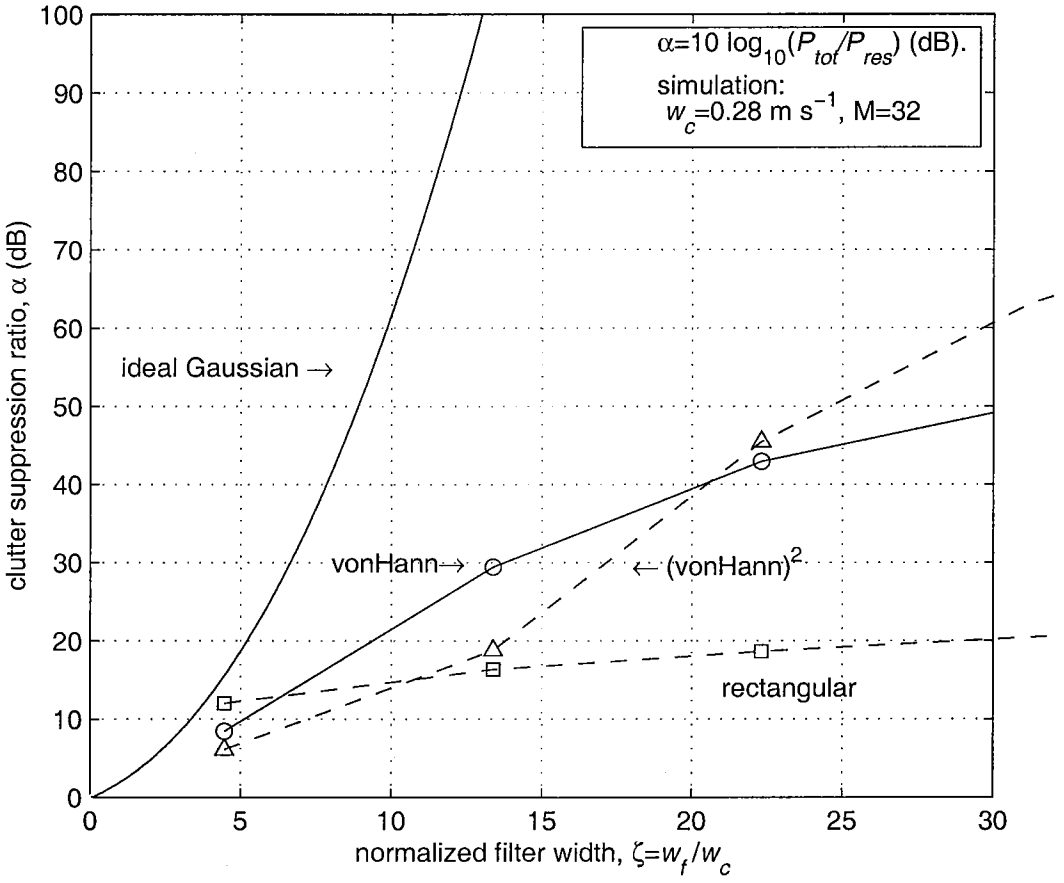

Fig.3.6. The clutter suppression ratio, α, as a function of the normalized clutter filter width for Guassian spectra with different window functions $\{\text{von Hann}\}^p$, p=0, 1, and 2. The curves are obtained from simulation; the simulation points are indicated by symbols (square, circle, and triangle). The number of staggered PRT samples, M, used in the simulation is 32.

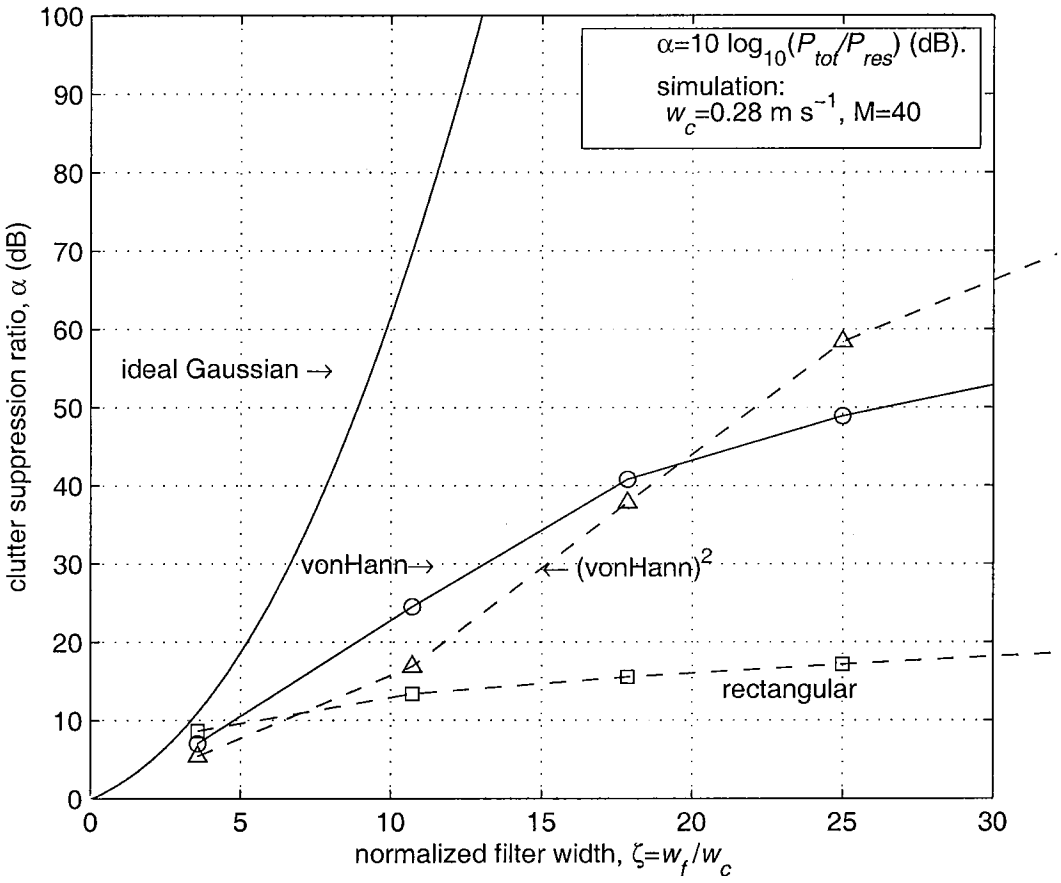

Fig.3.7. The clutter suppression ratio, α, as a function of the normalized clutter filter width for Guassian spectra with different window functions $\{\text{von Hann}\}^p$, p=0, 1, and 2. The curves are obtained from simulation; the simulation points are indicated by symbols (square, circle, and triangle). The number of staggered PRT samples, M, used in the simulation is 40.

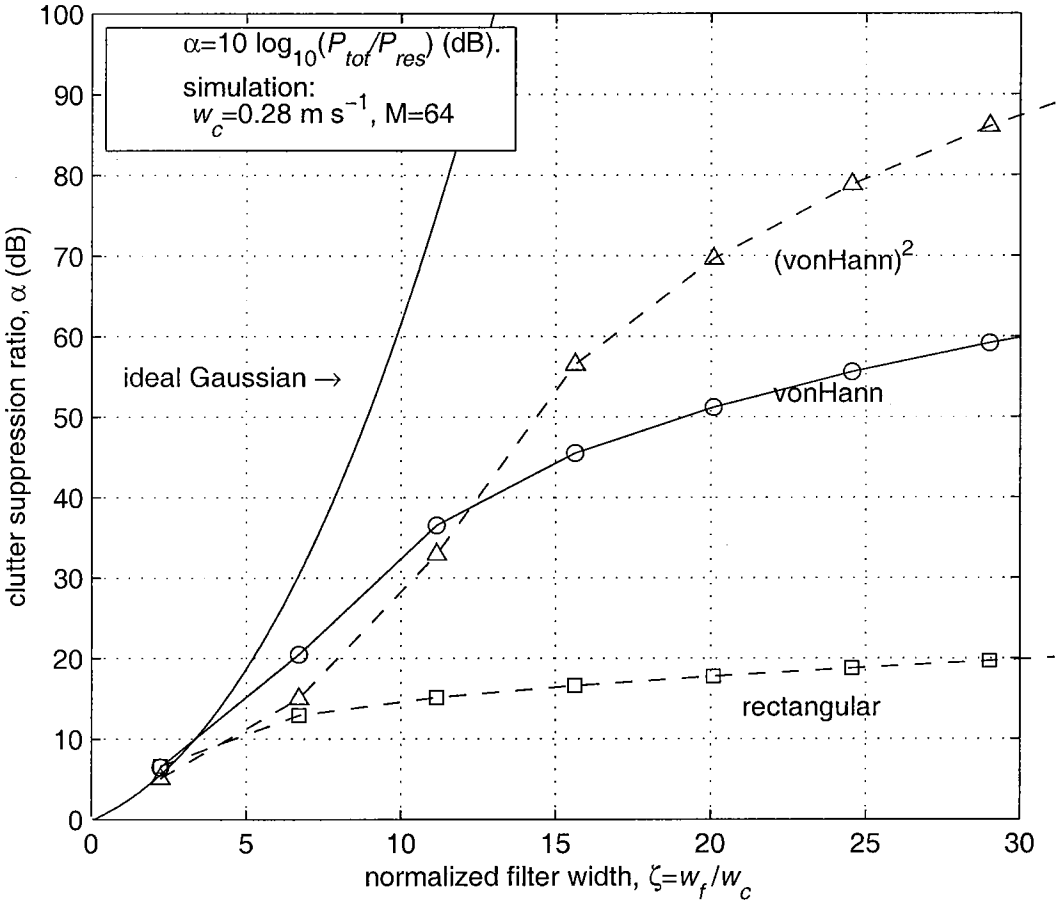

Fig.3.8. The clutter suppression ratio, α, as a function of the normalized clutter filter width for Guassian spectra with different window functions $\{\text{von Hann}\}^p$, p=0, 1, and 2. The curves are obtained from simulation; the simulation points are indicated by symbols (square, circle, and triangle). The number of staggered PRT samples, M, used in the simulation is 64.

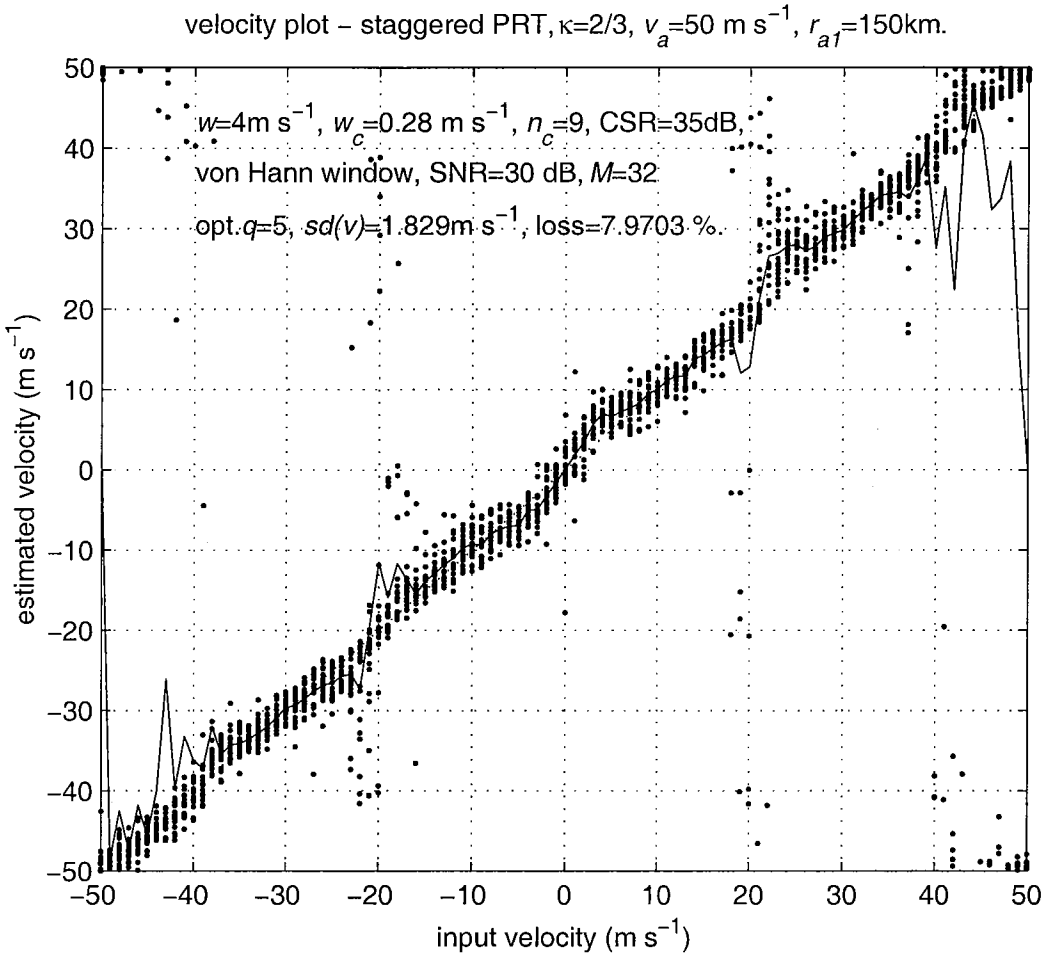

Fig.3.9. The weaker signal velocity recovery with von Hann window, M=32. The estimated velocity versus the input velocity using the proposed clutter filtering and bias correction algorithm. The parameters used in the simulation are as indicated in the figure and q=(n_c+1)/2. The abrupt change in data at the Nyquist velocity is an artifact inherent in plotting circular functions on a linear graph.

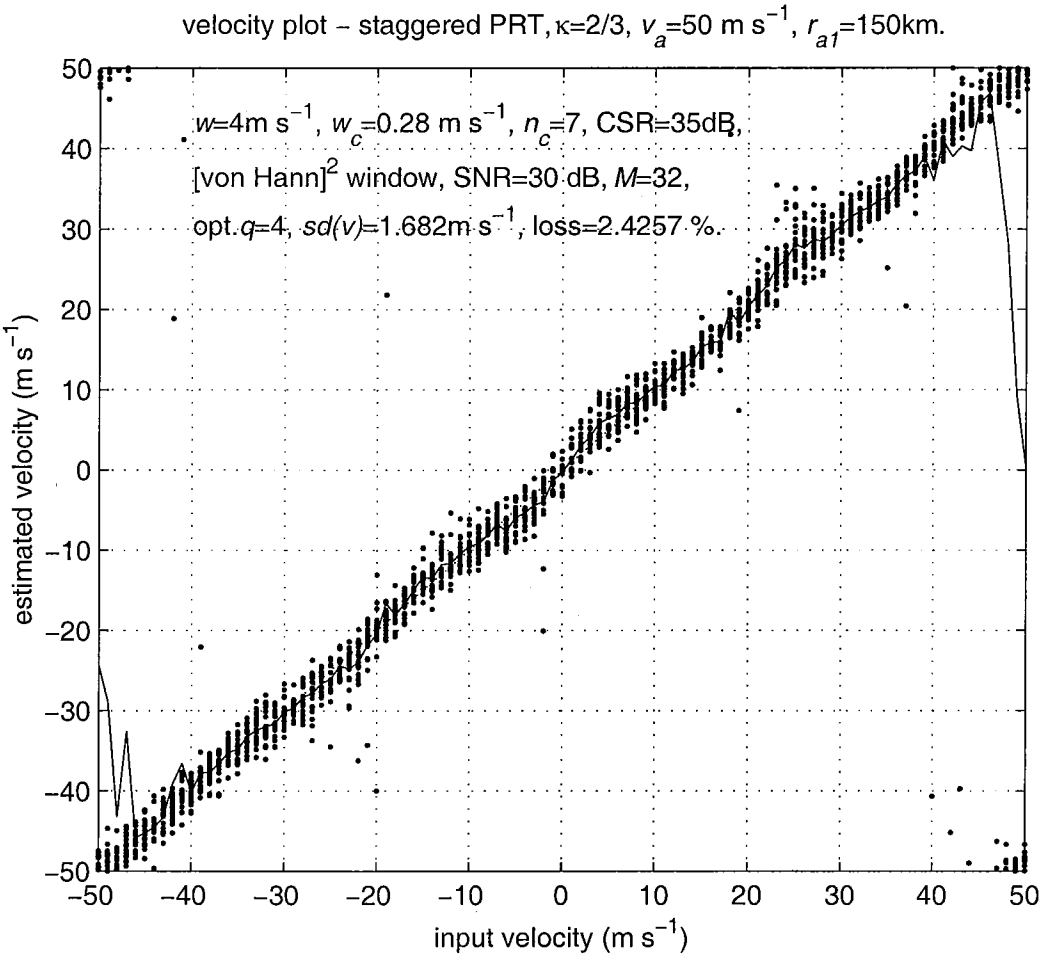

Fig.3.10. The weaker signal velocity recovery with {von Hann}^{2} window, M=32. The estimated velocity versus the input velocity using the proposed clutter filtering and bias correction algorithm. The parameters used in the simulation are as indicated in the figure and q=(n_c+1)/2. The abrupt change in data at the Nyquist velocity is an artifact inherent in plotting circular functions on a linear graph.

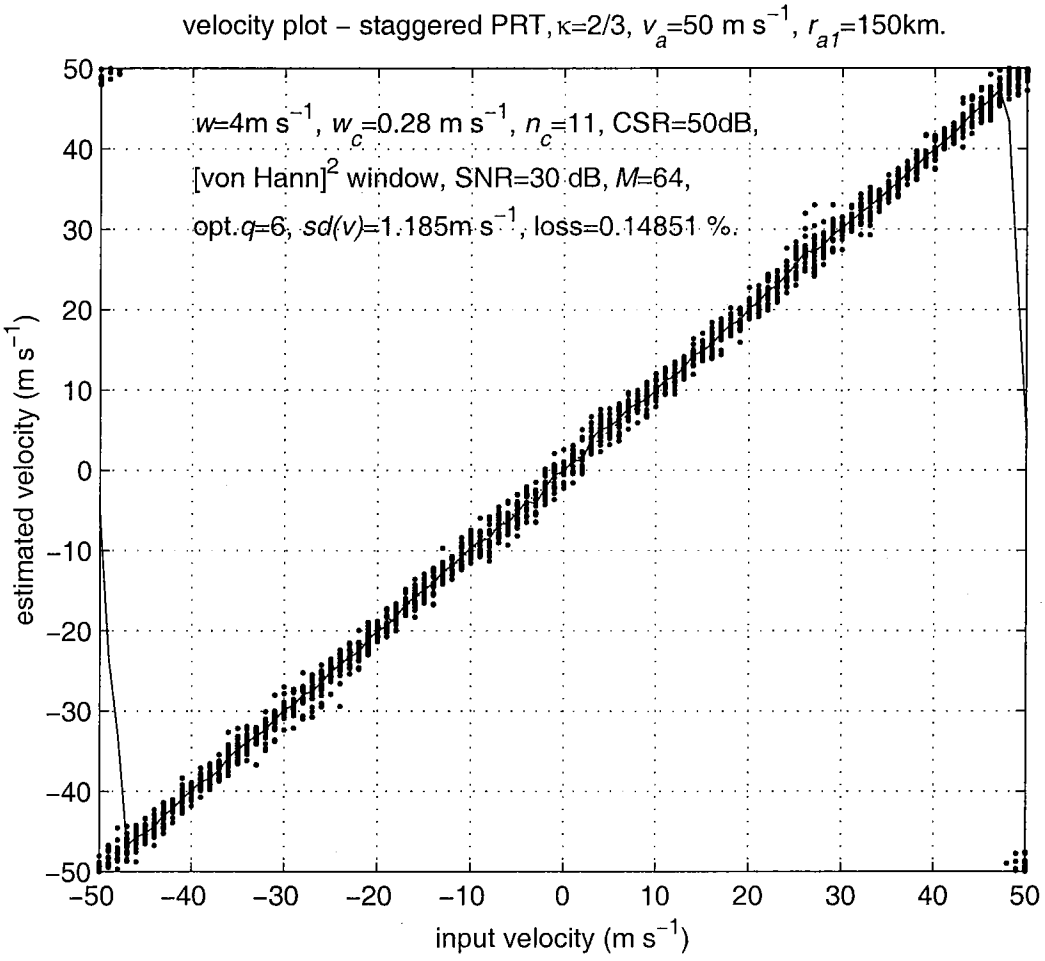

Fig.3.11. The weaker signal velocity recovery with {von Hann}^{2} window, M=64. The estimated velocity versus the input velocity using the proposed clutter filtering and bias correction algorithm. The parameters used in the simulation are as indicated in the figure and q=(n_c+1)/2. The abrupt change in data at the Nyquist velocity is an artifact inherent in plotting circular functions on a linear graph.

Table.3.3a. The clutter filter performance with von Hann window, M = 32, w_c=0.28 m s^{-1}, κ=2/3, T_u=0.5 ms, r_{al}=150 km, v_a=50 m s^{-1}.

w(m s^{-1})	CSR(dB)	optimum n_c	$sd(v)$(m s^{-1})	%loss
2	20	7	0.91	0.20
2	25	7	0.94	1.73
2	30	9	1.05	5.84
2	35	9	1.13	12.92
2	40	9	1.32	21.19
2	45	11	1.46	32.28
2	50	11	1.90	45.20
4	20	5	1.40	0.69
4	25	7	1.59	1.78
4	30	7	1.60	3.51
4	35	9	1.83	7.97
4	40	9	1.89	15.94
4	45	11	2.09	26.58
4	50	13	2.21	42.72
6	20	5	2.08	10.35
6	25	5	2.16	15.64
6	30	7	2.24	20.25
6	35	7	2.31	24.95
6	40	9	2.40	33.12
6	45	11	2.49	43.71
6	50	11	2.55	54.06

Table.3.3b. The clutter filter performance with {von Hann}^{2} window, M = 32, w_c=0.28 m s^{-1}, κ=2/3, T_u=0.5 ms, r_{al}=150 km, v_a=50 m s^{-1}.

w(m s^{-1})	CSR(dB)	optimum n_c	$sd(v)$(m s^{-1})	%loss
2	20	7	1.00	0.00
2	25	7	0.98	0.05
2	30	7	0.98	0.10
2	35	9	1.13	0.40
2	40	9	1.12	1.73
2	45	9	1.15	5.05
2	50	11	1.33	9.55
4	20	5	1.61	1.49
4	25	7	1.63	1.44
4	30	7	1.70	2.18
4	35	7	1.68	2.43
4	40	7	1.72	4.65
4	45	9	1.94	6.44
4	50	9	1.90	9.21
6	20	5	2.21	14.65
6	25	5	2.26	18.07
6	30	7	2.27	19.50
6	35	7	2.22	20.69
6	40	7	2.32	23.47
6	45	9	2.36	29.85
6	50	9	2.39	30.10

Table.3.3c. The clutter filter performance with von Hann window, $M = 64$, w_c=0.28 m s^{-1}, κ=2/3, T_u=0.5 ms, r_{al}=150 km, v_a=50 m s^{-1}.

w(m s^{-1})	CSR(dB)	optimum n_c	$sd(v)$(m s^{-1})	%loss
2	20	7	0.62	0.00
2	25	9	0.63	0.00
2	30	11	0.67	0.05
2	35	11	0.70	0.50
2	40	13	0.75	2.28
2	45	15	0.83	6.68
2	50	15	1.19	16.63
4	20	7	0.96	0.00
4	25	9	0.99	0.00
4	30	9	1.01	0.00
4	35	11	1.10	0.05
4	40	13	1.17	0.74
4	45	15	1.36	2.18
4	50	15	1.55	9.21
6	20	7	1.67	0.99
6	25	7	1.68	1.78
6	30	9	1.71	3.22
6	35	11	1.80	5.05
6	40	11	1.87	8.22
6	45	15	2.02	14.06
6	50	15	2.14	20.00

Table.3.3d. The clutter filter performance with {von Hann}^{2} window, M = 64, w_c=0.28 m s^{-1}, κ=2/3, T_u=0.5 ms, r_{al}=150 km, v_a=50 m s^{-1}.

w(m s^{-1})	CSR(dB)	optimum n_c	$sd(v)$(m s^{-1})	%loss
2	20	7	0.70	0.00
2	25	7	0.69	0.00
2	30	9	0.71	0.00
2	35	9	0.69	0.00
2	40	9	0.71	0.00
2	45	11	0.71	0.00
2	50	13	0.74	0.00
4	20	7	1.06	0.00
4	25	7	1.10	0.00
4	30	9	1.09	0.00
4	35	9	1.13	0.00
4	40	11	1.14	0.10
4	45	9	1.11	0.00
4	50	11	1.19	0.15
6	20	9	1.86	4.46
6	25	7	1.83	3.76
6	30	7	1.86	3.51
6	35	9	1.86	4.75
6	40	9	1.89	4.06
6	45	9	1.89	4.90
6	50	11	1.90	6.14

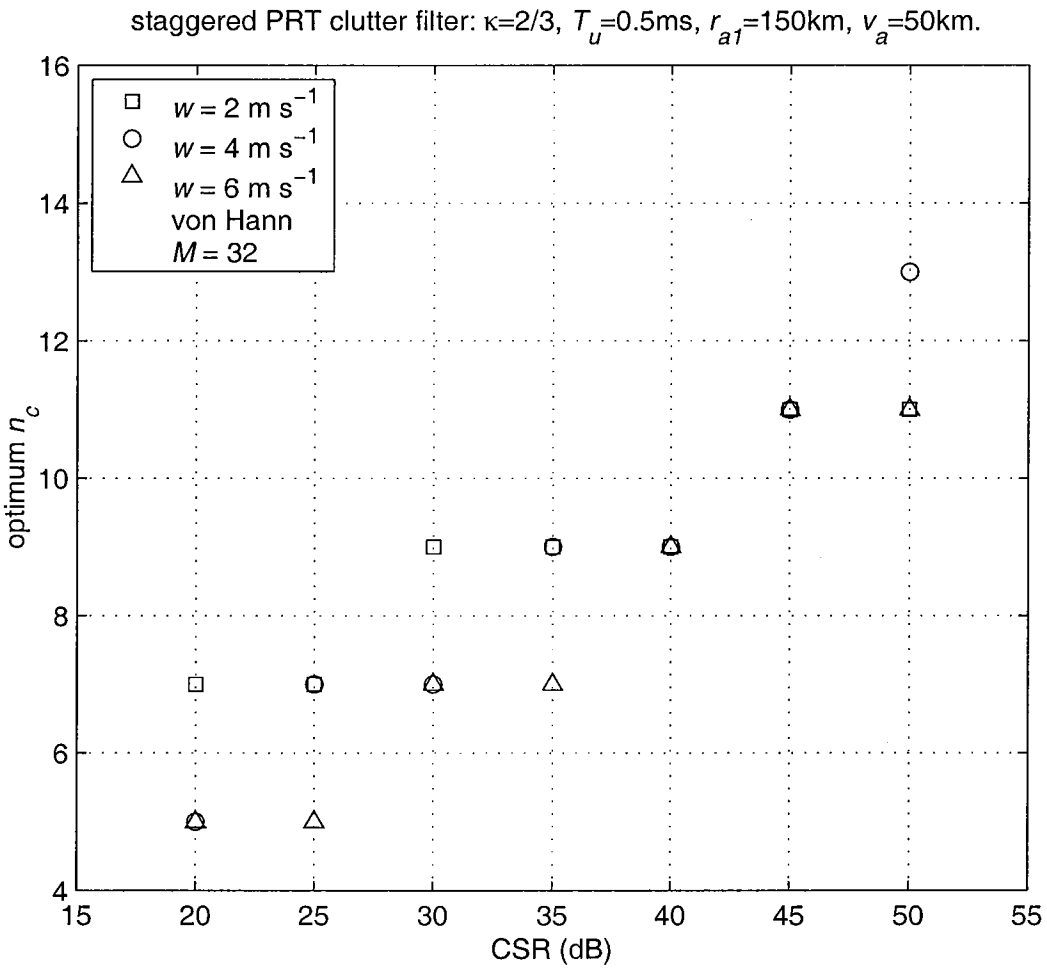

Fig.3.12. The optimum clutter filter width, n_c, versus the clutter-to-signal ratio, CSR, with spectrum width as a parameter, for M=32, and von Hann window.

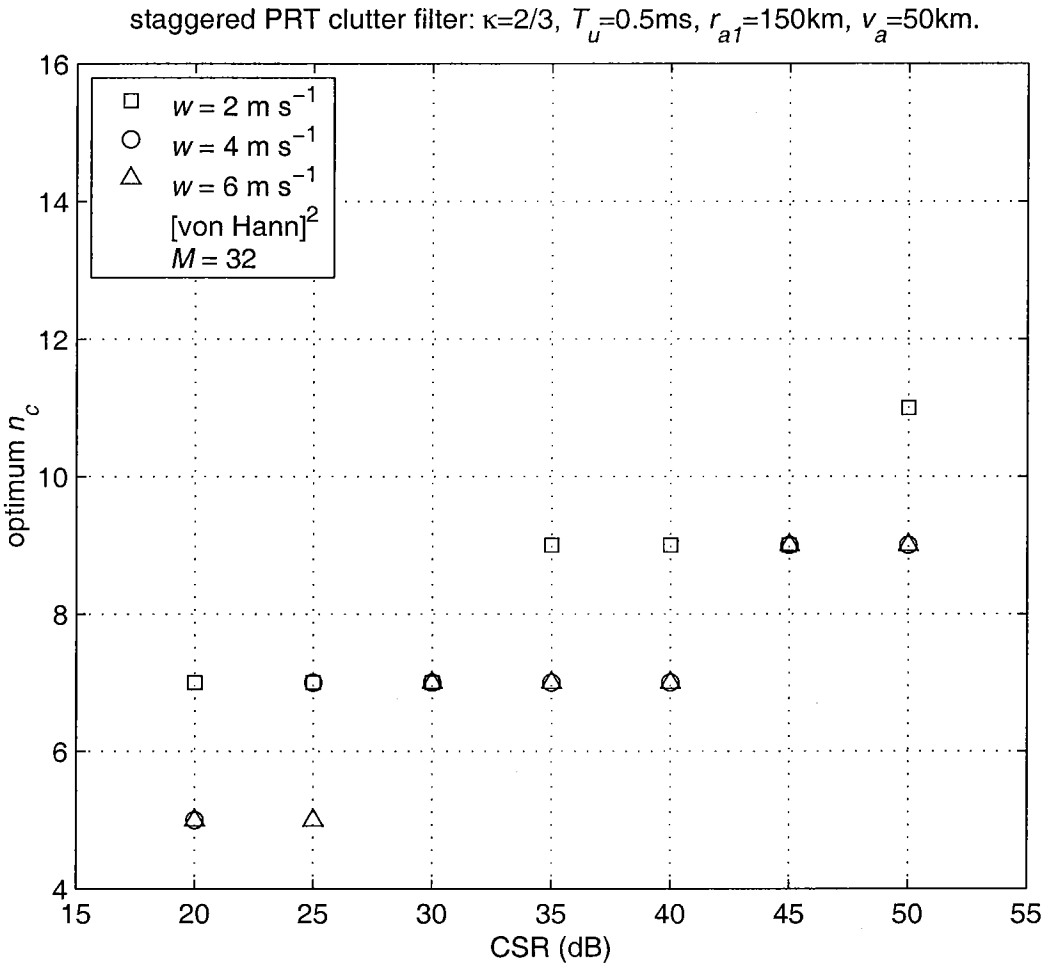

Fig.3.13. The optimum clutter filter width, n_c, versus the clutter-to-signal ratio, CSR, with spectrum width as a parameter, for M=32, and {von Hann}^{2} window.

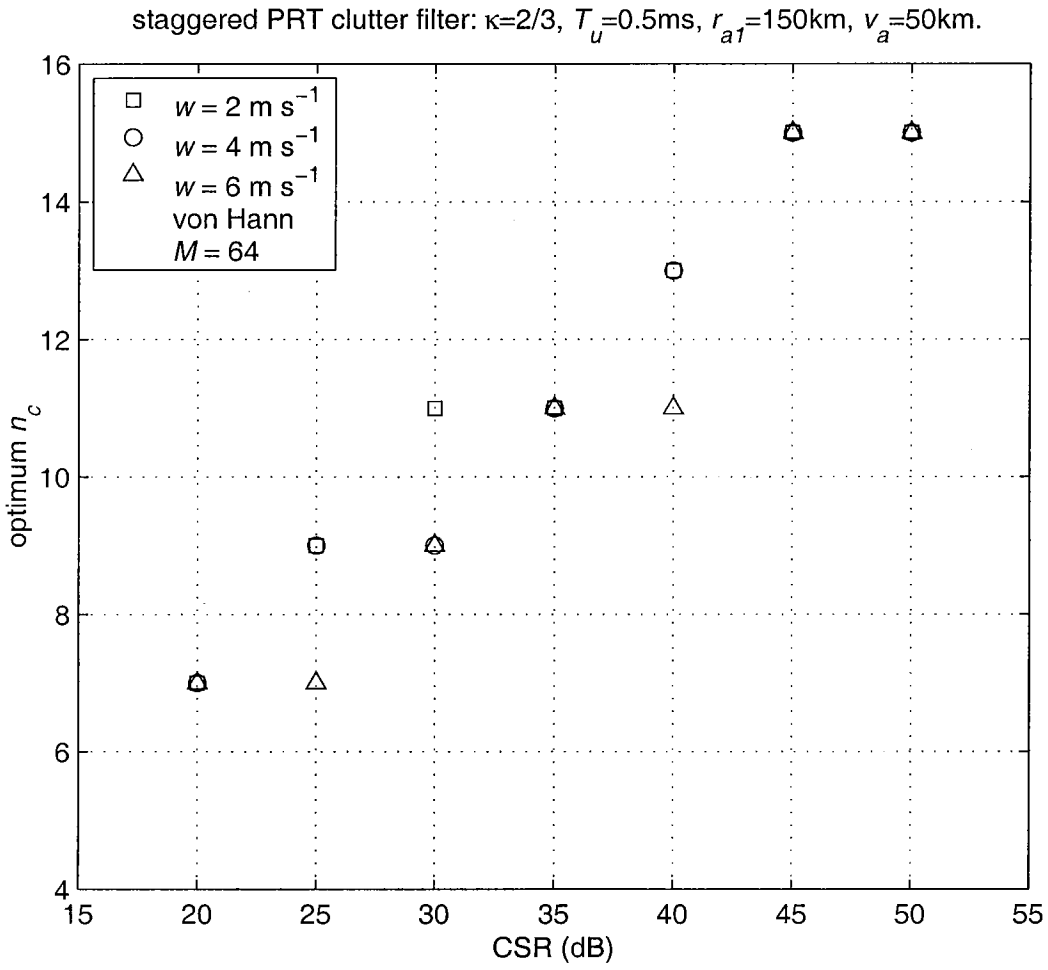

Fig.3.14. The optimum clutter filter width, n_c, versus the clutter-to-signal ratio, CSR, with spectrum width as a parameter, for M=64, and von Hann window.

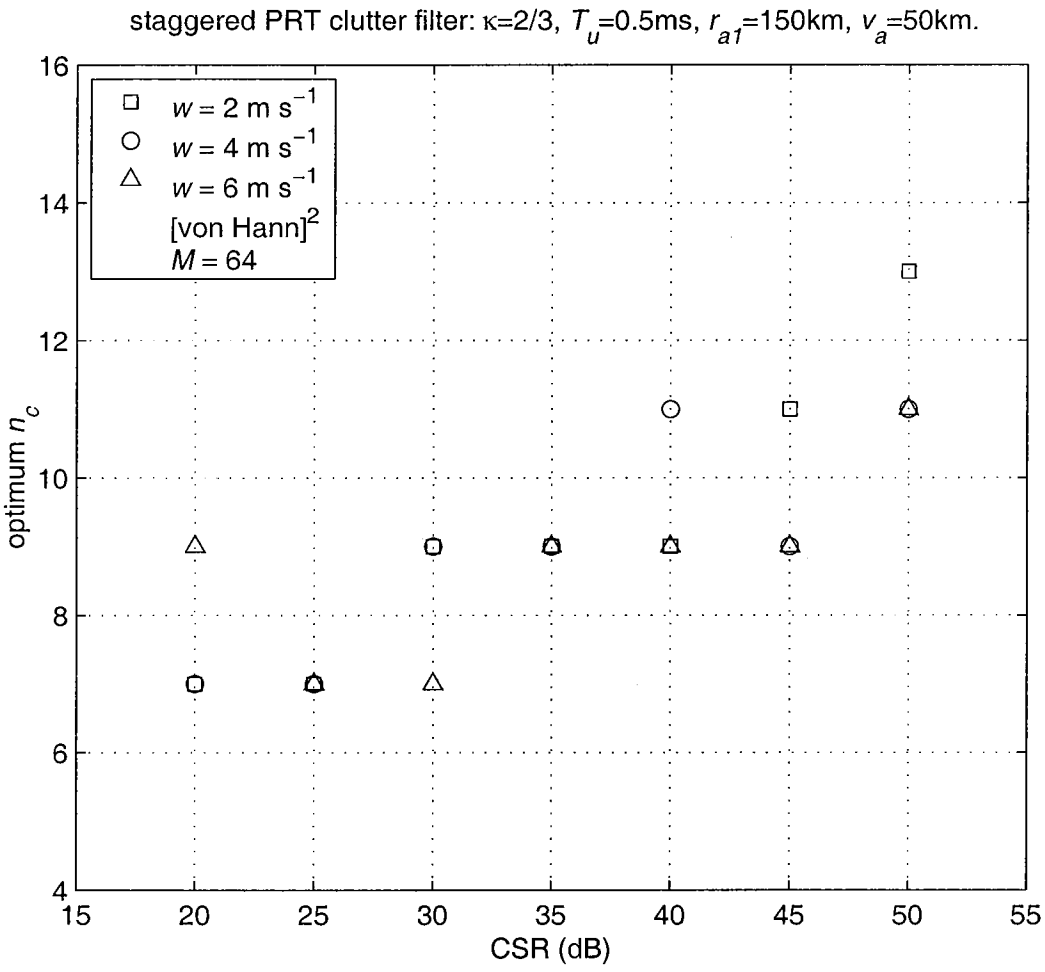

Fig.3.15. The optimum clutter filter width, n_c, versus the clutter-to-signal ratio, CSR, with spectrum width as a parameter, for M=64, and {von Hann}^{2} window.

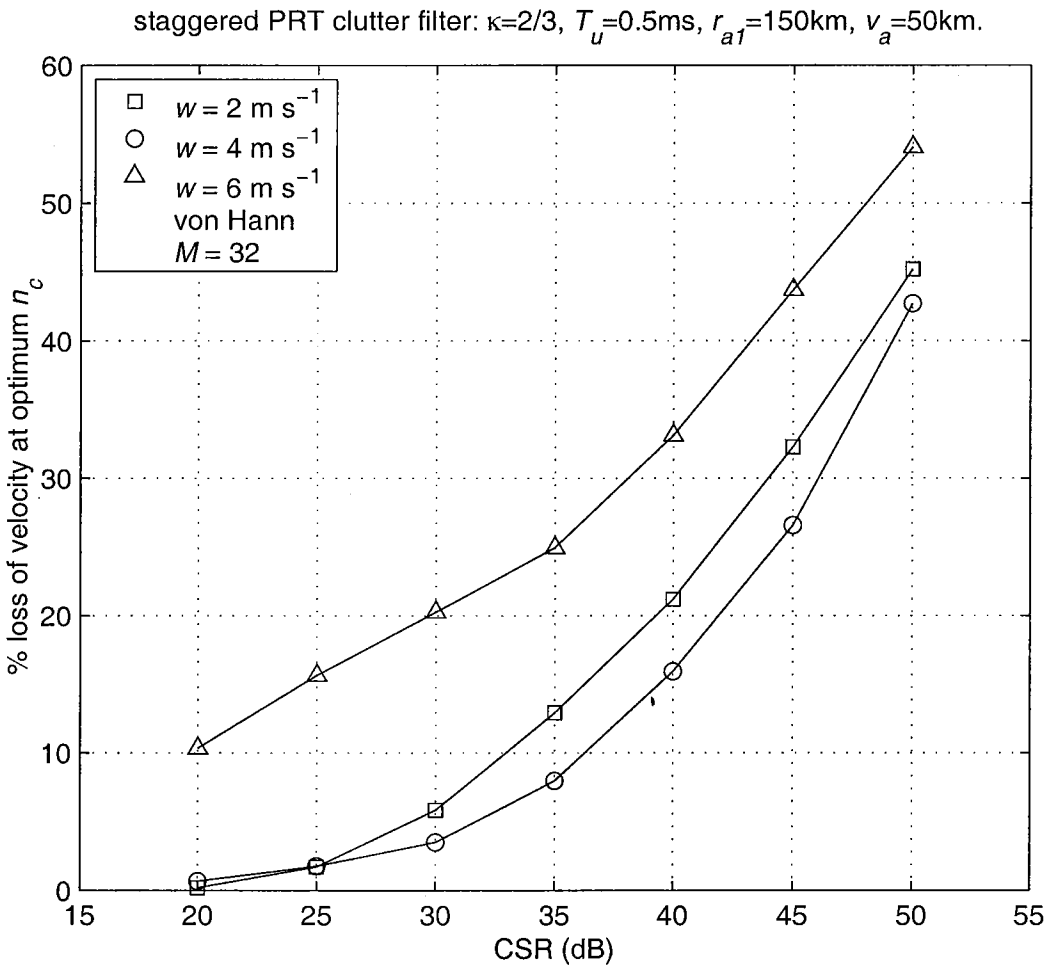

Fig.3.16. Percentage loss of velocity as a function of CSR, with spectrum width as a parameter, for M=32, and von Hann window.

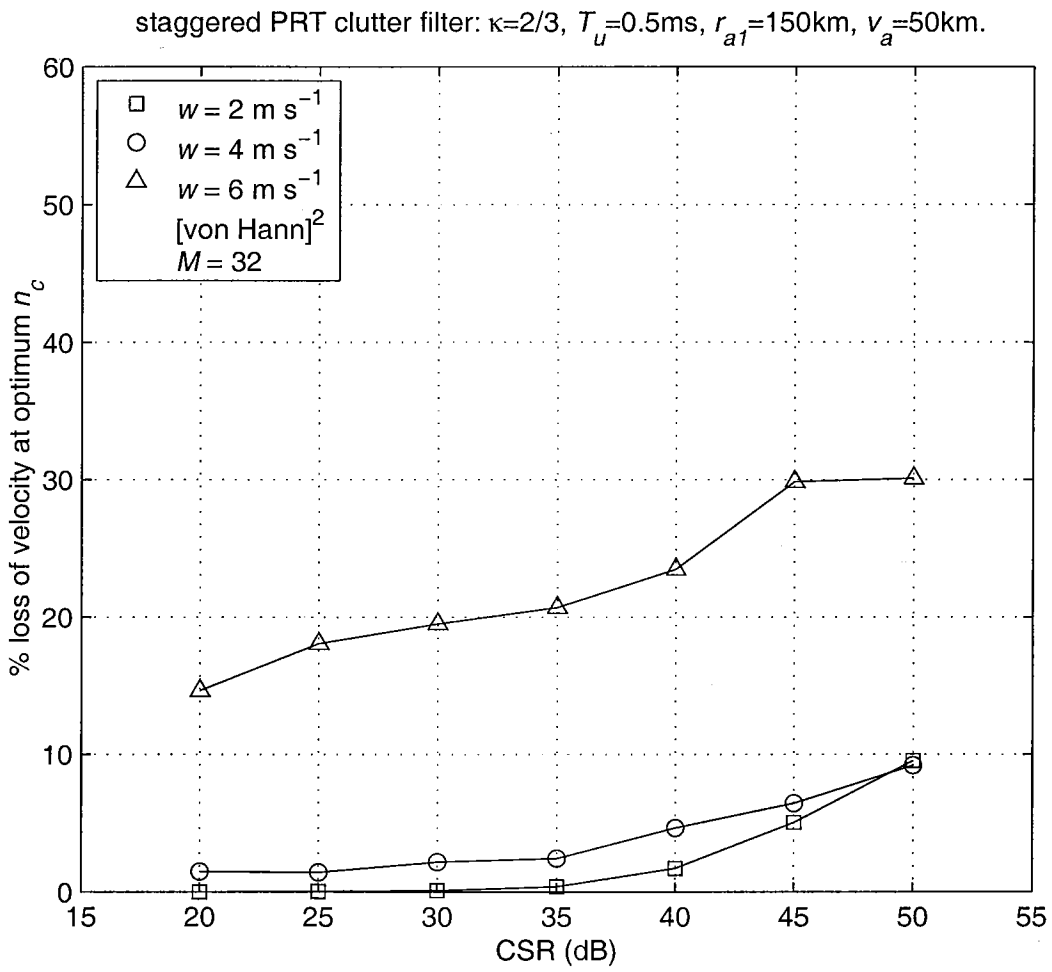

Fig.3.17. Percentage loss of velocity as a function of CSR, with spectrum width as a parameter, for M=32, and $\{\text{von Hann}\}^2$ window.

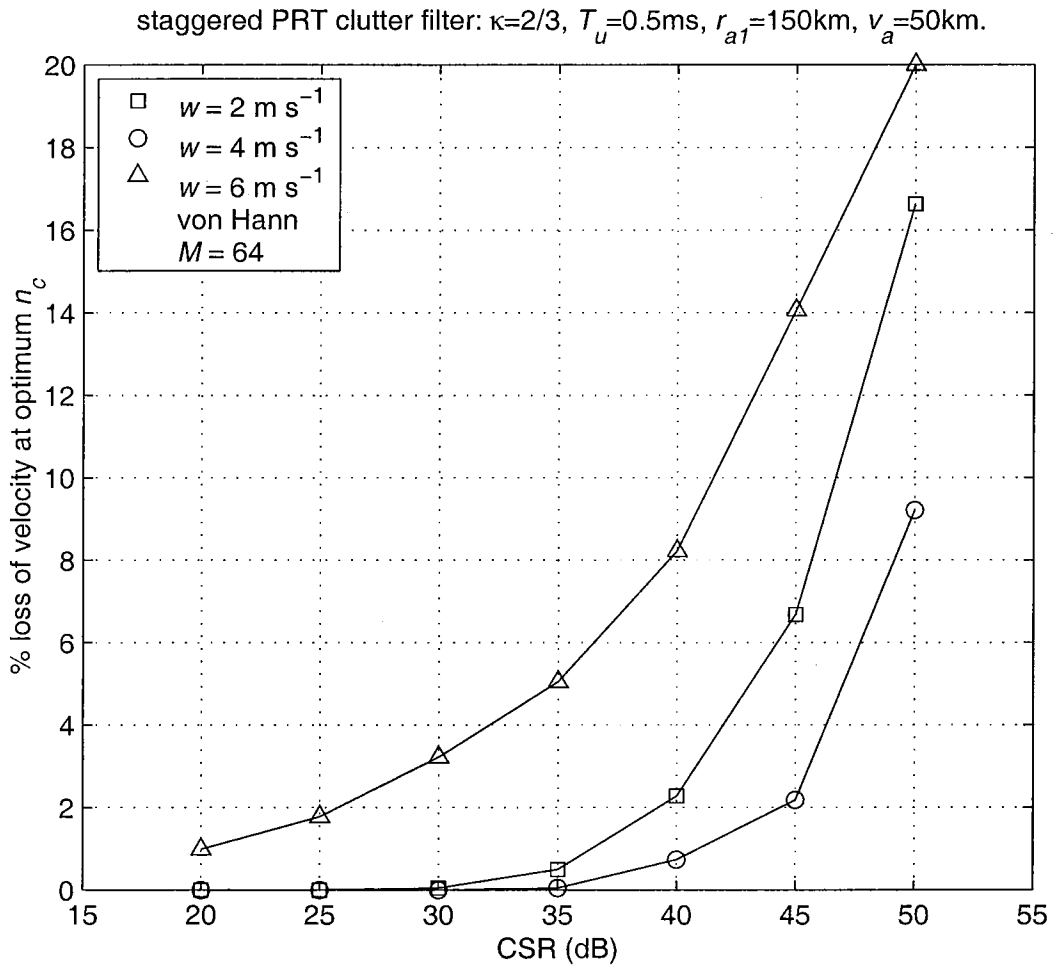

Fig.3.18. Percentage loss of velocity as a function of CSR, with spectrum width as a parameter, for M=64, and von Hann window.

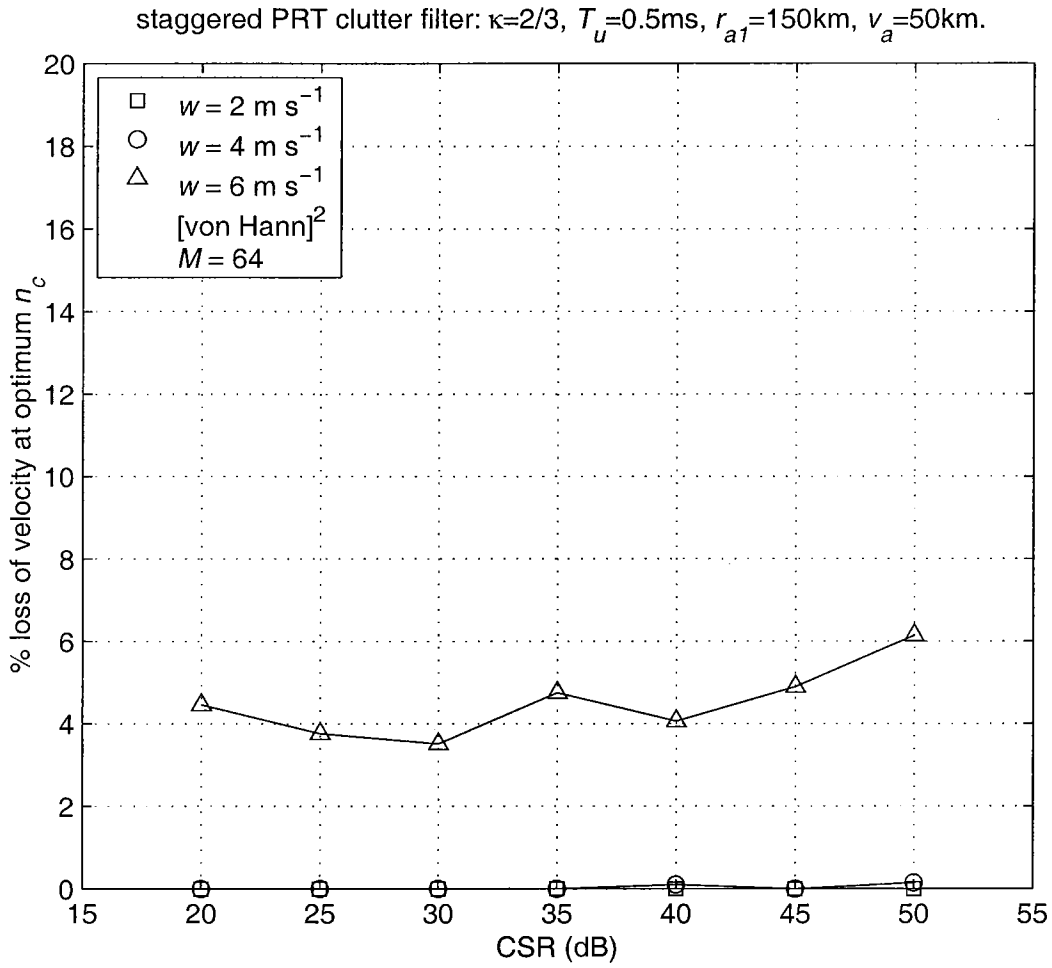

Fig.3.19. Percentage loss of velocity as a function of CSR, with spectrum width as a parameter, for M=64, and {von Hann}^{2} window.

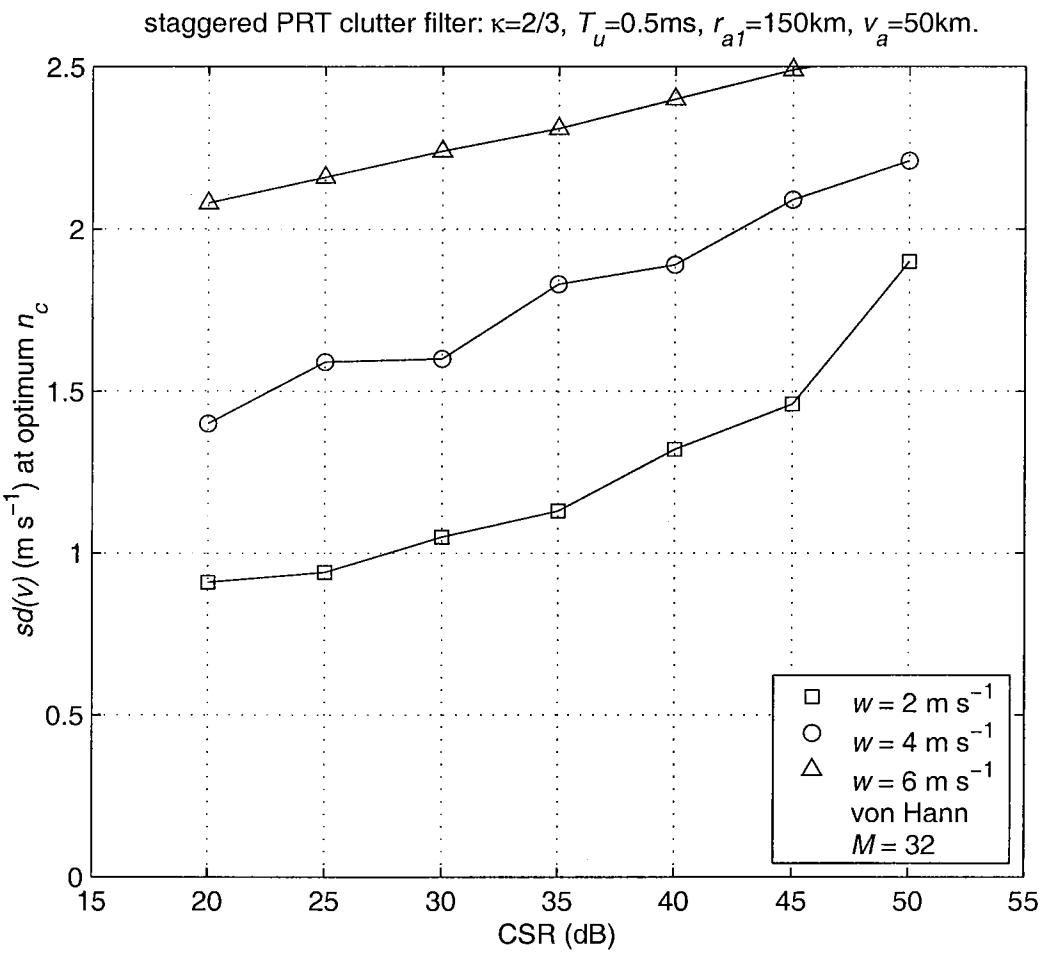

Fig.3.20. The standard error in the velocity estimate, *sd(v)*, at optimum clutter filter width, n_c, versus the clutter-to-signal ratio, CSR, with spectrum width as a parameter, for M=32, and von Hann window.

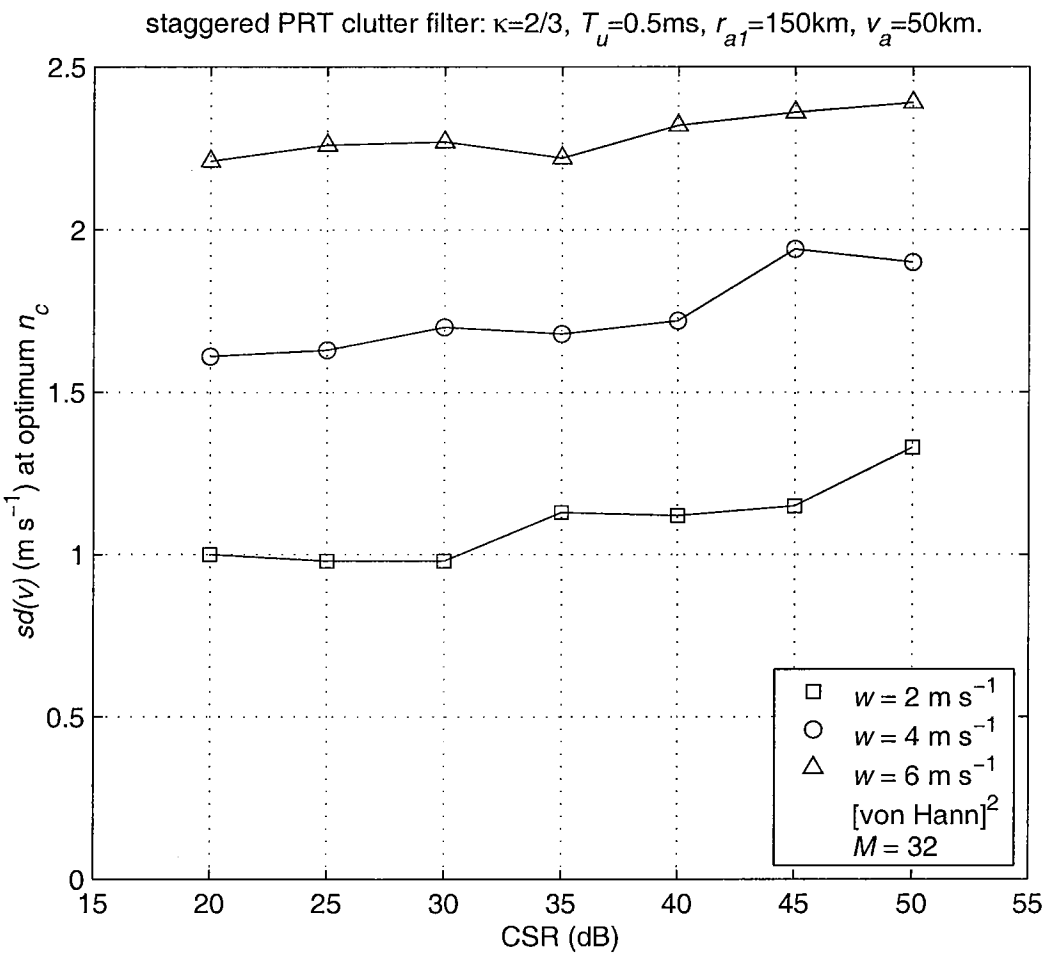

Fig.3.21. The *sd(v)* at optimum clutter filter width, n_c, versus the clutter-to-signal ratio, CSR, with spectrum width as a parameter, for M=32, and {von Hann}^{2} window.

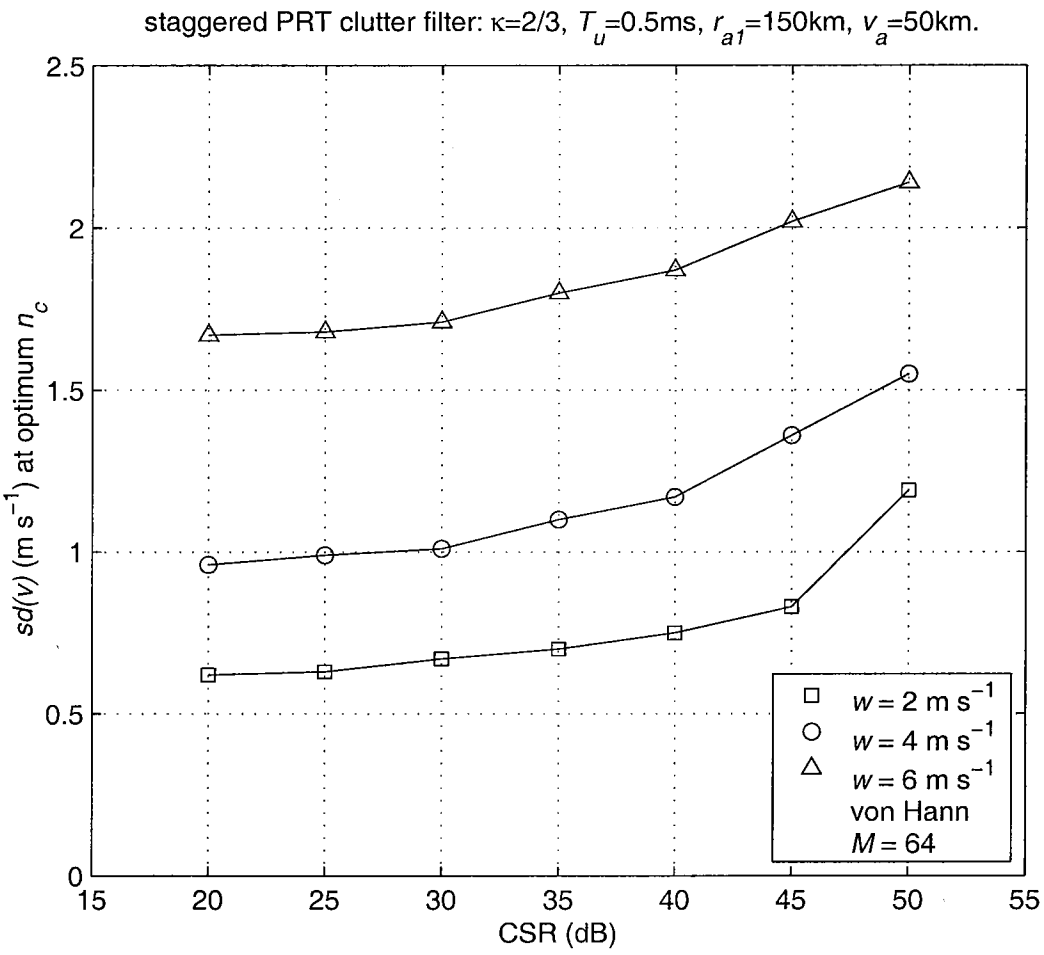

Fig.3.22. The *sd(v)* at optimum clutter filter width, n_c, versus the clutter-to-signal ratio, CSR, with spectrum width as a parameter, for M=64, and von Hann window.

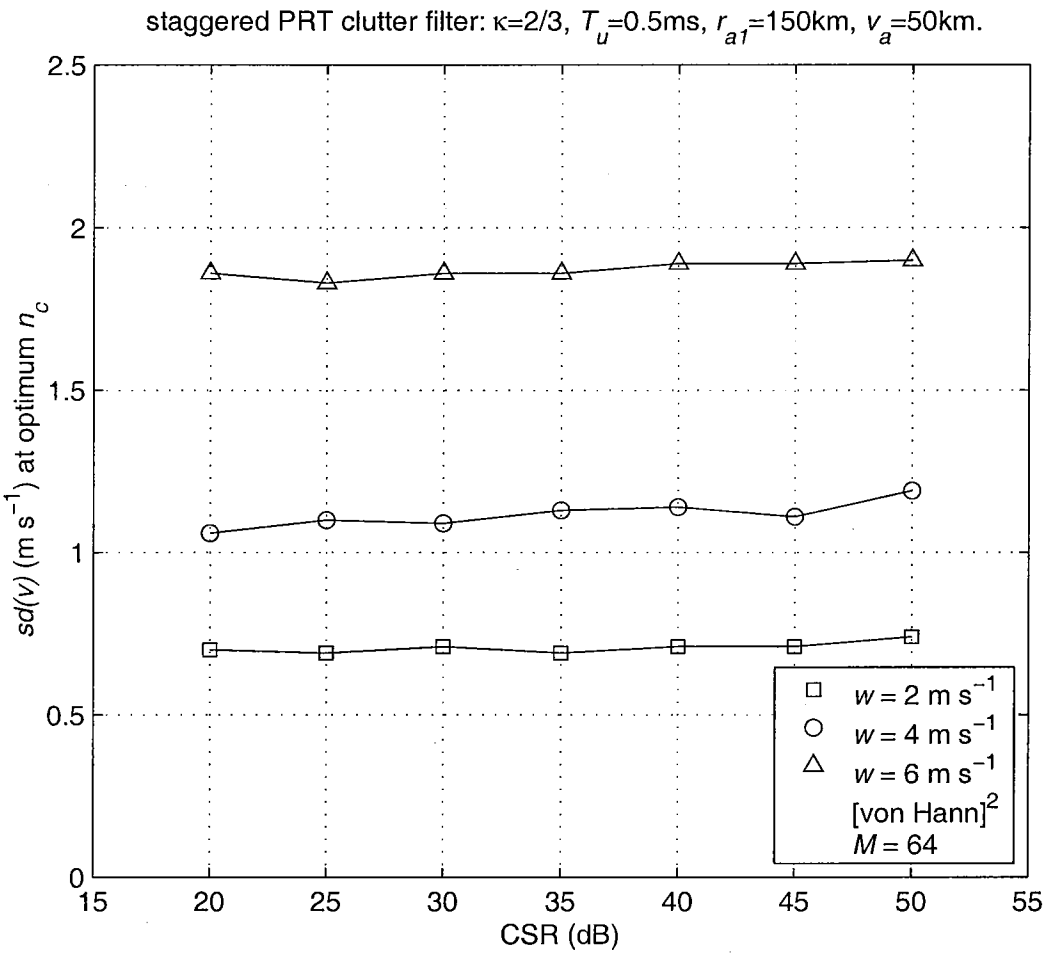

Fig.3.23. The *sd(v)* at optimum clutter filter width, n_c, versus the clutter-to-signal ratio, CSR, with spectrum width as a parameter, for M=64, and {von Hann}^{2} window.

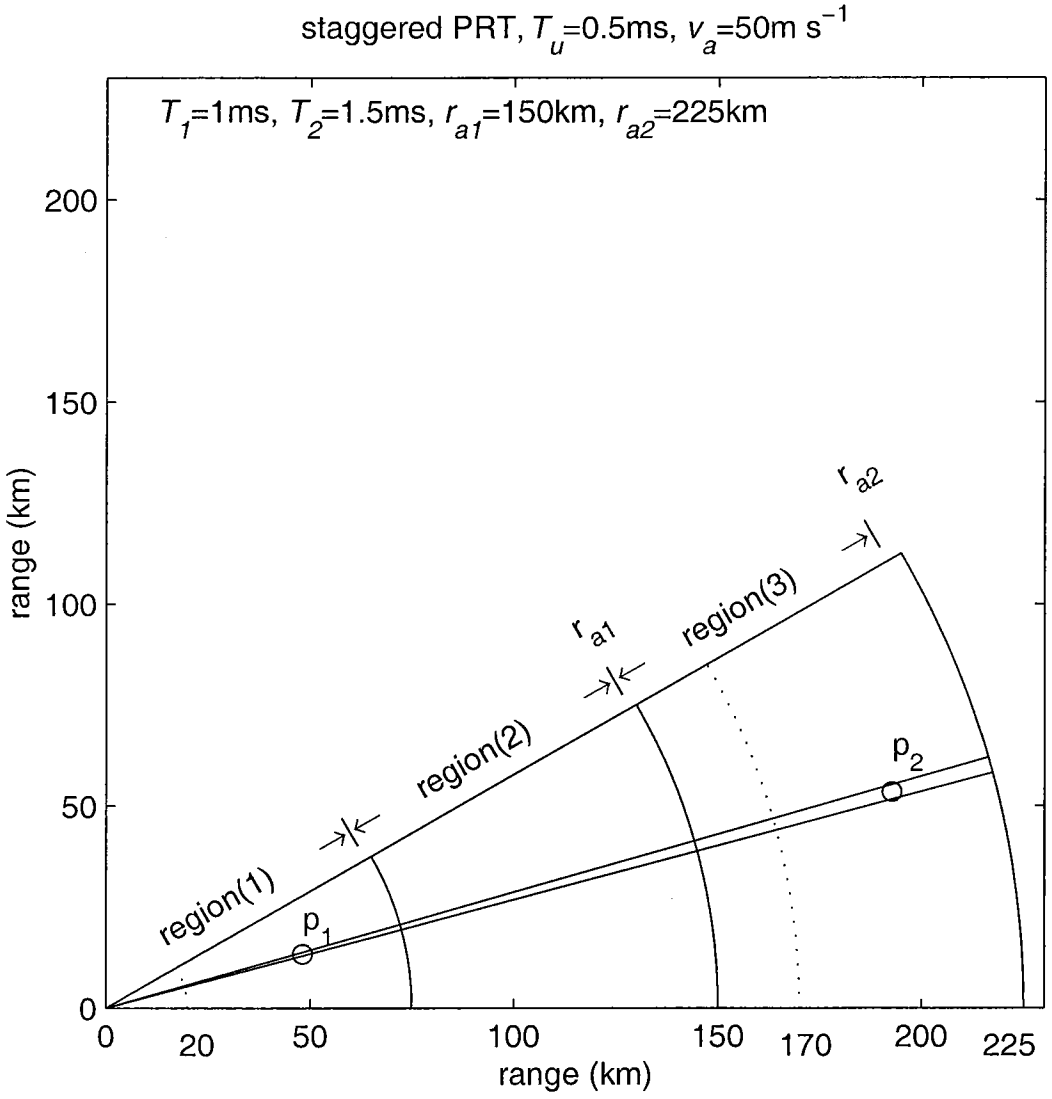

Fig. 4.1. Part of a PPI radar display showing the three $cT_u/2$ regions.

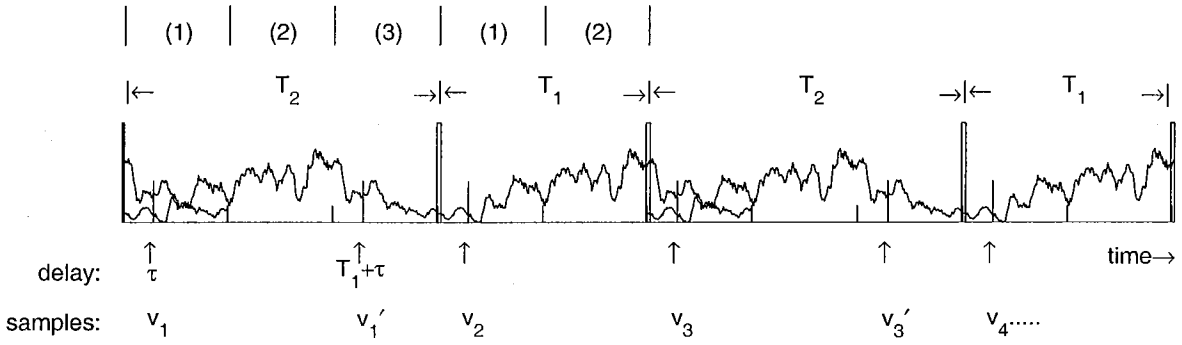

(a) Staggared PRT sampling scheme: one overlay, $\kappa = 2/3$.

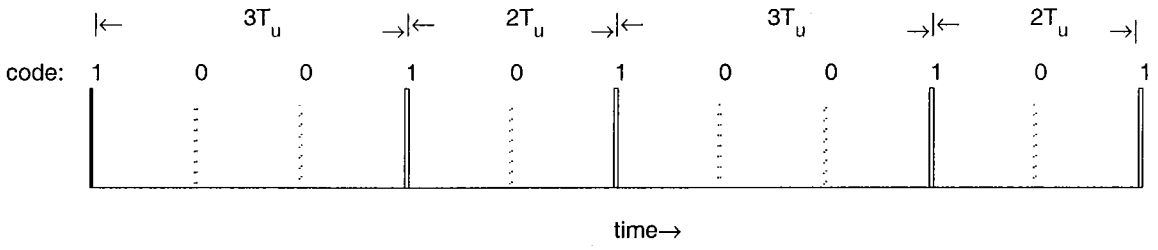

(b) Equivalent uniform PRT sampling for gate at τ.

Fig. 4.2. Staggered PRT sampling scheme - echoes with "one-overlay".

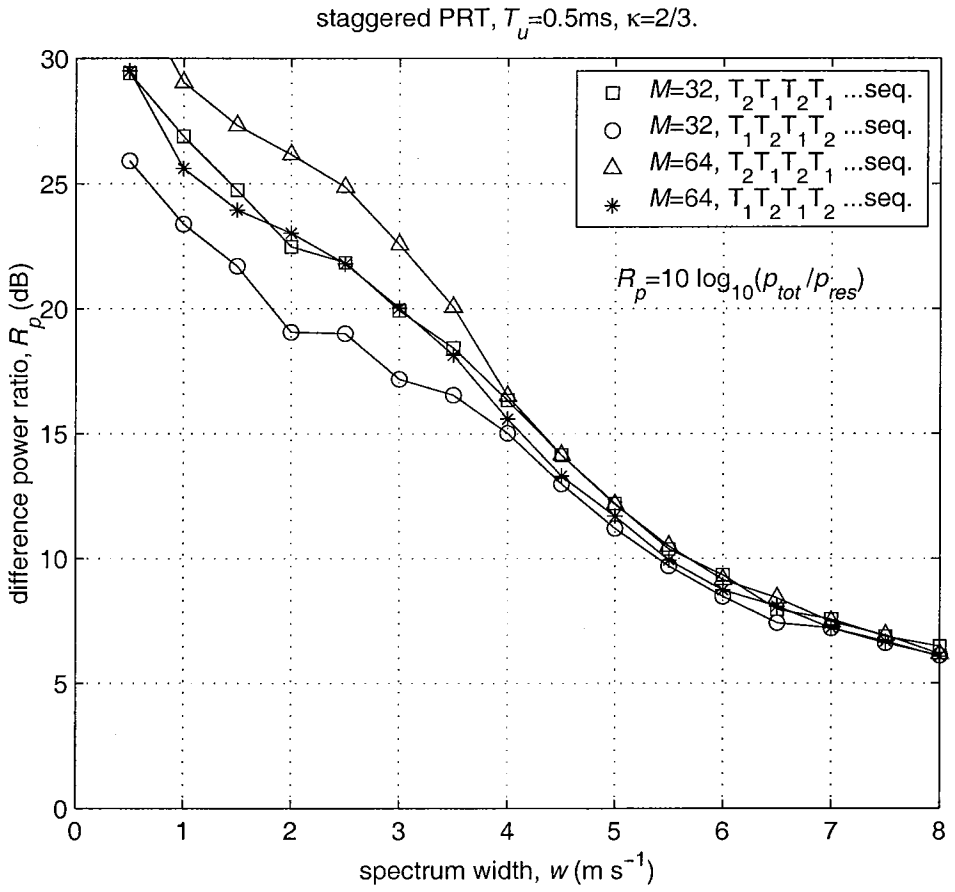

Fig. 4.3. Difference power ratio, R_p, versus the spectrum width of the overlaid signal for M=32 and 64.

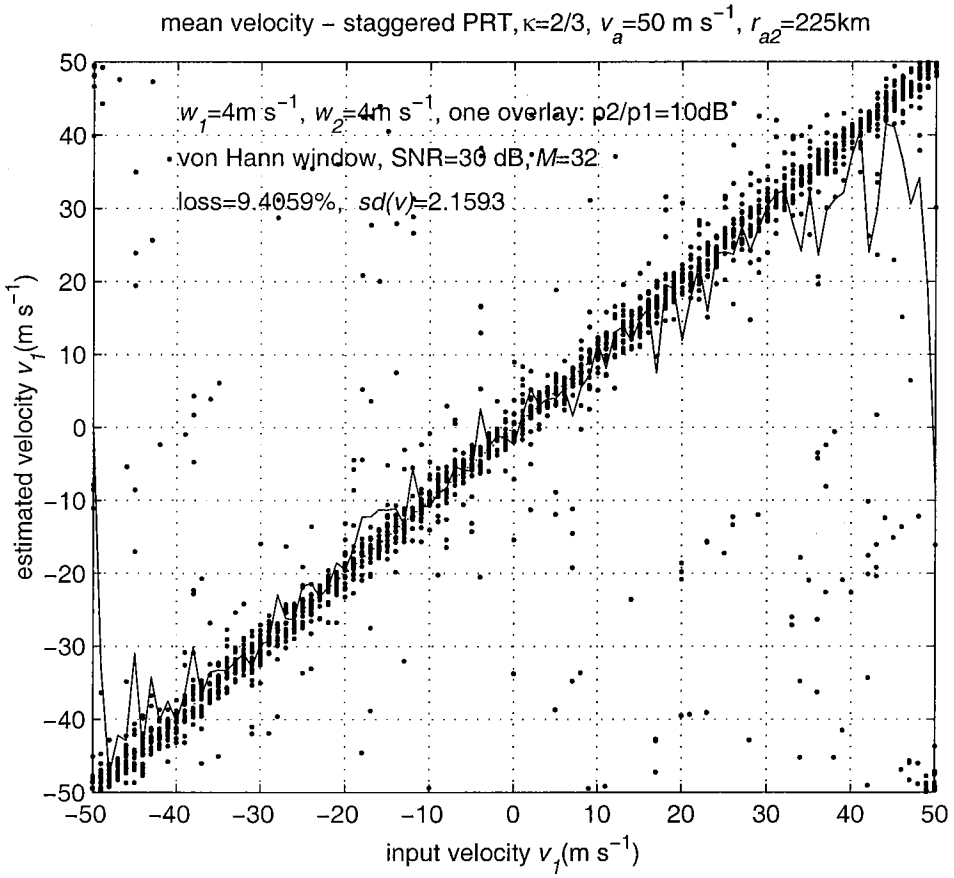

Fig. 4.4. Sample scatter plot of velocity recovery at the maximum overlay ratio, $\{p_2/p_1\}_{\max}$, for M=32, w_1=4 m s^{-1}, w_2=4 m s^{-1}. The abrupt change in data at the Nyquist velocity is an artifact inherent in plotting circular functions on a linear graph.

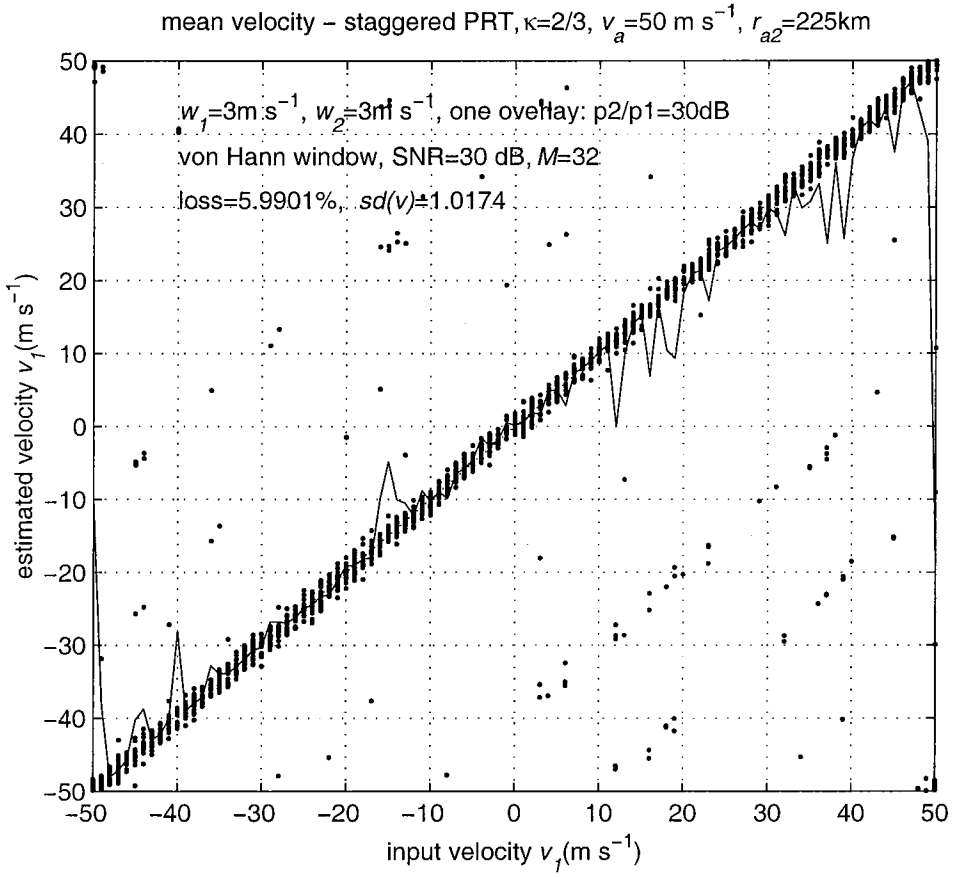

Fig. 4.5. Sample scatter plot of velocity recovery at the maximum overlay ratio, $\{p_2/p_1\}_{\max}$, for M=32, w_1=3 m s^{-1}, w_2=3 m s^{-1}. The abrupt change in data at the Nyquist velocity is an artifact inherent in plotting circular functions on a linear graph.

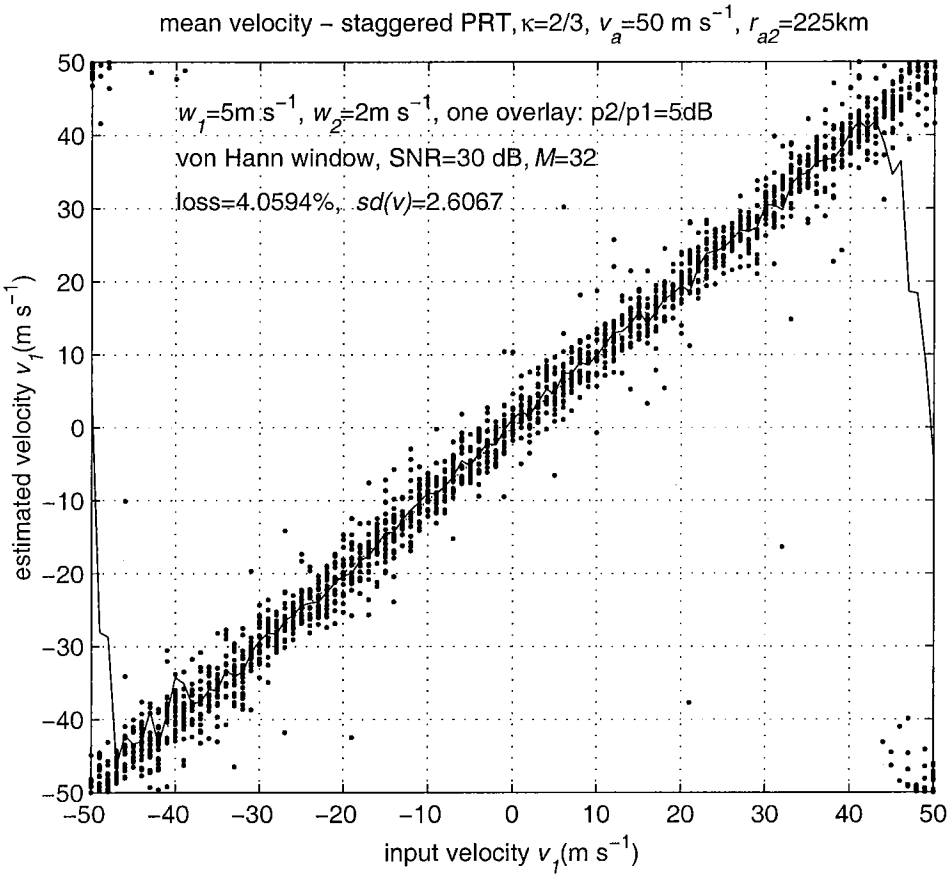

Fig. 4.6. Sample scatter plot of velocity recovery at the maximum overlay ratio, $\{p_2/p_1\}_{\max}$, for M=32, w_1=5 m s^{-1}, w_2=2 m s^{-1}. The abrupt change in data at the Nyquist velocity is an artifact inherent in plotting circular functions on a linear graph.

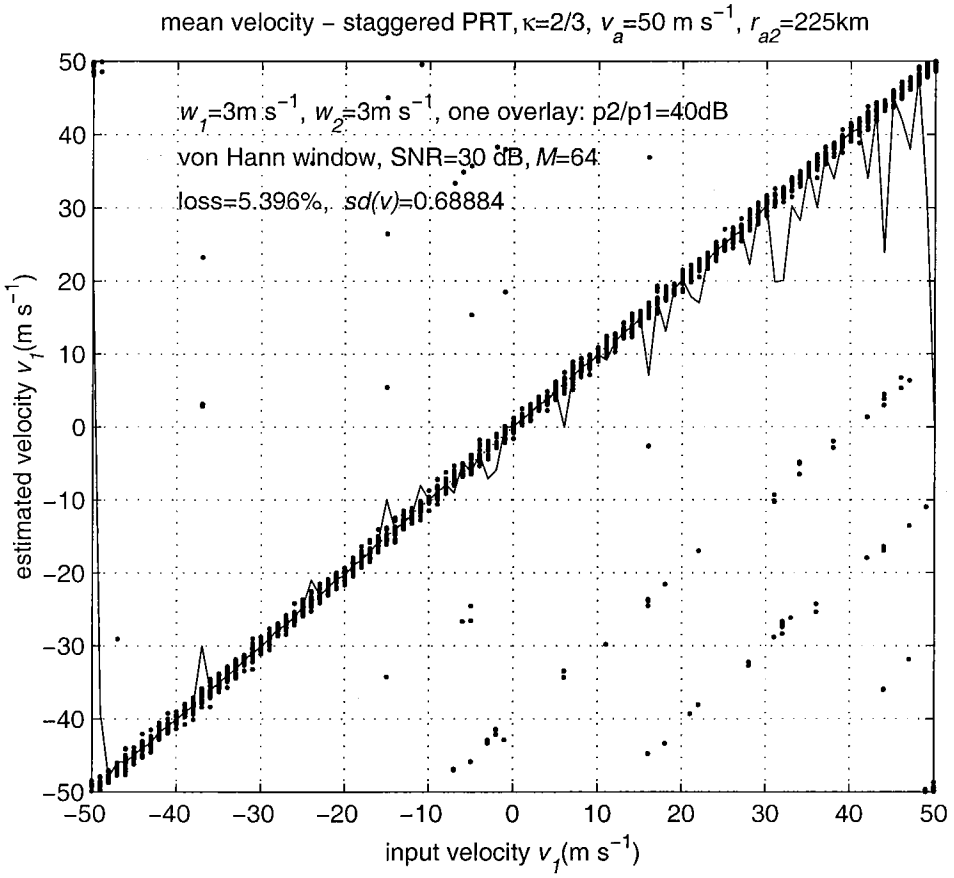

Fig. 4.7. Sample scatter plot of velocity recovery at the maximum overlay ratio, $\{p_2/p_1\}_{\max}$, for M=64, w_1=3 m s^{-1}, w_2=3 m s^{-1}. The abrupt change in data at the Nyquist velocity is an artifact inherent in plotting circular functions on a linear graph.

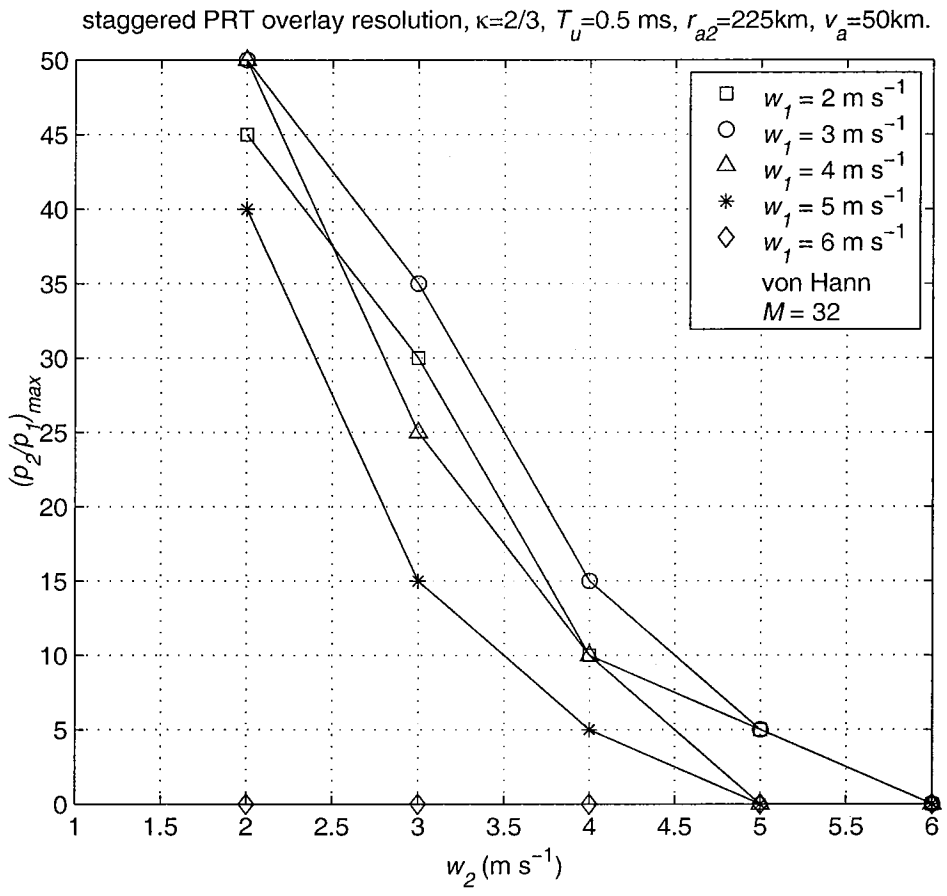

Fig. 4.8. The maximum overlay ratio, $\{p_2/p_1\}_{\max}$ (dB) as a function of spectrum width of the overlay signal for M=32.

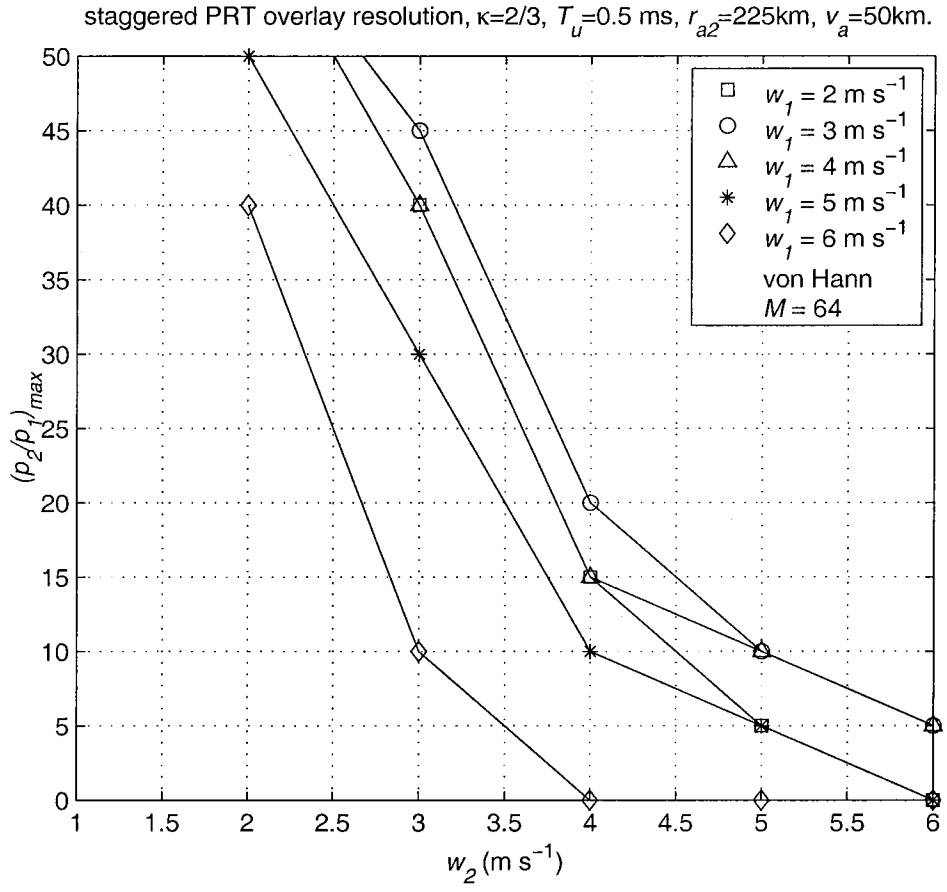

Fig. 4.9. The maximum overlay ratio, $\{p_2/p_1\}_{\max}$ (dB) as a function of spectrum width of the overlay signal for M=64.

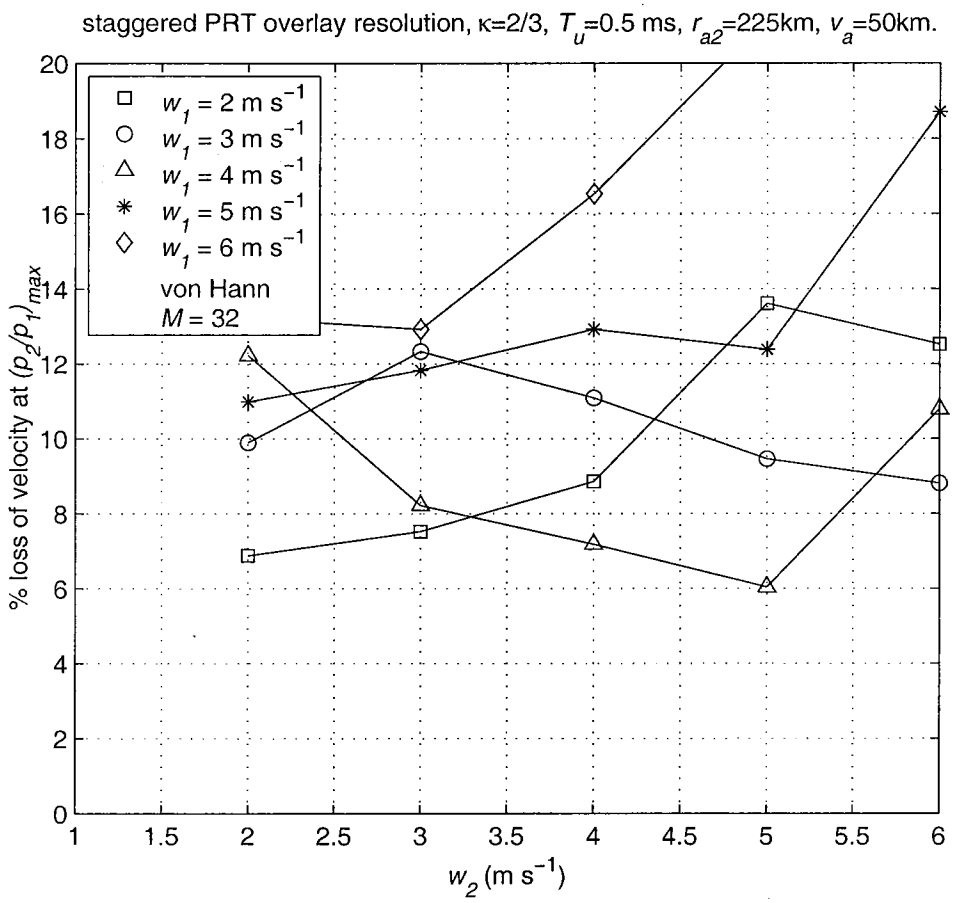

Fig. 4.10. The % loss at the maximum overlay ratio, $\{p_2/p_1\}_{\max}$ (dB) as a function of spectrum width of the overlay signal for M=32.

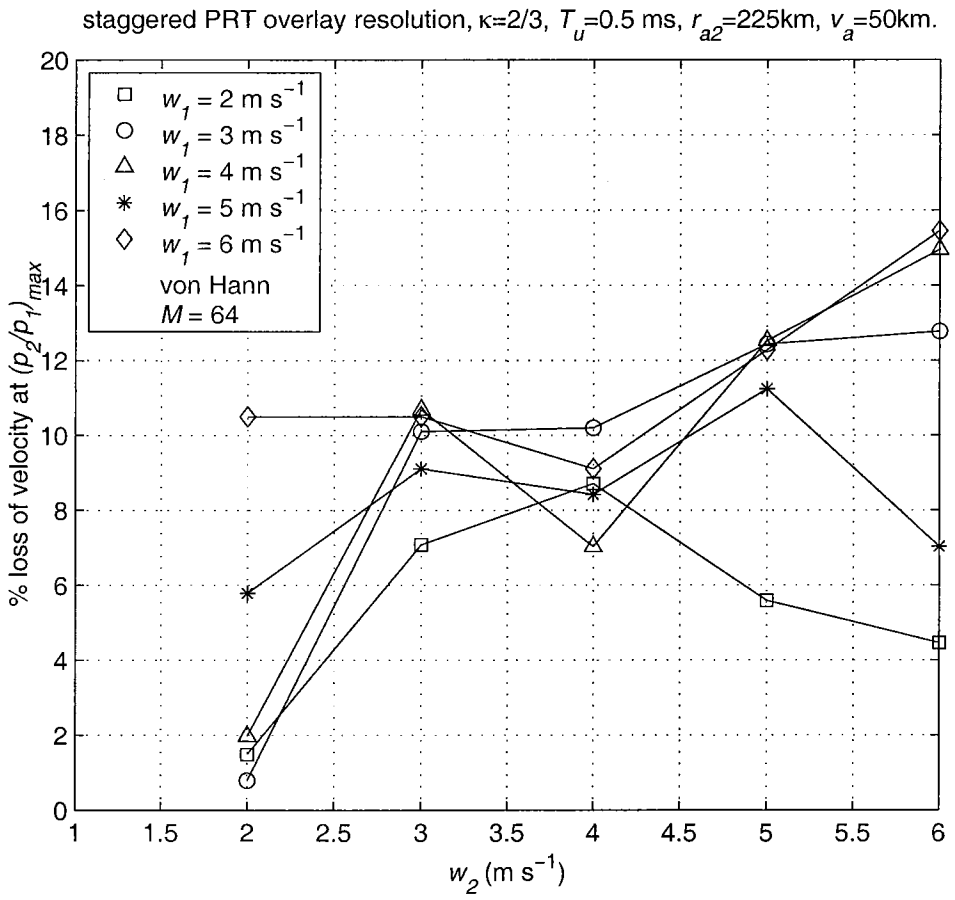

Fig. 4.11. The % loss at the maximum overlay ratio, $\{p_2/p_1\}_{\max}$ (dB) as a function of spectrum width of the overlay signal for M=64.

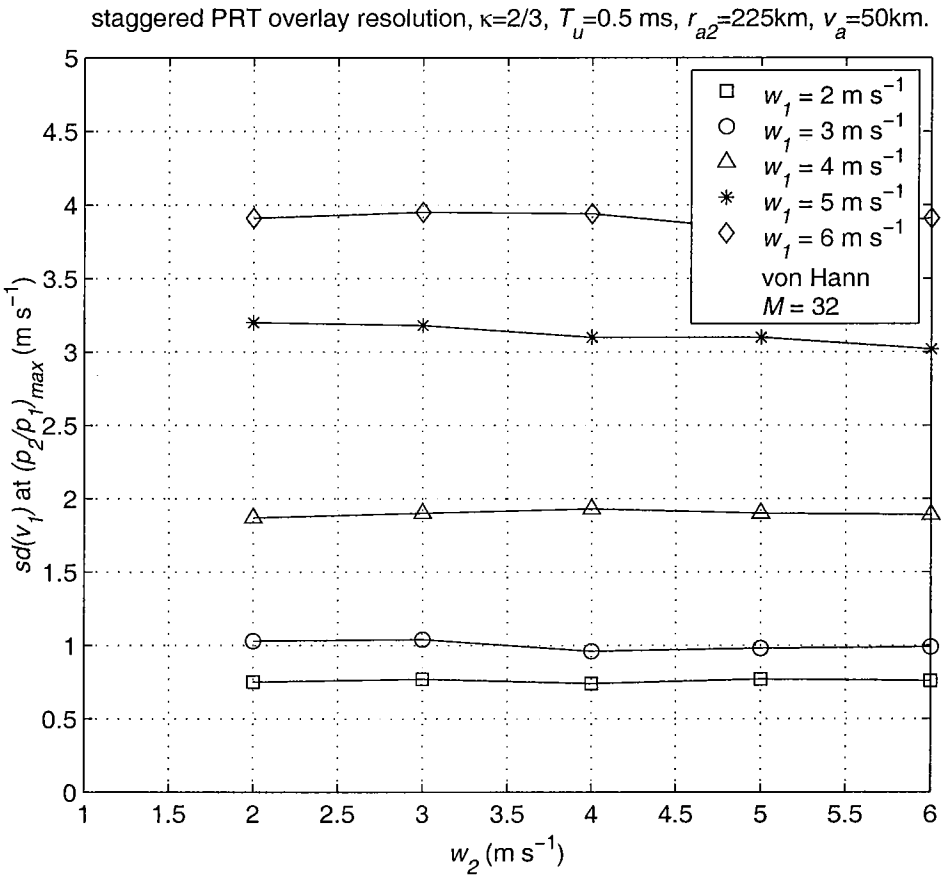

Fig. 4.12. The *sd(v)* at the maximum overlay ratio, $\{p_2/p_1\}_{\max}$ as a function of spectrum width of the overlay signal for M=32.

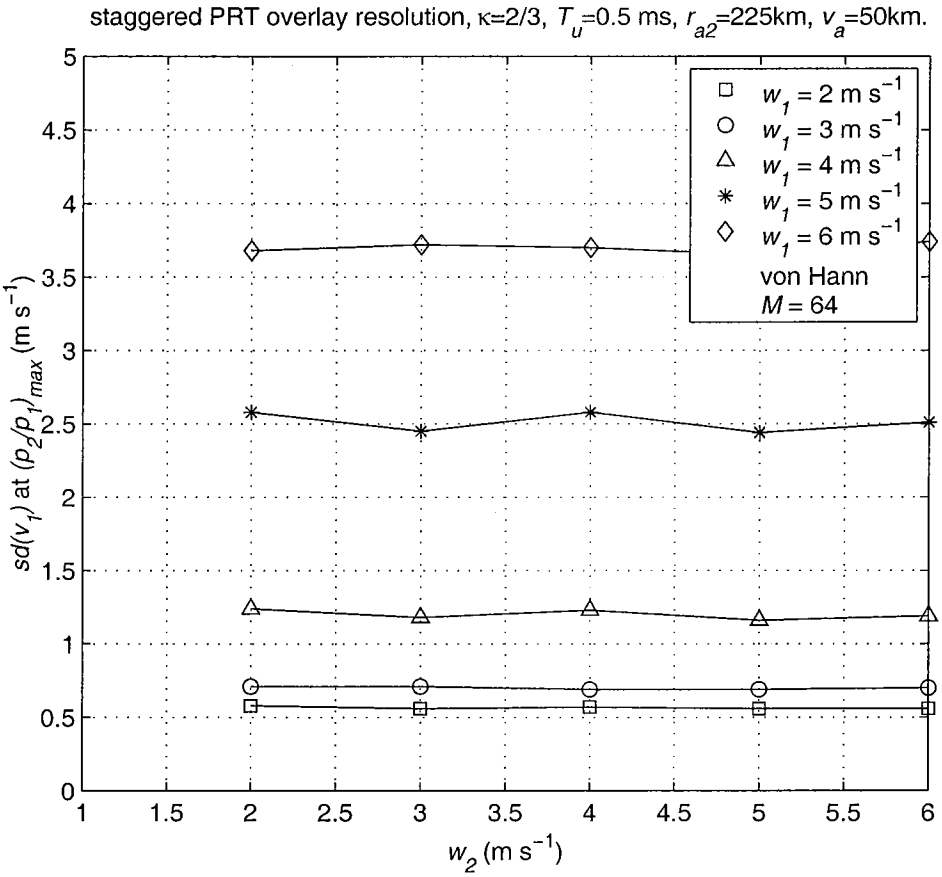

Fig. 4.13. The *sd(v)* at the maximum overlay ratio, $\{p_2/p_1\}_{\max}$ as a function of spectrum width of the overlay signal for M=64.

Table.5.1. Scan parameters for staggered PRT scheme(κ=2/3) - unambiguous range is r_{a2} with "one overlay" resolution. Velocity is estimated using pulse pair algorithm; von Hann window is used.

elv (deg)	dwell (ms)	range (km)[1]	T_1 (ms)	T_u (ms)	M	v_a (m s^{-1})	$2v_a/5$ (m s^{-1})	w_{max} (m s^{-1})[2]	$sd(v)$ (m s^{-1})[3] at w=4 m s^{-1}
0.50	104.1	460	2.04	1.02	41	24.46	9.78	2.8	7.20
1.45	101.0	379	1.68	0.84	48	29.68	11.87	3.39	2.06
2.40	69.9	303	1.34	0.67	42	37.13	14.85	4.24	0.85
3.35	53.9	247	1.10	0.55	39	45.55	18.22	5.21	0.82
4.30	53.9	207	0.92	0.46	47	54.35	21.74	6.21	0.77
5.25	55.9	177	0.78	0.39	57	63.56	25.42	7.26	0.76
6.20	55.9	154	0.68	0.34	65	73.05	29.22	8.35	0.73
7.50	39.2	131	0.58	0.29	54	85.88	35.35	9.81	0.86
8.70	39.9	115	0.51	0.26	62	97.83	39.13	11.18	0.85
10.0	39.9	100	0.44	0.22	72	112.50	45.00	12.86	0.89
12.0	39.9	85	0.38	0.19	84	132.35	52.94	15.13	0.84
14.0	39.9	73	0.32	0.16	98	154.11	61.64	17.61	0.87
16.7	39.9	62	0.28	0.14	116	181.45	72.58	20.74	0.84
19.5	39.9	54	0.24	0.12	133	208.33	83.33	23.81	0.98

Note:

(1) The maximum range is calculated based on a maximum height of 18km for all elevations except 0.5°, for which it is 16km.

(2) The values of w_{max} are calculated for M=64. These cause an error of less than about 1.5 m s^{-1} if there are no overlaid echoes.

(3) The $sd(v)$ is computed for the no-overlay case, and no window is used. With von Hann window and overlay resolution the value is higher (see table 5.2).

Table. 5.2. A proposed volume coverage pattern for the WSR-88D (revised).

(Proposed alternative to volume coverage pattern-11)

Elev. deg	AZ rate °/sec	WF Type	M	T_u [2] ms	v_a m/s	r_a km	max[3] p_1/p_2 dB	standard errors[1]		
								$sd(p)$ dB	$sd(v)$ m s^{-1}	$sd(w)$ m s^{-1}
0.5	18.7	CS, 1	17	3.11	-	466		1.12	-	-
0.5	19.2	SZ(8/64)	52	0.78	32.05	234	20	1.53, 1.87	1.02, 1.29	0.68, 1.37
1.45	19.8	CS, 1	16	3.11	-	466		1.2	-	-
1.45	19.2	SZ(8/64)	52	0.78	32.05	234	20	1.53, 1.87	1.02, 1.29	0.68, 1.37
2.4	16.1	ST(2/3)	45(44)	0.61	40.98	274	5	0.99, 1.02	2.71, 2.67	0.58, 0.57
3.35	17.9	ST(2/3)	43(44)	0.50	50.00	225	16	1.08, 1.14	1.01, 1.75	0.70, 0.64
4.3	17.9	ST(2/3)	46(44)	0.46	54.35	207	20	1.16, 1.09	1.04, 1.40	0.68, 0.70
5.25	17.5	ST(2/3)	56(56)	0.39	64.10	176	40.5	1.08, 1.11	0.99, 0.98	0.59, 0.59
6.2	17.5	ST(2/3)	65(64)	0.35	71.42	158	55	1.08, 1.12	0.95, 0.96	0.58, 0.59
7.5	25.2	ST(2/3)	53(52)	0.30	83.33	135	57	1.27, 1.30	1.17, 1.16	0.69, 0.65
8.7	25.4	ST(2/3)	53(52)	0.30	83.33	135	57	1.27, 1.30	1.17, 1.16	0.69, 0.65
10.0	25.4	ST(2/3)	53(52)	0.30	83.33	135	57	1.27, 1.30	1.17, 1.16	0.69, 0.65
12.0	25.5	ST(2/3)	53(52)	0.30	83.33	90		1.29	0.88	0.59
14.0	25.5	ST(2/3)	53(52)	0.30	83.33	90		1.29	0.88	0.59
16.7	25.6	ST(2/3)	53(52)	0.30	83.33	90		1.29	0.88	0.59
19.5	25.7	ST(2/3)	53(52)	0.30	83.33	90		1.29	0.88	0.59

Notes:

(1) For the SZ(8/64) scheme, (elevations 0.5 ° and 1.45 °) the standard errors are computed for w_1=4 m s^{-1} and w_2=4 m s^{-1}. The standard errors pairs are for the stronger and the weaker signals, p_1/p_2=20dB for SZ(8/64) scheme and with max (p_2/p_1) overlay for ST(2/3) scheme. The von Hann window is used for SZ(8/64) scheme and also for ST(2/3) scheme whenever one overlay resolution algorithm is applied, i.e.,the shaded part - elevations 2.4 ° to 10 °. A further reduction in the standard error is possible by taking about 30% more samples using the sample overlap scheme (see rep-3, p71).

(2) The short PRT for the ST(2/3) mode is $2T_u$. The Klystron duty cycle may limit the shortest PRT that can be used at higher elevation scans. (Here shortest T_1 is limited to 0.6 ms)

(3) The max (p_1/p_2) is computed at 10% loss of velocity data, and the standard errors given for ST(2/3) scheme is at this limiting (p_2/p_1).

Abbreviations: CS - contiguous surveillance (same as the original WSR-88D scheme).
SZ(n/M) - SZ phase coded contiguous Doppler.
ST(κ) - Staggered PRT.

Table. 5.3a. Performance of the staggered PRT overlay algorithm for different elevation scans.

elv. deg.	T_u ms	*M*	v_a m s^{-1}	r_{a2} km	p_2/p_1 dB	w_1	w_2 m s^{-1}	$sd(p_1)$ dB	$sd(p_2)$ dB	$sd(v_1)$ m s^{-1}	$sd(v_2)$ m s^{-1}	$sd(w_1)$ m s^{-1}	$sd(w_2)$ m s^{-1}	$loss_1$ %	$loss_2$ %
2.40	0.61	44	40.98	274.5	0.0	4	4	1.03	1.02	2.65	2.58	0.57	0.57	4.01	4.16
2.40	0.61	44	40.98	274.5	0.5	4	4	1.02	1.02	2.55	2.60	0.56	0.56	4.75	3.47
2.40	0.61	44	40.98	274.5	1.0	4	4	1.02	1.01	2.62	2.63	0.57	0.56	4.21	3.17
2.40	0.61	44	40.98	274.5	1.5	4	4	1.00	1.00	2.67	2.65	0.55	0.57	5.35	2.38
2.40	0.61	44	40.98	274.5	2.0	4	4	0.99	1.03	2.63	2.54	0.56	0.55	5.74	2.23
2.40	0.61	44	40.98	274.5	2.5	4	4	0.98	0.99	2.67	2.60	0.56	0.58	7.62	2.48
2.40	0.61	44	40.98	274.5	3.0	4	4	1.01	1.01	2.72	2.62	0.56	0.58	7.77	2.43
2.40	0.61	44	40.98	274.5	3.5	4	4	1.02	1.00	2.56	2.58	0.56	0.56	6.49	2.03
2.40	0.61	44	40.98	274.5	4.0	4	4	1.03	1.01	2.63	2.60	0.58	0.56	10.74	1.98
2.40	0.61	44	40.98	274.5	4.5	4	4	1.01	1.04	2.49	2.66	0.54	0.58	9.26	1.34
2.40	0.61	44	40.98	274.5	5.0	4	4	0.99	1.02	2.67	2.71	0.57	0.58	9.75	1.44
2.40	0.61	44	40.98	274.5	5.5	4	4	1.01	0.99	2.64	2.55	0.57	0.59	12.38	1.73
2.40	0.61	44	40.98	274.5	6.0	4	4	1.03	1.02	2.43	2.70	0.57	0.64	12.97	1.78
2.40	0.61	44	40.98	274.5	6.5	4	4	1.07	1.03	2.54	2.61	0.57	0.68	14.36	1.14
2.40	0.61	44	40.98	274.5	7.0	4	4	1.00	1.03	2.76	2.44	0.56	0.72	15.15	1.53
2.40	0.61	44	40.98	274.5	7.5	4	4	0.99	1.02	2.53	2.37	0.56	0.75	15.99	0.74
2.40	0.61	44	40.98	274.5	8.0	4	4	1.01	1.02	2.47	2.14	0.56	0.80	17.77	0.64
2.40	0.61	44	40.98	274.5	8.5	4	4	1.01	1.00	2.68	1.91	0.57	0.80	19.36	0.25
2.40	0.61	44	40.98	274.5	9.0	4	4	1.00	1.00	2.68	1.62	0.57	0.78	19.65	0.35
2.40	0.61	44	40.98	274.5	9.5	4	4	1.00	1.04	2.64	1.53	0.56	0.76	20.99	0.30
2.40	0.61	44	40.98	274.5	10.0	4	4	1.00	1.01	2.60	1.37	0.57	0.71	23.47	0.05
3.35	0.50	44	50.00	225.0	0.0	4	4	1.10	1.14	1.74	1.82	0.68	0.71	1.39	1.58
3.35	0.50	44	50.00	225.0	1.0	4	4	1.06	1.13	1.70	1.76	0.67	0.70	1.34	1.29
3.35	0.50	44	50.00	225.0	2.0	4	4	1.07	1.10	1.71	1.82	0.66	0.69	0.74	1.53
3.35	0.50	44	50.00	225.0	3.0	4	4	1.12	1.11	1.77	1.77	0.69	0.68	1.88	0.84
3.35	0.50	44	50.00	225.0	4.0	4	4	1.12	1.09	1.72	1.77	0.67	0.68	1.44	0.64
3.35	0.50	44	50.00	225.0	5.0	4	4	1.08	1.07	1.70	1.79	0.69	0.70	2.28	0.50
3.35	0.50	44	50.00	225.0	6.0	4	4	1.09	1.11	1.71	1.82	0.68	0.78	2.08	0.79
3.35	0.50	44	50.00	225.0	7.0	4	4	1.08	1.11	1.75	1.81	0.68	0.90	2.38	0.94
3.35	0.50	44	50.00	225.0	8.0	4	4	1.12	1.09	1.78	1.64	0.68	0.94	2.87	0.45
3.35	0.50	44	50.00	225.0	9.0	4	4	1.07	1.08	1.68	1.42	0.69	0.91	4.01	0.35
3.35	0.50	44	50.00	225.0	10.0	4	4	1.10	1.10	1.68	1.36	0.65	0.86	3.42	0.10
3.35	0.50	44	50.00	225.0	11.0	4	4	1.09	1.11	1.76	1.17	0.68	0.84	5.79	0.00
3.35	0.50	44	50.00	225.0	12.0	4	4	1.08	1.12	1.64	1.13	0.68	0.82	5.74	0.05
3.35	0.50	44	50.00	225.0	13.0	4	4	1.11	1.13	1.72	1.07	0.69	0.80	7.08	0.00
3.35	0.50	44	50.00	225.0	14.0	4	4	1.08	1.12	1.66	1.09	0.66	0.74	9.70	0.00
3.35	0.50	44	50.00	225.0	15.0	4	4	1.09	1.07	1.75	1.06	0.68	0.69	8.56	0.00
3.35	0.50	44	50.00	225.0	16.0	4	4	1.14	1.08	1.75	1.01	0.69	0.70	10.00	0.00
3.35	0.50	44	50.00	225.0	17.0	4	4	1.13	1.09	1.68	1.01	0.67	0.66	14.06	0.00
3.35	0.50	44	50.00	225.0	18.0	4	4	1.07	1.09	1.80	1.02	0.69	0.67	12.72	0.00
3.35	0.50	44	50.00	225.0	19.0	4	4	1.09	1.10	1.68	1.01	0.67	0.66	17.33	0.00
3.35	0.50	44	50.00	225.0	20.0	4	4	1.10	1.08	1.72	1.03	0.68	0.66	17.43	0.00

Table. 5.3b. Performance of the staggered PRT overlay algorithm for different elevation scans.

elv. deg.	T_u ms	*M*	v_a m s^{-1}	r_{a2} km	p_2/p_1 dB	w_1	w_2 m s^{-1}	$sd(p_1)$ dB	$sd(p_2)$ dB	$sd(v_1)$ m s^{-1}	$sd(v_2)$ m s^{-1}	$sd(w_1)$ m s^{-1}	$sd(w_2)$ m s^{-1}	$loss_1$ %	$loss_2$ %
4.30	0.46	44	54.35	207.0	0.0	4	4	1.14	1.14	1.42	1.53	0.68	0.70	0.69	0.50
4.30	0.46	44	54.35	207.0	1.3	4	4	1.14	1.16	1.49	1.34	0.71	0.68	0.59	0.64
4.30	0.46	44	54.35	207.0	2.5	4	4	1.14	1.15	1.46	1.52	0.69	0.73	0.25	0.84
4.30	0.46	44	54.35	207.0	3.8	4	4	1.11	1.16	1.51	1.42	0.69	0.69	0.69	0.40
4.30	0.46	44	54.35	207.0	5.0	4	4	1.17	1.13	1.38	1.50	0.71	0.75	0.64	0.54
4.30	0.46	44	54.35	207.0	6.3	4	4	1.15	1.14	1.47	1.51	0.69	0.89	0.74	0.25
4.30	0.46	44	54.35	207.0	7.5	4	4	1.15	1.16	1.41	1.45	0.71	0.97	1.24	0.35
4.30	0.46	44	54.35	207.0	8.8	4	4	1.18	1.11	1.45	1.31	0.69	0.98	1.44	0.20
4.30	0.46	44	54.35	207.0	10.0	4	4	1.12	1.14	1.45	1.34	0.69	0.97	1.34	0.15
4.30	0.46	44	54.35	207.0	11.3	4	4	1.15	1.14	1.34	1.20	0.67	0.93	1.73	0.05
4.30	0.46	44	54.35	207.0	12.5	4	4	1.16	1.13	1.33	1.17	0.69	0.86	2.92	0.00
4.30	0.46	44	54.35	207.0	13.8	4	4	1.13	1.13	1.43	1.12	0.71	0.80	3.27	0.00
4.30	0.46	44	54.35	207.0	15.0	4	4	1.11	1.12	1.41	1.11	0.71	0.77	3.66	0.00
4.30	0.46	44	54.35	207.0	16.3	4	4	1.11	1.13	1.46	1.06	0.70	0.73	4.55	0.00
4.30	0.46	44	54.35	207.0	17.5	4	4	1.13	1.15	1.37	1.03	0.69	0.71	6.29	0.00
4.30	0.46	44	54.35	207.0	18.8	4	4	1.15	1.12	1.40	1.04	0.69	0.69	6.98	0.00
4.30	0.46	44	54.35	207.0	20.0	4	4	1.09	1.16	1.40	1.04	0.70	0.68	7.18	0.00
4.30	0.46	44	54.35	207.0	21.3	4	4	1.15	1.11	1.42	1.03	0.70	0.65	10.40	0.00
4.30	0.46	44	54.35	207.0	22.5	4	4	1.12	1.15	1.40	1.02	0.68	0.63	11.53	0.00
4.30	0.46	44	54.35	207.0	23.8	4	4	1.12	1.15	1.34	1.01	0.70	0.63	12.33	0.00
4.30	0.46	44	54.35	207.0	25.0	4	4	1.16	1.13	1.30	1.03	0.69	0.63	14.41	0.00
5.25	0.39	56	64.10	175.5	0.0	4	4	1.09	1.08	0.99	0.98	0.58	0.59	0.05	0.05
5.25	0.39	56	64.10	175.5	2.3	4	4	1.11	1.09	0.98	1.03	0.59	0.59	0.00	0.00
5.25	0.39	56	64.10	175.5	4.5	4	4	1.12	1.08	0.99	1.03	0.59	0.65	0.00	0.00
5.25	0.39	56	64.10	175.5	6.8	4	4	1.08	1.10	1.02	1.07	0.59	1.00	0.00	0.00
5.25	0.39	56	64.10	175.5	9.0	4	4	1.13	1.11	1.01	1.15	0.60	1.15	0.00	0.00
5.25	0.39	56	64.10	175.5	11.3	4	4	1.13	1.11	1.00	1.20	0.60	1.09	0.00	0.00
5.25	0.39	56	64.10	175.5	13.5	4	4	1.12	1.09	0.99	1.11	0.59	0.93	0.10	0.00
5.25	0.39	56	64.10	175.5	15.8	4	4	1.11	1.10	0.99	1.06	0.59	0.77	0.00	0.00
5.25	0.39	56	64.10	175.5	18.0	4	4	1.11	1.12	1.00	1.04	0.61	0.71	0.05	0.00
5.25	0.39	56	64.10	175.5	20.3	4	4	1.13	1.11	1.03	1.02	0.59	0.65	0.25	0.00
5.25	0.39	56	64.10	175.5	22.5	4	4	1.08	1.08	1.05	0.98	0.59	0.63	0.30	0.00
5.25	0.39	56	64.10	175.5	24.8	4	4	1.11	1.09	0.98	1.00	0.60	0.64	0.50	0.00
5.25	0.39	56	64.10	175.5	27.0	4	4	1.09	1.11	1.02	0.95	0.58	0.59	1.49	0.00
5.25	0.39	56	64.10	175.5	29.3	4	4	1.09	1.07	1.01	0.98	0.58	0.60	1.73	0.00
5.25	0.39	56	64.10	175.5	31.5	4	4	1.11	1.09	1.00	0.99	0.59	0.61	2.77	0.00
5.25	0.39	56	64.10	175.5	33.8	4	4	1.11	1.06	0.99	0.99	0.59	0.60	3.56	0.00
5.25	0.39	56	64.10	175.5	36.0	4	4	1.10	1.11	0.98	0.99	0.59	0.60	4.85	0.00
5.25	0.39	56	64.10	175.5	38.3	4	4	1.12	1.09	1.01	0.99	0.59	0.59	8.12	0.00
5.25	0.39	56	64.10	175.5	40.5	4	4	1.11	1.08	0.98	0.99	0.59	0.59	8.76	0.00
5.25	0.39	56	64.10	175.5	42.8	4	4	1.12	1.13	0.97	1.00	0.61	0.58	14.50	0.00
5.25	0.39	56	64.10	175.5	45.0	4	4	1.11	1.13	0.97	0.98	0.60	0.60	15.25	0.00

Table. 5.3c. Performance of the staggered PRT overlay algorithm for different elevation scans.

elv. deg.	T_u ms	*M*	v_a m s^{-1}	r_{a2} km	p_2/p_1 dB	w_1	w_2 m s^{-1}	$sd(p_1)$ dB	$sd(p_2)$ dB	$sd(v_1)$ m s^{-1}	$sd(v_2)$ m s^{-1}	$sd(w_1)$ m s^{-1}	$sd(w_2)$ m s^{-1}	$loss_1$ %	$loss_2$ %
6.20	0.35	64	71.43	157.5	0.0	4	4	1.10	1.02	0.96	0.95	0.56	0.57	0.00	0.00
6.20	0.35	64	71.43	157.5	2.8	4	4	1.07	1.08	1.00	0.95	0.58	0.57	0.00	0.00
6.20	0.35	64	71.43	157.5	5.5	4	4	1.10	1.08	0.97	0.96	0.58	0.75	0.00	0.00
6.20	0.35	64	71.43	157.5	8.3	4	4	1.06	1.10	0.97	1.22	0.58	1.43	0.00	0.05
6.20	0.35	64	71.43	157.5	11.0	4	4	1.10	1.09	0.97	1.22	0.58	1.25	0.00	0.00
6.20	0.35	64	71.43	157.5	13.8	4	4	1.07	1.11	0.95	1.11	0.59	1.02	0.00	0.00
6.20	0.35	64	71.43	157.5	16.5	4	4	1.06	1.06	0.95	1.03	0.58	0.81	0.00	0.00
6.20	0.35	64	71.43	157.5	19.3	4	4	1.09	1.11	0.99	1.00	0.58	0.70	0.00	0.00
6.20	0.35	64	71.43	157.5	22.0	4	4	1.10	1.10	0.97	0.96	0.58	0.63	0.00	0.00
6.20	0.35	64	71.43	157.5	24.8	4	4	1.08	1.07	0.94	0.98	0.58	0.61	0.00	0.00
6.20	0.35	64	71.43	157.5	27.5	4	4	1.08	1.06	0.97	0.98	0.58	0.58	0.05	0.00
6.20	0.35	64	71.43	157.5	30.3	4	4	1.12	1.11	0.96	0.97	0.58	0.59	0.10	0.00
6.20	0.35	64	71.43	157.5	33.0	4	4	1.12	1.07	0.95	0.99	0.59	0.58	0.15	0.00
6.20	0.35	64	71.43	157.5	35.8	4	4	1.10	1.06	0.98	0.97	0.58	0.58	0.35	0.00
6.20	0.35	64	71.43	157.5	38.5	4	4	1.10	1.08	0.97	0.97	0.58	0.57	0.54	0.00
6.20	0.35	64	71.43	157.5	41.3	4	4	1.07	1.08	0.97	0.94	0.59	0.58	0.69	0.00
6.20	0.35	64	71.43	157.5	44.0	4	4	1.09	1.12	0.96	0.95	0.59	0.59	2.82	0.00
6.20	0.35	64	71.43	157.5	46.8	4	4	1.08	1.09	0.97	0.95	0.58	0.57	3.47	0.00
6.20	0.35	64	71.43	157.5	49.5	4	4	1.12	1.11	0.96	0.95	0.58	0.59	5.15	0.00
6.20	0.35	64	71.43	157.5	52.3	4	4	1.10	1.08	0.96	0.96	0.57	0.58	11.24	0.00
6.20	0.35	64	71.43	157.5	55.0	4	4	1.12	1.08	0.96	0.95	0.59	0.58	11.34	0.00
7.50	0.30	52	83.33	135.0	0.0	4	4	1.32	1.27	1.15	1.11	0.68	0.68	0.00	0.00
7.50	0.30	52	83.33	135.0	3.0	4	4	1.30	1.29	1.18	1.15	0.69	0.73	0.00	0.00
7.50	0.30	52	83.33	135.0	6.0	4	4	1.28	1.30	1.16	1.20	0.68	1.14	0.00	0.00
7.50	0.30	52	83.33	135.0	9.0	4	4	1.29	1.33	1.16	1.42	0.68	1.71	0.00	0.00
7.50	0.30	52	83.33	135.0	12.0	4	4	1.28	1.29	1.12	1.38	0.66	1.51	0.00	0.00
7.50	0.30	52	83.33	135.0	15.0	4	4	1.33	1.28	1.17	1.26	0.68	1.19	0.00	0.00
7.50	0.30	52	83.33	135.0	18.0	4	4	1.29	1.30	1.15	1.18	0.68	0.96	0.00	0.00
7.50	0.30	52	83.33	135.0	21.0	4	4	1.29	1.31	1.13	1.16	0.68	0.81	0.00	0.00
7.50	0.30	52	83.33	135.0	24.0	4	4	1.28	1.31	1.14	1.19	0.69	0.74	0.00	0.00
7.50	0.30	52	83.33	135.0	27.0	4	4	1.26	1.32	1.17	1.14	0.68	0.71	0.00	0.00
7.50	0.30	52	83.33	135.0	30.0	4	4	1.29	1.30	1.14	1.14	0.67	0.68	0.00	0.00
7.50	0.30	52	83.33	135.0	33.0	4	4	1.28	1.30	1.16	1.15	0.68	0.66	0.00	0.00
7.50	0.30	52	83.33	135.0	36.0	4	4	1.33	1.29	1.15	1.13	0.68	0.67	0.00	0.00
7.50	0.30	52	83.33	135.0	39.0	4	4	1.31	1.29	1.14	1.13	0.69	0.69	0.00	0.00
7.50	0.30	52	83.33	135.0	42.0	4	4	1.27	1.34	1.18	1.15	0.68	0.68	0.10	0.00
7.50	0.30	52	83.33	135.0	45.0	4	4	1.28	1.29	1.12	1.12	0.66	0.67	0.35	0.00
7.50	0.30	52	83.33	135.0	48.0	4	4	1.30	1.31	1.15	1.11	0.68	0.67	1.14	0.00
7.50	0.30	52	83.33	135.0	51.0	4	4	1.27	1.31	1.17	1.15	0.66	0.69	2.62	0.00
7.50	0.30	52	83.33	135.0	54.0	4	4	1.25	1.27	1.15	1.14	0.68	0.69	4.60	0.00
7.50	0.30	52	83.33	135.0	57.0	4	4	1.30	1.27	1.16	1.17	0.65	0.69	10.05	0.00
7.50	0.30	52	83.33	135.0	60.0	4	4	1.34	1.32	1.13	1.08	0.68	0.68	14.26	0.00

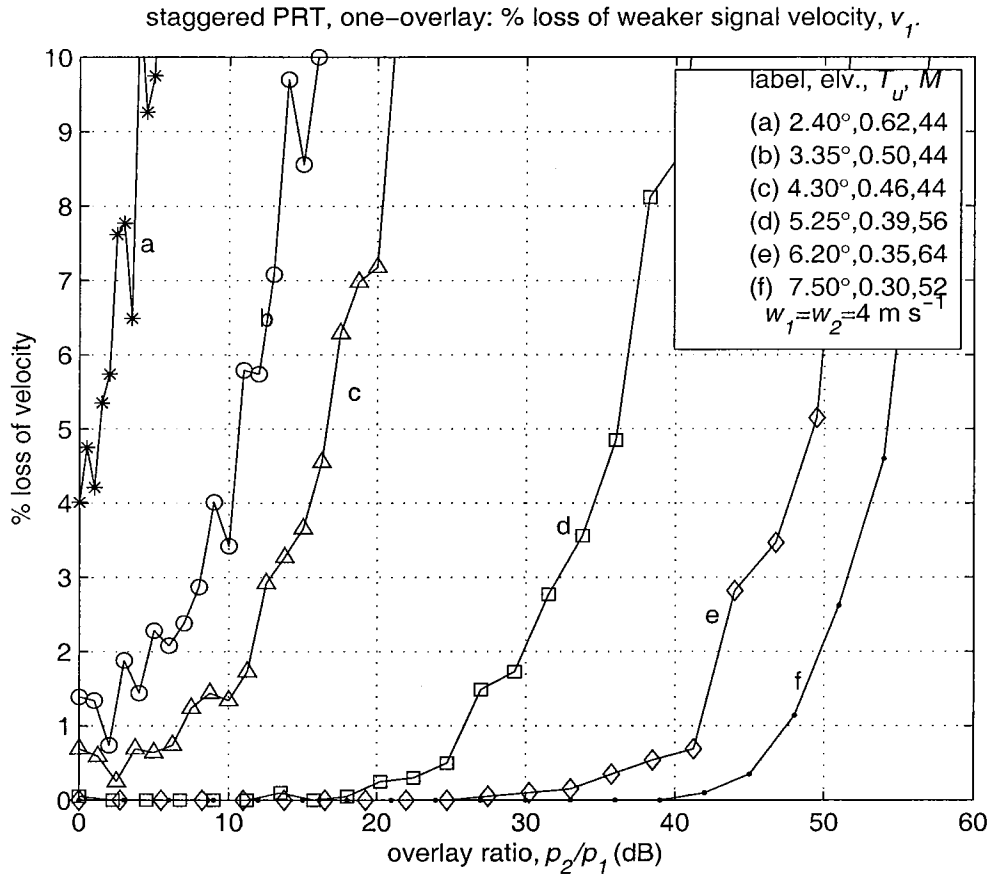

Fig. 5.1. The percentage loss of velocity as a function of the overlay power ratio, p_2/p_1, for different elevation scans of the vcp-11 of the WSR-88D. The PRTs are chosen appropriately to give the required range coverage for each elevation. The spectrum width used for both signals is 4 m s^{-1}.

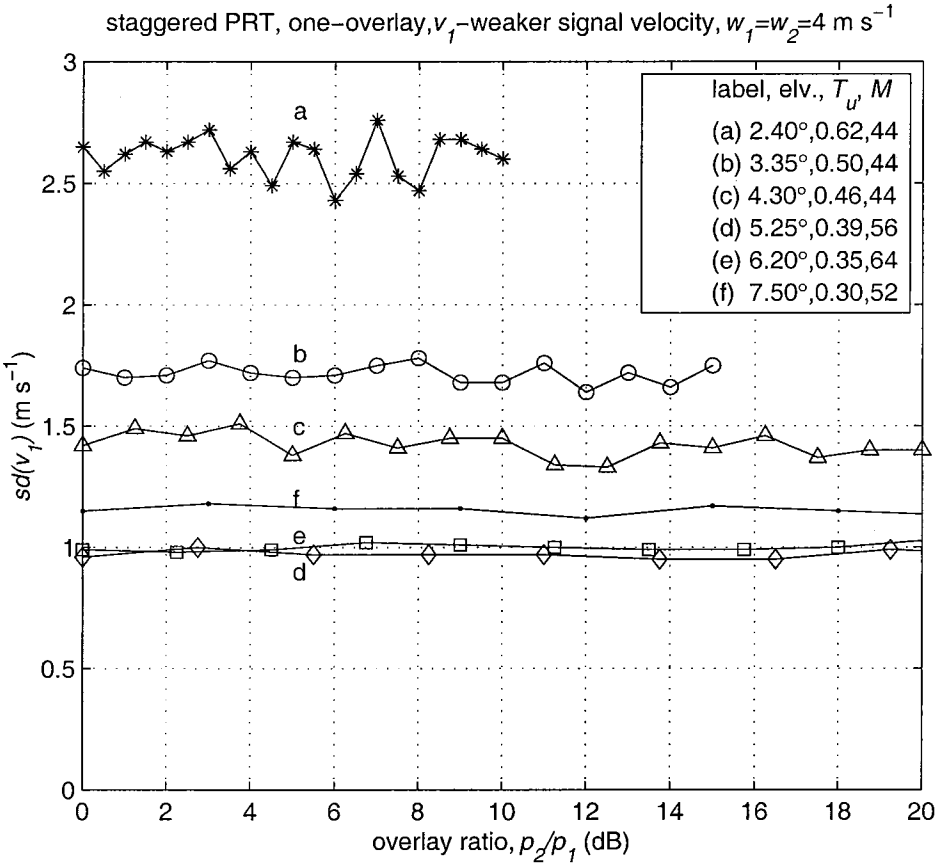

Fig. 5.2. The $sd(v_1)$, the standard error in the weaker signal velocity as a function of the overlay power ratio, p_2/p_1, for different elevation scans of the vcp-11 of the WSR-88D. The PRTs are chosen appropriately to give the required range coverage for each elevation. The spectrum width used for both signals is 4 m s^{-1}.

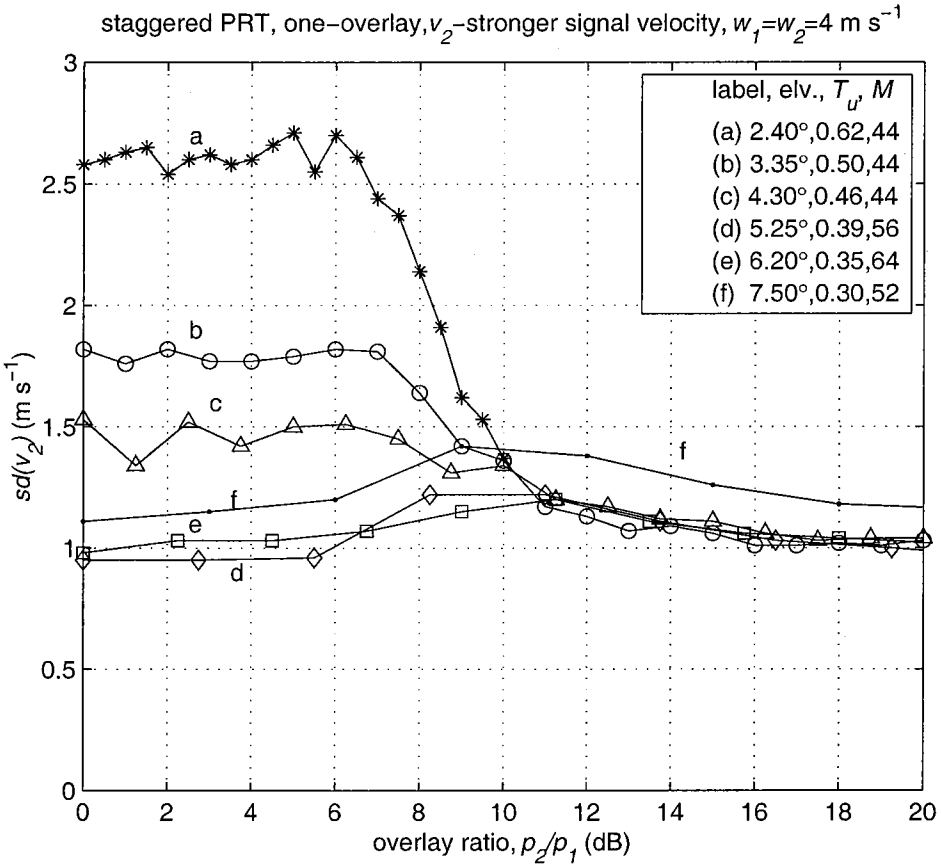

Fig. 5.3. The $sd(v_2)$, the standard error in the stronger signal velocity as a function of the overlay power ratio, p_2/p_1, for different elevation scans of the vcp-11 of the WSR-88D. The PRTs are chosen appropriately to give the required range coverage for each elevation. The spectrum width used for both signals is 4 m s^{-1}.

9. References.

Doviak, R.J. and D.S. Zrnic, 1993: *Doppler Radar and Weather Observations.*, Academic Press, New York, 562pp.

Sachidananda, M., D.S. Zrnic, and R.J. Doviak, 1997: Signal design and processing techniques for WSR-88D ambiguity resolution, Part-1. *National Severe Storms Laboratory*, July 1997, 100 pp.

Sachidananda, M., D.S. Zrnic, and R.J. Doviak, 1998: Signal design and processing techniques for WSR-88D ambiguity resolution, Part-2. *National Severe Storms Laboratory*, June 1998, 105 pp.

Sachidananda, M., D.S. Zrnic, and R.J. Doviak, 1998: Signal design and processing techniques for WSR-88D ambiguity resolution, Part-3. *National Severe Storms Laboratory*, June 1998, 81 pp.

Sachidananda, M., and D.S. Zrnic, 2000: Clutter filtering and spectral moment estimation for Doppler weather radars using staggered pulse repetition time (PRT). *J. Atmos. Oceanic Technol.*, **17**, 323-331.

Zrnic, D.S., and P.R. Mahapatra, 1985: Two methods of ambiguity resolution in pulsed Doppler weather radars. *IEEE Trans. on Aerospace and Electronic Systems.*, **AES-21**, 470-483.

LIST OF NSSL REPORTS FOCUSED ON
POSSIBLE UPGRADES TO THE WSR-88D RADARS.

Doviak, R.J. and D.S. Zrnic, 1998: NOAA/NSSL's WSR-88D Radar for Research and Enhancement of Operations: Polarimetric Upgrades to Improve Rainfall Measurements, 110 pp.

Sachidananda, M., 1999: Signal Design and Processing Techniques for WSR-88D Ambiguity Resolution, Part 3, 81 pp.

Sachidananda, M., 1998: Signal Design and Processing Techniques for WSR-88D Ambiguity Resolution, Part 2, 105 pp.

Sachidananda, M., 1997: Signal Design and Processing Techniques for WSR-88D Ambiguity Resolution, Part 1, 100 pp.

Sirmans, D., D.S. Zrnic, and M. Sachidananda, 1986: Doppler radar dual polarization considerations for NEXRAD, Part 1, 109 pp.

Sirmans, D., D.S. Zrnic, and N. Balakrishnan, 1986: Doppler radar dual polarization considerations for NEXRAD, Part 2, 70 pp.